NASA CR-72442

FINAL REPORT

ANALYTIC AND EXPERIMENTAL STUDY OF REENTRANT STREAM CROSSED-FIELD AMPLIFIERS

by

G. E. Dombrowski and W. C. Price

prepared for

NATIONAL AERONAUTICS AND SPACE ADMINISTRATION

July, 1968

CONTRACT NAS 3-9710

Technical Management
NASA Lewis Research Center
Cleveland, Ohio
Henry G. Kosmahl

UNIVERSITY OF CONNECTICUT
Department of Electrical Engineering
Storrs, Connecticut

NOTICE

This report was prepared as an account of Government sponsored work. Neither the United States, nor the National Aeronautics and Space Administration (NASA), nor any person acting on behalf of NASA:

A) Makes any warranty or representation expressed or implied, with respect to the accuracy, completeness, or usefulness of the information contained in this report, or that the use of any information, apparatus, method, or process disclosed in this report may not infringe privately owned rights; or

B) Assumes any liabilities with respect to the use of, or for damages resulting from the use of any information, apparatus, method or process disclosed in this report.

As used above, "person acting on behalf of NASA" includes any employee or contractor of NASA, or employee of such contractor, to the extent that such employee or contractor of NASA, or employee of such contractor prepares, disseminates, or provides access to, any information persuant to his employment or contract with NASA, or his employment with such contractor.

Requests for copies of this report should be referred to:

National Aeronautics and Space Administration
Office of Scientific and Technical Information
Washington, D. C. 20545

Attention: AFSS-A

ANALYTIC AND EXPERIMENTAL STUDY OF

REENTRANT STREAM CROSSED-FIELD AMPLIFIERS

by G. E. Dombrowski and W. C. Price

University of Connecticut

SUMMARY

Electronic interaction in an injected beam forward-wave amplifier was analyzed by simulation in a digital computer. The computations show that gains as high as 15 db with efficiencies in the range of 50 to 70 percent can be attained with a proposed design which uses a network 6 wavelengths long. Attempted simulation of high gain operation with low rf input signals was hampered by instability. After considerable study it was concluded that reentrant stream feedback was the cause, although fluctuations are normally present in the simulation.

Studies of a second design of the amplifier, using 13 wavelengths, show higher gain and greater computational stability with less stream feedback. Early indications are that the efficiency of this design is greater.

The analysis of the injected reentrant beam crossed-field amplifier is not complete. Further computations are required to cover a wider range of parameters. Such work, however, should be more closely related to the actual device development.

Amplitron noise power measurements were made on type QKS-1300 tubes. Spectral density of total noise was found to be -68 dbm/Hz for a broad range of frequency in the Amplitron pass band. Near the carrier (within 70 KHZ) the noise is higher, reaching -58 dbm/Hz 10 KHZ from the carrier. Attempts to measure the f-m noise failed. The reason is thought to be that a microwave limiter used was too noisy.

TABLE OF CONTENTS

Page	Section	
ii		SUMMARY
v		LIST OF ILLUSTRATIONS
vii		LIST OF SYMBOLS
1	1.	OBJECTIVES
1	1.1	Analytic Studies
1	1.2	Experiments
3	PART I	ANALYTIC STUDIES
3	2.	INTRODUCTION
3	2.1	Self-Consistent Field Calculations
4	2.2	Traveling-Wave Calculations
4	2.3	Transient Calculations
5	3.	FORMULATION OF THE COMPUTER SIMULATION
5	3.1	Nomenclature
8	3.2	Assumptions
10	3.3	Notation
10	3.4	Laws Governing Simulation
11	4.	THE COMPUTER PROGRAM FOR THE SIMULATION
11	4.1	Outline
12	4.2	Details of the Computer Program
12	4.2.1	Computation of Space-Charge Fields
14	4.2.2	Computation of the Circuit Fields and Induced Anode Charge
15	4.2.3	Network Computations
16	4.2.4	Trajectories
17	4.2.5	Cathode Emission
21	4.2.6	Beam Injection
21	4.2.7	Waveform Analysis
21	4.2.8	Graphic Output
24	4.3	Running of a Computation
24	4.3.1	Input
24	4.3.2	Output
26	5.	AMPLITRON CALCULATIONS
26	5.1	Parameters
27	5.2	Results
27	5.3	Termination
27	6.	INJECTED BEAM FORWARD-WAVE AMPLIFIER CALCULATIONS
28	6.1	Parameters
29	6.2	Results
29	6.2.1	Preliminary Calculations

TABLE OF CONTENTS (cont.)

Page	Section	
31	6.2.2	Demodulation & Feedback Through the Stream
31	6.2.3	Instability at High Gain
42	6.3	Amplifier Performance at Moderate Gain
47	6.4	Effect of Parameters on Operation
47	6.4.1	Dc Anode Voltage
47	6.4.2	Dc Injected Current
51	6.4.3	Rf Input Power Level
51	6.4.4	Rf Impedance Level
57	6.5	Second Design of the Injected Beam Amplifier
59	7.	CONCLUSIONS OF ANALYTIC STUDY
59	7.1	Conclusions
59	7.2	Recommendations
64	PART II	AMPLITRON NOISE MEASUREMENTS
64	8.	INTRODUCTION
64	9.	MEASUREMENTS
64	9.1	Scope
64	9.2	Measurement Techniques
66	9.3	Results
68	9.4	Conclusions
72	APPENDIX	
72	A.	COMPUTER PROGRAM LISTING
72	A.1	Control Program
76	A.2	Input Program
82	A.3	Space-Charge Green's Function
84	A.4	Anode Green's Function
86	A.5	Graphic Display
90	A.6	Space-Charge Field Calculation
98	A.7	Induced Charge, Network Response, & Circuit Fields
103	A.8	Cathode Emission
106	A.9	Trajectory Calculations
109	A.10	Merge, Collect and Output
116	A.11	Fourier Analysis
119	DISTRIBUTION LIST	

LIST OF ILLUSTRATIONS

Page	Figure No.	Title
6	3.1	Interaction Space Nomenclature
7	3.2	Lumped Constant Network Models
9	3.3	Phase Characteristics of Networks of Figure 3.2
18	4.1	Construction for Trajectory Calculation
19	4.2	Test Calculations of Electron Orbit in Static 1/r Field
20	4.3	Net Cathode Emission as a Function of Cathode Field
22	4.4	Specimen of Graphic Display for Amplitron Calculation
23	4.5	Specimen of Graphic Output (Injected Beam Amplifier)
30	6.1	Extension of CFA Calculation #010268: Failure to Reach Steady State
32	6.2	Example of Instability
34	6.3	Calculation #6012: Space-Charge Forces Omitted; Artificial Stream Demodulation
35	6.4	Standing Wave Resulting from Mismatch of Amplifier. Reflection Coefficient: 1/3
36	6.5	Calculation Carried for Extended Period
37	6.6	Spectrum Analysis of Output Voltage Waveform
39	6.7	Transition from Uniform DC Drift Potential to Tapered Drift Potential
40	6.8	Variation of Length of Drift and Active Sections
41	6.9	Drift Section Removed
43	6.10	Comparison of Calculations With and Without Stream Reentrance
44	6.11	Calculation #6007: Configuration at T=96.0
45	6.12	Calculation #6007: Configuration at T=96.5
46	6.13	Calculation #6007: Configuration at T=97.0
48	6.14	Distribution of Current and Voltage on Network; Calculation #6007, T=97.0
49	6.15	Calculation #6007: Collector Histogram
50	6.16	RF Current Distribution as Function of Injected Current
52	6.17	Effect of Injected Current on Performance
53	6.18	RF Current in Stream vs. RF Drive Power
55	6.19	Power Transfer Characteristic
56	6.20	Start-up Transient with Very Small RF Input Signal
58	6.21	Calculation #7004: Internal Voltage Distribution
60	6.22	Calculation #5010: Configuration at T=40.8
61	6.23	Calculation #5010: Configuration at T=41.2
62	6.24	Calculation #5010: Configuration at T=41.8
65	9.1	Amplitron Noise Measuring Bridge System

LIST OF ILLUSTRATIONS (Cont.)

Page	Figure No.	Title
67	9.2	Effect of Heater Current on Noise
69	9.3	Noise Power as a Function of RF Drive Power
70	9.4	F-M Noise Power Density Measurement: "Cold" Tube
71	9.5	F-M Noise Power Density Measurement: Operating Tube

LIST OF SYMBOLS

SYMBOL	PAGE	CORRESPONDING COMPUTER VARIABLE	DESCRIPTION
ACF	25	ACF	Autocorrelation function
B	11		Magnetic flux density
B_o	28		Critical (scaling)magnetic flux density
C	11		Capacitance element
C'	16		Effective capacitance
$\underline{\underline{C}}$, $\underline{\underline{C}}^{-1}$	16		Capacitance matrix inverse
C_a,C_b,C_c	7	CA,CB,CC	Network capacitance elements
C_{nn}, C_{nm}	15		Self, mutual capacitances
C_o	10		Scaling capacitance parameter
C_1, C_2	7	C1; C2	Network terminating capacitances
I_1, I_2	7	CIN1,CIN2	Network source currents
I_1, I_2	7	COUT1,COUT2	Network source currents
		CNST	Emitted charge element
d_a	26		Anode diameter
d_c	26		Cathode (sole) diameter
EX, EY	11	EX, EY	Electric field components
EX_o, EY_o	16		Initial values of EX, EY
G	11		Conductance element
G, G_k	12		Green's functions
G_a,G_b,G_c	24	GA,GB,GC	Network conductance elements
G_{nn}, G_{nm}	15		Self, mutual conductances
G_o	10		Scaling conductances
G_1, G_2	7	G1, G2	Network terminating (load) conductances
$\underline{\underline{G}}$	16		Conductance matrix
GAP	6	GAP	Fractional intervane spacing
h_t	16	HT	Time increment
h	10		Axial length of interaction space
I_b	26		Dc anode current
I_c	26		Dc collector current
I_i(N)	48		Induced current of Nth electrode

LIST OF SYMBOLS (cont.)

SYMBOL	PAGE	CORRESPONDING COMPUTER VARIABLE	DESCRIPTION
I_k	28		Dc injected (cathode) current
I_n	15		Current into Nth electrode
I_o	10		Scaling current
I_1, I_2	7		Source currents
$\underline{\underline{I}}$	16		Current matrix
J	20		Current density
J_s	20		Saturation emission current density
K_o	28		Coupling impedance, $EE^*/2\beta^2P$
k	16		Boltzmann constant
k_o	10		Reference mode number
L_o	10		Scaling inductance
NE	5	NE	Number of anode sectors
NG	5	NG	Number of active anode sectors
NK	21	NK	Number of emission sites
PS	24	PS	Normalized mean particle diameter
P_o	10		Scaling power
P_{in}	28		Signal input power
P_{out}	26		Signal output power
p		P	Radial coordinate; p=0 is cathode (sole)
p_{in}	24	PIN	Injection radius
p'		PD	Radial velocity
p'_{in}	24	PDIN	Injection radial velocity
Q	11	Q	Normalized charge
$Q_i(N)$	14		Induced charge at Nth electrode
Q_j	14		Particle charge
$Q_m(N)$	53		Amplitude of signal frequency component of $Q_i(N)$
Q_o	10		Scaling charge
r	6		Radial coordinate
$\underline{r}$	12		Position vector
r_a	10		Anode radius

LIST OF SYMBOLS (cont.)

SYMBOL	PAGE	CORRESPONDING COMPUTER VARIABLE	DESCRIPTION
r_c	10		Cathode (sole) radius
r_s	6		Sole radius
S_k	14		Surface of kth electrode
s	11		Normalized radius
$\underline{s}$	11		Position vector (normalized)
$\underline{s}_i$	11		Initial position vector
s_o	6	SZ	Normalized cathode (sole) radius
T	11	T	Normalized time, vt
T	16		Temperature
t	11		Real time
$\underline{U}$	11		Normalized velocity vector
u_x, u_y	11	UX, UY	Velocity components
V	10		Electric potential
V'	11		Time derivative of electric potential
V_o	10		Scaling voltage
V_b	26	VDC	Anode voltage
		VDD	Dc drift section voltage
V_c	14		Circuit component of potential
V_c	26		Average collector potential
V_H	11		Hartree voltage
V_n, V_m	15		RF potential of nth, mth electrodes
V'_n, V'_m	15		Time derivatives of V_n and V_m
$V_n(N)$	32		Amplitude of r-f voltage on nth electrode
$\underline{\underline{V}}$, $\underline{\underline{V}}'$	16		Voltage matrix, time-derivative
$\underline{\underline{W}}$	16		Excitation matrix
w	26		Anode vane width
β	16		$1/(2\eta kT)=11600/T$
Γ	11		Reciprocal inductance
Γ_a,Γ_b,Γ_c	7	GAMA,GAMB,GAMC	Network inductance elements
Γ_{nn},Γ_{nm}	15		Self, mutual inductance parameters

LIST OF SYMBOLS (cont.)

SYMBOL	PAGE	CORRESPONDING COMPUTER VARIABLE	DESCRIPTION
Γ_o	10		Scaling reciprocal inductance
Γ_1, Γ_2	24	GL1, GL2	Network terminating inductances
$\underline{\underline{\Gamma}}$	16		Inductance matrix
δ	12		Dirac delta function
ε_o	10		Free space dielectric permittivity
η	10		Magnitude of electron specific
θ	5	TH	Azimuthal coordinate
		THD	Azimuthal time rate ("velocity")
	24	THDIN	Azimuthal velocity of injected charge
θ'	17		Increment in azimuth
θ_m	24	THM	Range of space charge Green's fcn.
θ_{mp}	24	THMP	Range of anode Green's fcn.
θ^o	11		Cyclotron time, $\omega_c t$
θ_s	6	THS	Azimuth of one sector
ν_o	10		Reference frequency
P	10		Normalized charge density
τ	24	TLIFE	Electron axial transit time
ϕ	20		Electric potential
ω	9		Frequency
ω_o			Reference (angular) frequency, $2\pi\nu$.

1. OBJECTIVES

1.1 ANALYTIC STUDIES

1.1.1 General Objectives

The general objectives of this phase of the research are the development and application of a computer model to the study of high-efficiency, high power crossed-field amplifiers using reentrant electron streams.

The operational characteristics of the amplifier of interest are:

a. Gain;
b. Output;
c. Efficiency;
d. Bandwidth;
e. Linearity;
f. Phase distortion.

A determination is to be made of how these characteristics are affected by such operating variables and design parameters as

a. dc magnetic field intensity;
b. dc anode voltage
c. dc anode current;
d. rf input level;
e. rf interaction space length;
f. rf network impedance;
g. rf network phase characteristics;
h. rf network attenuation;
i. number and shape of anode electrodes;
j. length of demodulation (drift) section, if any.

1.1.2 Specific Objectives

Originally, the amplifier device on which calculations were to have been made was the Amplitron. This crossed-field amplifier uses a reentrant beam derived by thermionic or secondary emission from a cylindrical cathode. Its rf network encompasses the entire perimeter of the interaction region (there is no drift region), but is itself not reentrant. It may be thought of as the result of severing the straps of a conventional strapped-vane magnetron.

Inasmuch as Amplitrons have been well understood and in widespread use for many years, and also because a computer program for its large-signal analysis had been in existence, these computations take on the nature of the collection of a body of information for design refinement.

Subsequently, however, the application for which the Amplitron was intended was modified to the extent that the Amplitron was no longer desired. It was replaced in the intended application and this study by a different reentrant-stream crossed-field amplifier. The new device uses

a forward-wave network, has a demodulating section, and obtains its electron stream by axial injection of a hollow beam. The scope of the study therefore is extended to consider the effects of injection parameters on the amplifier performance.

The new form of amplifier is at an early stage of development, however. The applicability of the computations thus to some degree takes on the character of pointing out the directions for further device development rather than design refinement.

1.2 EXPERIMENTS

1.2.1 Amplitron Performance

In conjunction with the numerical analysis, measurements were to have been made, especially at high magnetic fields and with such parameters as indicated by computer results, on a commercial Amplitron of medium power. The objective of this phase was to verify as much of the computer optimization as possible.

When the Amplitron was discarded as a candidate for the application as the transmitter tube, this phase of the project was abandoned.

1.2.2 Amplitron Noise Measurements

As a separate issue, measurements were to be made of the noise inherent in the Amplitron as a transmitter tube for general application. The total noise was to be measured as a function of frequency relative to the amplified signal, and was to have been resolved into its f-m and a-m components.

PART I. ANALYTIC STUDIES

2. INTRODUCTION

There is a clear need for information with which to optimize the design of high power microwave tubes. This is especially true of such highly efficient ones as crossed-field devices, since the dissipation within the device--and consequent heating and heat dissipation problems--is more radically affected by a given change in efficiency for them.

Because high power devices inevitably involve nonlinear interactions, numerical analysis is usually necessary. Large capacity, high speed computers are readily available for this purpose. The primary limitation involved in resorting to numerical work is the difficulty in making generalizations from the specific cases studied.

The computers presently available are attractive instruments for making simulations of a wide variety of complex systems, of which the microwave electron device is surely a member. Such computer experiments are much cheaper to run than tests on actual high power tubes. Parameter changes can be more easily made in the computer, and the results thereof more readily discerned. The computer, however, is limited by the validity of the model used to represent the real device.

2.1 Self-consistent Field Calculations

Some of the earliest numerical analysis of electron tubes was the application to the magnetron of Hartree's method of self-consistent fields. In its use here, the calculations proceed somewhat as outlined below:

a. The space-charge configuration is assumed (by guess--educated or otherwise);

b. the electric potential of the interaction region is computed from the space-charge and the applied rf and dc potentials. This is the solution of Poisson's equation;

c. electron trajectories are computed from the cathode in this field;

d. the currents carried on each trajectory are adjusted so that the potential gradient at the cathode is zero. Space-charge-limited conditions are thus assumed;

e. the resulting total space-charge configuration is compared with that from which it was derived. In a series of iterations, new configurations are generated with which to repeat the sequence outlined above.

According to the simple theory of the Amplitron, the space-charge is very much like that in the magnetron in spite of the amplification of the rf signal with azimuth. The reasons for this are the absence

of a drift region to allow for debunching and the rather short recirculation time of the electrons. A good self-consistent field calculation would thus be a starting point for Amplitron analysis.

The success of the self-consistent method obviously depends on one's ability to make wise guesses of the space-charge. It also requires freedom from instability in the sense that small deviations from the correct answer must not lead one into making guesses that are even wilder. Unfortunately, previous workers in this area have not met success. The underlying cause seems to be the presence of dense space-charge, its consequent effect on the electric field, and the critical dependence of the electron paths of the electric field through the partial balance of the Lorentz force. There is, indeed, considerable doubt whether the magnetron is really a stable device.

2.2 Traveling-Wave Tube Calculations

Subsequent to the invention of the traveling-wave tube by Kompfner and the development of an elegant small signal theory by Pierce, large-signal computer studies were made. At that time computers were in a very early stage of development, and many approximations were made in order to get solutions. One of these is that interaction takes place only with the circuit component wave traveling in near synchronism with the electrons. This is reasonable only with injected beam devices such as the O-type traveling wave tube and the injected beam class of crossed-field amplifiers (non-reentrant). It does not seem to be applicable to the Amplitron, which has important nonsynchronous components and a multi-velocity stream. Another assumption is that of small gain rate, which allows the computation of space charge forces without regard to the variation from one bunch to the next and an overall calculation as an integration pass from input end to output end of the system. In such crossed-field devices as the Amplitron and other emitting sole tubes, the gain rate is quite high and space-charge forces cannot be computed this way. Moreover, stream reentrancy without demodulation makes it impossible to know the conditions at the input end of the system until the output conditions are determined. This method, nevertheless appears to be quite applicable to handling the forward-wave CFA with the injected beam.

2.3 Transient Calculations

The self-consistent field technique not only fails in the case of the magnetron, but as with all iterative methods, the intermediate stages fail to yield any physically meaningful results. In the transient method one attempts to simulate a physically possible situation, such as the start-up of an oscillator, and then to follow its development into steady state. It eliminates the need to guess at any charge configuration. Rather one starts with, say, no charge at all, from which one computes the fields, thence the emission, and the resulting charge configuration a very short time later. The fields of the new configuration are then computed, and the calculation marches on with time.

Transient calculations had been made during the course of early magnetron research to determine the static distribution in the cut-off magnetron. The extension to include time-varying fields has been made only recently.

In the case of the Amplitron and other crossed-field amplifiers, this technique appears to be quite promising--assuming that steady state is reached, as it has in many cases. An additional factor involved in amplifiers is the variation of space-charge and circuit fields from spoke to spoke and with distance along the signal path. This can be handled in modern computers without the restrictions of the past to only one or a few Hartree (space) harmonics. Indeed, the transient calculation may properly be regarded as a case of simulation of both the stream and the network in the computer.

The transient calculation, or more generally, computer simulation in the time domain, is the method that was applied to previous analysis of the Amplitron. It is used in the present research and is described fully in Section 4.

It must be remembered, however, that the magnetron and related crossed-field devices are critically dependent on space charge and on the balance between electrostatic and Lorentz forces for focusing. The self-consistent field calculations failed because of these factors, i.e., because the calculated electron paths did not go where the electrons were supposed to have been. In the computer simulation this is not a problem: the electron positions are known, and their effects on the fields are known. The difficulty of the calculation appears in attaining a steady state and in the fluctuations and/or oscillations therefrom. To some extent the determination of steady state results is a statistical problem because of the fluctuations. It is expected that if a large enough system of particles is used to simulate the actual electron stream, these fluctuations will be small. This certainly depends on the inherent stability of the system under simulation.

3. FORMULATION OF THE COMPUTER SIMULATION

3.1 Nomenclature

Figure 3.1 shows the nomenclature of the interaction region. In the computer it is possible to keep account of a large number of variables, hence the electrodes are numbered, starting with #1 at $\theta=0$, and proceeding counterclockwise to #NE. Of these electrodes, the first NG are active; the remainder have only d-c potentials as a drift section. In the Amplitron, NG=NE, i.e., there is no drift section. The r-f signal is applied at #1 for a backward-wave network, as most Amplitrons use, and propagates counterclockwise. The electrons move in the clockwise direction with positive anode voltage and axial magnetic field.

Figure 3.2(a) shows the rf network typical of Amplitrons. It is essentially a balanced two-wire line (the straps) with resonator (vanes) loading. A balance-to-unbalance transition is usually connected to the ends of the network to transform to the external signal paths. Figure

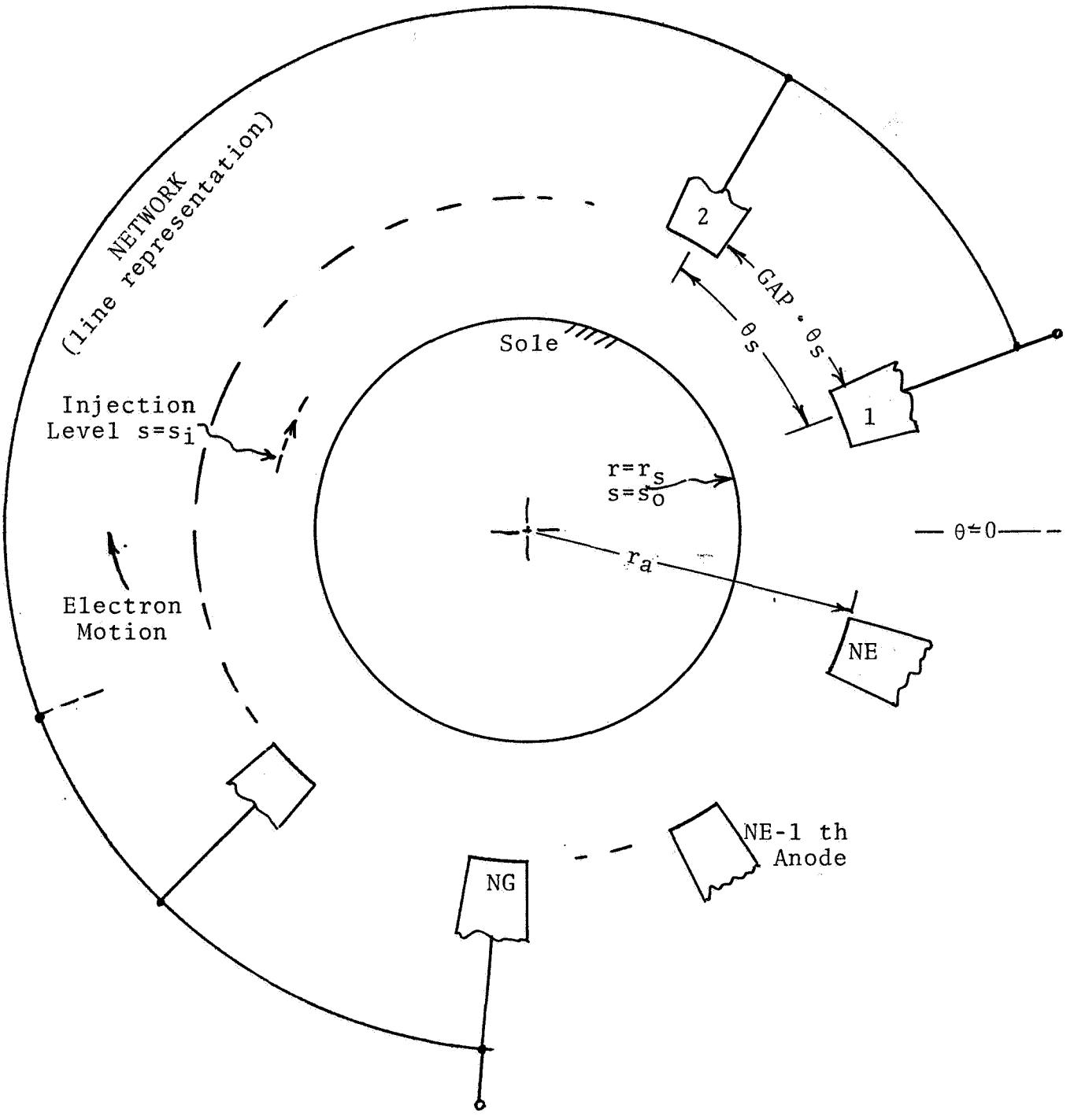

Figure 3.1. Interaction Space Nomenclature.

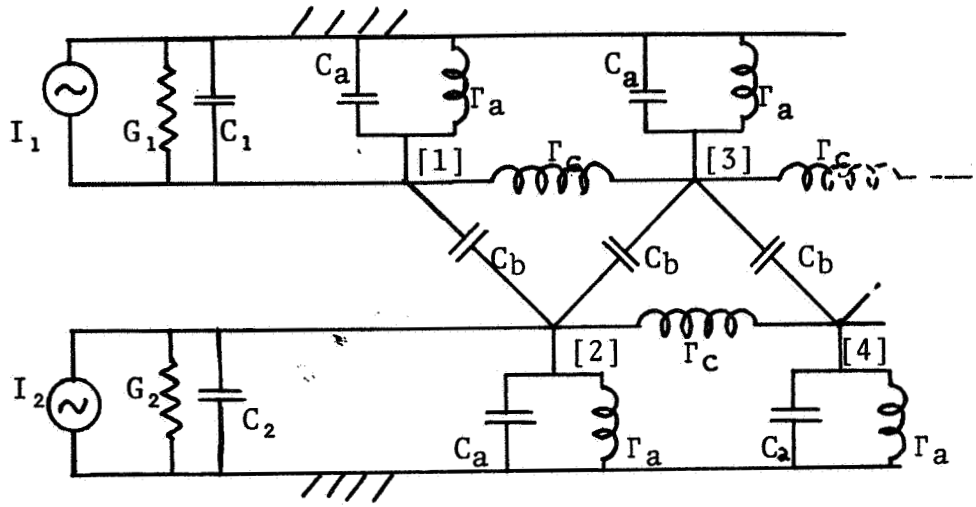

a. Network for Amplitrons (strapped vanes).

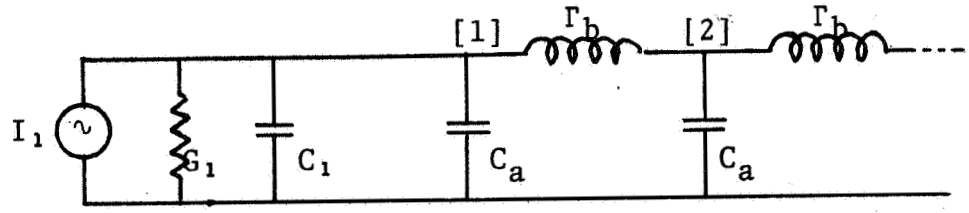

b. Forward-wave network.

Figure 3.2. Lumped constant network models. Electrode numbers in brackets.

3.3(a) shows the phase characteristic of such a network.

Figure 3.2(b) shows an elementary forward-wave network used to simulate the injected beam, forward-wave amplifier. Precise details of the network used in the actual tube are not known, but this representation is considered to be the best known one inasmuch as its dispersion is minimal. Its phase characteristic is shown in Figure 3.3(b).

The analysis of the injected beam forward-wave device is based on Figure 3.1 with the specification that electrons are emitted at some intermediate radius and have clockwise angular velocity. The signal input is at the NGth electrode; propagation is also clockwise, the load being connected to the first electrode.

3.2 Assumptions

The following assumptions are made:

a. The dc magnetic field is uniform and axial.
b. Cathode is circular cylinder concentric with the anode.
c. All anode electrodes are identical and equally spaced.
d. All network elements are identical and ideal.
e. Cathode emission is uniform.
f. Electron motion is nonrelativistic.
g. No neutral or ionized gas atoms are present.
h. Electric field retardation effects are negligible.
i. Rf magnetic field forces are negligible.
j. No secondary electron emission takes place.

These are the basic assumptions necessary for expeditious handling of microwave tube problems. It is of course necessary that the network representation used be a realistic model for the actual microwave network; this is a matter of degree of approximation.

In the analysis of the injected beam device, assumption (e) is to be replaced by

(e) injection takes place equally at equally spaced sites located on the injection circle. All injected electrons have the same axial velocity, which is such that after TLIFE rf cycles they emerge from the interaction process and are eliminated therefrom;

In addition to the basic assumptions made above are added the specific assumptions below, which are subject to modification as the problem changes or the model improves:

a. All anode electrodes are identical and equally spaced. They have circular inner faces and radial sides. The field is assumed to be purely azimuthal between radial faces of adjacent electrodes;

Other restrictions in the model take on the nature of the approximations made; they will be described in connection with the specific

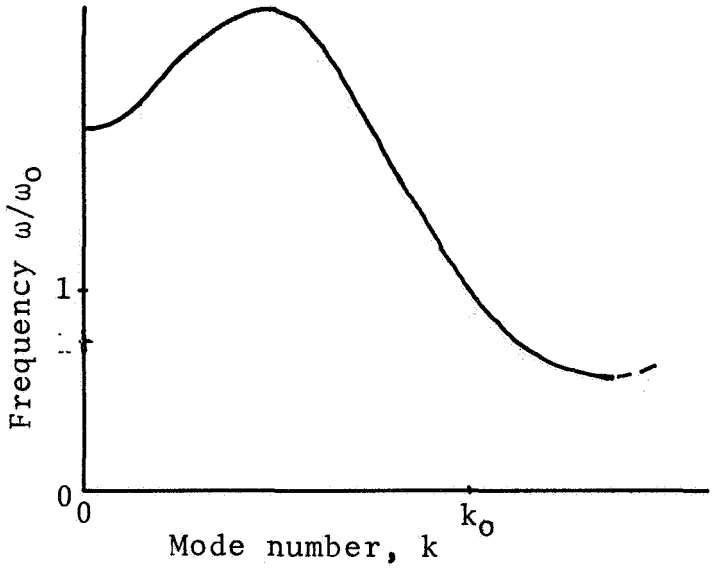

a. Amplitron network (strapped vanes)

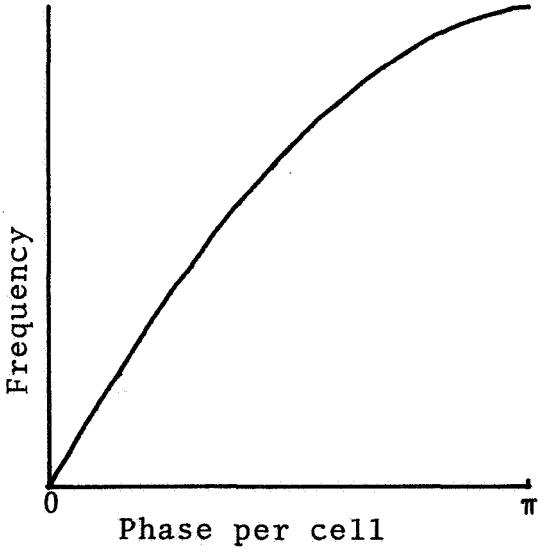

b. Forward-wave Network

Figure 3.3. Phase Characteristics of Networks of Figure 3.2.

portions of the analysis below.

3.3 Notation

3.3.1 Interaction Space Geometry

As indicated in Figure 3.1, the following notation applies:

- r_a Anode radius
- r_c Sole radius
- s_o Ratio: sole radius/anode radius
- h Axial length of interaction system
- GAP Fraction of anode circle for intervane gap
- NE Number of anode electrode sectors
- NG Number of active anodes

3.3.2 Normalization

For reference purposes only, a reference frequency and mode number are defined. Voltages are normalized with respect to the synchronous value, which is the electron kinetic energy for synchronism in the reference mode at reference frequency. This voltage is described in Table 3.1. A reference capacitance, C_o, is also listed. The reference current, I_o, is the rf current flowing through C_o with V_o applied at frequency ν_o. Other scaling values follow.

Table 3.1 Normalizing Variables

Voltage	V_0	$(2\pi\nu_0 r_a/k_0)^2/2\eta$
Capacitance	C_0	$\omega_0\varepsilon_0 h$
Charge	Q_0	C_0V_0
Current	I_0	ν_0Q_0
Power	P_0	I_0V_0
Conductance	G_0	$I_0/V_0 = \nu_0C_0$
Inductance	L_0	R_0/ν_0
1/Inductance	Γ_0	$\nu_0G_0 = \nu^2C_0$

3.4 Laws Governing Simulation

The laws that govern the computer model are mainly the same as those of a physical system: Poisson's, Newton's, and Kirchoff's.

In the computer model, using normalized potential, charge, and distance, Poisson's Law takes the form

$$\nabla^2 V = P, \tag{3.1}$$

where the Laplacian operation is in the normalized coordinate system. The charge density P is positive for electrons (it is like a number density), accounting for the odd algebraic sign of this equation.

In dealing with the equations of motion in the computer it is convenient to define a velocity variable which is directly commensurate with the electric field. This is done with the machine velocities

$$UY = u_y\ (r_a B/V_o);\ UX = u_x\ (r_a B/V_o) \tag{3.2}$$

Then, using normalized electric fields and cyclotron time, $\theta^o \equiv \omega_c t$ Newton's nonrelativistic equations become

$$\frac{d\ UY}{d\theta^o} = EY + UX$$

$$\frac{d\ UX}{d\theta^o} = EX - UY \tag{3.3}$$

Normalized distance along a trajectory is

$$\underline{s} - \underline{s_i} = \left(\frac{1}{2}\frac{\omega_0}{k_0\omega}\right)^2 \int \underline{U}\ d\theta^o \tag{3.4}$$

and kinetic energy of a charge is, normalized to $Q_o V_o$,

$$K.E. = Q\left(\frac{\omega_0}{2k_0\omega}\right)^2 \{UX^2 + UY^2\}$$

The Kirchoff node equations are quite straight-forwardly scaled in terms of charge, admittance elements, and time, to yield equations of the type

$$I = GV + CV' + \Gamma\int VdT, \tag{3.6}$$

where the prime denotes the derivative with respect to normalized time, $T \equiv \nu_0 t$.

For reference purposes, the Hartee voltage in the normalized system is

$$V_H = k_0\frac{\omega}{\omega_0}(1 - s_0^2) - 1 \tag{3.7}$$

Aside from some assumed law of emission (cathode for Amplitrons; injection for the injected beam device), these three laws are the only ones built into the computer model. The use of the frequency ν_o and the mode number k_o are solely for reference; nothing is assumed as to the frequency or mode of interaction, if indeed there is any.

4. The Computer Program for the Simulation

4.1 Outline

The transient calculation has the following steps:

1. The space-charge force between each electron and all others

is calculated;
2. The induced charge on each electrode is calculated;
3. From the previously known induced charge, the induced currents are calculated. With this information and the network variables and parameters, the new network rf voltages are calculated;
4. From the r-f voltages and the d-c voltages, the circuit field forces on each particle are calculated. This is added to the space-charge force to get the total electric force;
5. From the known electron velocity at the beginning of the time step and the electric force, the trajectory is computed at the end of the next time step;
6. From the known electric field at the cathode the cathode thermionic emission is computed;
7. The emitted particles are merged into the set of all particles, intercepted particles are eliminated, and time is advanced one step;
8. After printout of the intermediate results, the computation returns to step #1.

The above outline governs the Amplitron calculation. For the injected beam, step #6 is replaced by computing new charges not dependent on r-f conditions. Charges are also removed after expiration of their transit (life) through the interaction space. The problem with an injected beam has some three-dimensional aspects. In order to treat it as a two-dimensional one, the axial variation of forces on an electron during its transit through the interaction are neglected. Details of the various steps in the calculation process are given in separate sections below. The program listing is given in Appendix A.

4.2 Details of the Computer Program

4.2.1 Computation of Space-Charge Fields

The choice of the method for calculation of the space-charge fields is a critical one. In most analyses, this is the most time-consuming portion of the program. In crossed-field devices, the role played by space-charge forces is not completely understood, yet is heavily involved in the performance of the device, especially when high power is required.

The method used here is the evaluation and summation of the binary forces between particles. For this determination the anode and sole are considered to be perfectly circular cylinders at zero potential. The binary force is computed by taking the gradient of a Green's space-charge potential function, defined by

$$\nabla^2 G(\underline{r},\underline{r}') = 2\pi\, \delta(\underline{r}-\underline{r}')$$
$$G(\underline{r},\underline{r}') = 0 \text{ on } s=s_o,1 \qquad (4.1)$$

where $\underline{r}$ is the position vector at the point at which the field is to be evaluated, and $\underline{r}'$ is the position vector of the source charge. Hence, the space-charge potential of a charge element is the Green's function

multiplied by the normalized charge, Q, of the source.

The Green's function is one of three variables: the radial coordinates of source and observation points, and the azimuth between them.

The Green's function is needed N^2 times for an ensemble of N charges. It would be completely impractical to compute it directly each time it is needed. The technique used here is to compute and store the function for the mesh points of a three-dimensional grid covering the ranges of the three variables in which the force is appreciable. The gradient components are computed when required by interpolation using the mesh point values of the potential.

This technique has the speed of table look-up and interpolation as developed for computers. The table look-up involves storage address arithmetic; the interpolation, a few floating point operations. These have been optimized for speed by machine-language programming (IBM 7040 MAP and IBM 360 Assembler). The powerful instruction set and register structure of modern computers make this attractive.

The accuracy of this method depends mainly on the accuracy of the Green's function, on the mesh size, and on the interpolation formula used. The first of these three is related to the time spent in "set-up" calculation. The second is limited by machine storage capacity. The last factor--the use of simple or complex interpolation methods-- affects the execution time during the simulation, and is the most critical.

The program for pre-computing the Green's functions is based on an expansion of the source charge (the Dirac delta function in Equation 4.1) in a Fourier series in azimuth. Although the series is infinite, a finite number of terms is adequate in view of the fact that the charge to be represented is not a true line charge, but has finite size. To each Fourier term there is a well-known and easily-computed potential; these are summed to yield the Green's function. The program to do this is listed in Appendix A.3; it is called SPACH.

When two electrons are close to each other the use of the precomputed Green's functions poses difficulties because of its logarithmic singularity. In handling this situation, the existence of the anode and sole electrodes is ignored and the Green's function is taken to be its limiting expression

$$\lim_{\underline{r}\to\underline{r}'} G(\underline{r},\underline{r}') = \ell n|\underline{r}-\underline{r}'| . \qquad (4.2)$$

When two 'electrons' are so close that the diffuse charge groups which they represent actually are enmeshed, the average force between the groups is diminished by comparison with the force between line charges. In the computer the average 'diameter' of an 'electron' is designated PS. This value is used to compute a linear reduction of the interparticle force when the electrons interpenetrate one another.

Another consideration in the calculation of space-charge forces concerns particles just after emission from the cathode, at which time

it behaves more as a curved sheet than a rod (line). The computer then calculates the space-charge field as that between the sheet and its image in the cathode, which is approximated by a plane surface.

The program for evaluating the space-charge forces under the above conditions is a subroutine named COOL. It is written in IBM 360 Assembler language, as shown in Appendix A.6.

4.2.2 Computation of the Circuit Fields and Induced Anode Charge

The circuit components of the electric fields on the particles are also calculated from Green's functions. In this case the Green's function satisfies the equations

$$\nabla^2 G_k(\underline{r}) = 0$$

$$G_k = \begin{cases} 1 \text{ on } S_k \\ 0 \text{ on } S_j,\ j \neq k \end{cases} \tag{4.3}$$

S_k is the surface of the kth electrode; all others, including the sole (cathode) are designated S_j. If, as is assumed here, all electrodes of the anode are identical and equally spaced, the Green's functions are all alike when a suitable multiple of azimuthal sector angle is used for rotation. In any case, the circuit potential at any point, $\underline{r}$, is

$$V_c(\underline{r}) = \sum V(k)\ G_k(\underline{r}) \tag{4.4}$$

where the summation is over all NE electrodes and, if necessary, the cathode (sole) as well.

The anode electrode Green's functions serve another purpose in the computation. Ramo's induced charge theorem is invoked, according to which the induced charge on the kth electrode is given by

$$Q_i(K) = \sum Q_j\ G_k(\underline{r}_j), \tag{4.5}$$

the summation being taken over all charges.

The circuit fields and the induced charges are computed by interpolation from stored mesh point values.

There is a number of methods that can be used for the calculation of the Green's functions. Relaxation is quite generally applicable; it would be used for irregular or irregularly spaced electrodes. In the present case, calculations were made for a simple anode shape: the inner faces of the vanes are assumed to be segments of the anode circle; the side faces are assumed to be purely radial. Also, the potential is assumed to vary linearly with azimuth from vane tip to adjacent vane tip. The Green's function at the anode circle is completely specified. It can easily be resolved into Fourier components in azimuth, each term of which series can be extended inward toward the cathode (sole). Com-

plex variable theory could also have been used. The program for precomputing the electrode Green's function is listed in Appendix A.4.

The program for using the precomputed Green's functions proceeds in three steps: (1) the induced charge is computed; (2) new network potentials are computed from induced and externally applied currents; (3) the circuit fields are computed. These steps are executed in the sub-routine listed as Appendix A.7.

4.2.3 Network Computations

In many numerical analyses it is assumed that the electron stream interacts primarily with the dc fields and the rf field of a synchronously traveling wave. This wave is only one of the several components referred to by the term Hartree harmonic. It is valid where there is essential synchronism over a long period of time, i.e., where traveling-wave interaction occurs and is predominant. This may not be a very good assumption however, even in the traveling-wave tube, for in the high-level regions the non-synchronous components (as part of the total wave) {Dow} are large, and the interaction may be rather diode-like more than of a traveling-wave type. In the emitting-sole crossed-field tube or in the magnetron, rf fields are present at the cathode and influence emission as well as beam-forming. It seems necessary to account for all components of the field, both rf and dc here.

The computer program written with the idea of simulation in mind is pertinent here. No assumption of synchronism or selection of field components more important than others is made. What is assumed is first, that retardation effects are negligible, and second, that a lumped-constant network can be found that reasonably well resembles the actual one. The first assumption is certainly fulfilled when the interaction space dimensions are small in comparison with the free-space wavelength. This is in turn true when the electron velocities are small in comparison with that of light, and this is a characteristic feature of crossed-field tubes. The second assumption is increasingly well satisfied with the networks being used with more recently developed amplifiers.

The network equations are based on the nodal formulation of Kirchoff's equations, i.e., on the continuity of current. For each node of the network, an anode electrode, the equation of continuity may be written

$$I_n = G_{nn}V_n + C_{nn}V'_n + \Gamma_{nn}\int V_n dT + \sum_m (G_{nm}V_m + C_{nm}V'_m + \Gamma_{nm}\int V_m dT) \tag{4.6}$$

where the symbols G, C, and Γ have their usual meanings as normalized conductance, capacitance, and (1/inductance); where the subscript nn denotes the self-parameter, and where the subscript nm denotes a mutual parameter. The term on the left consists of impressed currents entering the node. These consist of externally impressed currents (at the

end nodes) and the electron stream induced currents. The externally applied current is assumed to be sinusoidal, but no assumption is otherwise made as to the time-variation of any network quantity. This allows the calculation of all components of signals that the interaction might generate, including harmonics, subharmonics, and cyclotron frequency phenomena.

An equation of the above type can be written for each node. The set of equations has the matrix form

$$\underline{\underline{I}} = \underline{\underline{G}}\ \underline{V} + \underline{\underline{C}}\ \underline{V}' + \underline{\underline{\Gamma}}\ \underline{\int V dT}, \tag{4.7}$$

where each doubly underscored quantity is a matrix. These equations are regarded as a set from which the time-derivative, V', can be determined from a knowledge of the currents, the present state of the network (V), and the past states (VdT). To do this the equations are rewritten in the form

$$\underline{\underline{C}}\ \underline{V}' = \underline{I} - \underline{\underline{G}}\ \underline{V} - \underline{\underline{\Gamma}}\int V dT \equiv \underline{W}, \tag{4.8}$$

which defines $\underline{W}$. Multiplying this equation by $\underline{\underline{C^{-1}}}$, the inverse of $\underline{\underline{C}}$, yields the derivative

$$\underline{V}' = \underline{\underline{C^{-1}}}\ \underline{W}. \tag{4.9}$$

$\underline{\underline{C}}$ is a large matrix (it is NG square), but it need only be inverted once. This is done at the same time that the Green's functions are computed.

The actual equations to be solved are difference equations rather than differential equations. The quantity V' corresponds to an average derivative over the time step. To improve accuracy, terms such as GV are written

$$G\ V(T) \simeq G\ V(0) + G\ V'(0)\ T \tag{4.10}$$

When this is averaged over the time step, HT, there results a term proportional to V'(0); its coefficient, G HT/2, is added to the corresponding capacitance. Similarly, the inductance element yields a contribution given by $\Gamma(HT^2/6)$; the result is that the capacitance matrix contains elements given by

$$C' = C + G\ HT/2 + \Gamma\ HT^2/6. \tag{4.11}$$

4.2.4 Trajectories

The problem is: given the initial position and velocity of an electron at the start of a short time interval in which the electric field is assumed constant, to determine the particle position and velocity at the end of the interval. It is also necessary to determine if the particle hits the cathode (sole) or any anode electrode and, if it does, to collect bombardment data and to generate secondary particles if they are to occur.

Some improvement became necessary for the trajectory calculation in the course of the development of crossed-field programs. Previously, the trajectories could be computed as segments of cycloidal-trochoidal motion based on constant, uniform fields in the time interval. This is adequate if the time interval is small in terms of cyclotron periods as well as rf periods, and if the field is truly uniform. The last requirement is not met by a dc field if the cathode has much curvature. It has been found that both trajectory and energy balance are lost if the magnetic field is high enough to make the time interval more than 1/4 cyclotron period even though this may be only a much smaller fraction of the rf period. This is particularly true near a small cathode, where the radial field vector rotates along the trajectory in the Cartesian frame fixed relative to the initial point.

As shown in Figure 4.1, a fixed Cartesian coordinate system is set up at the initial point, P, at the beginning of a time step. As the electron moves along its trajectory to some point such as Q, the radial vector, $\hat{r}$, rotates by a small angle, θ'. Assuming that the field EY_o at point P represents a radial field (as in a static device), the Y-component of field at point Q is

$$EY(\theta') = EY_0 \cos\theta' - EX_0 \sin\theta', \tag{4.12}$$

which for small angles is

$$EY(\theta') \simeq EY_0 - EX_0\ \theta' \tag{4.13}$$

Similarly, the X-component of electric field is approximately written

$$EX(\theta') \simeq EX_0\ \theta' \tag{4.14}$$

These approximations were incorporated into the differential equations, Eq. 3.3. To solve them, a power series in θ^o was assumed and the coefficients thereof evaluated. A new algorithm using five terms in the series was thus obtained. This method of trajectory calculation is clearly superior to previously used ones, as can be seen from Figure 4.2. The energy balance is also much improved.

Also, in order to handle trajectories for which the time interval is small in comparison with the signal period but long in terms of cyclotron periods, the above algorithm is applied to submultiple intervals of the full time step.

4.2.5 Cathode Emission

Thermionic cathode emission is not involved in the injected beam device; this section may be skipped by those interested solely in that device. It is presented here for the sake of completeness.

Figure 4.3 shows the relation between the fraction of saturation current escaping the potential minimum in a nonmagnetic diode and the potential gradient at the cathode surface. The relation can be reasonably well approximated by a linear function. It is then considered to

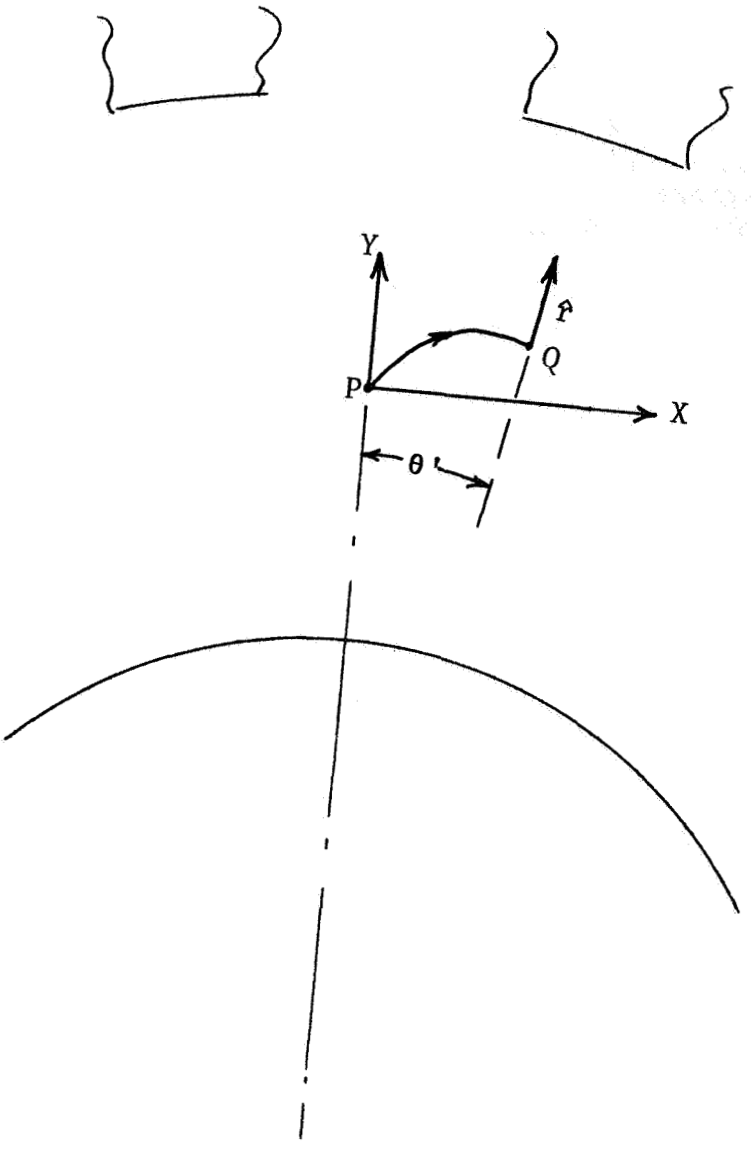

Figure 4.1. Construction for Trajectory Calculation.

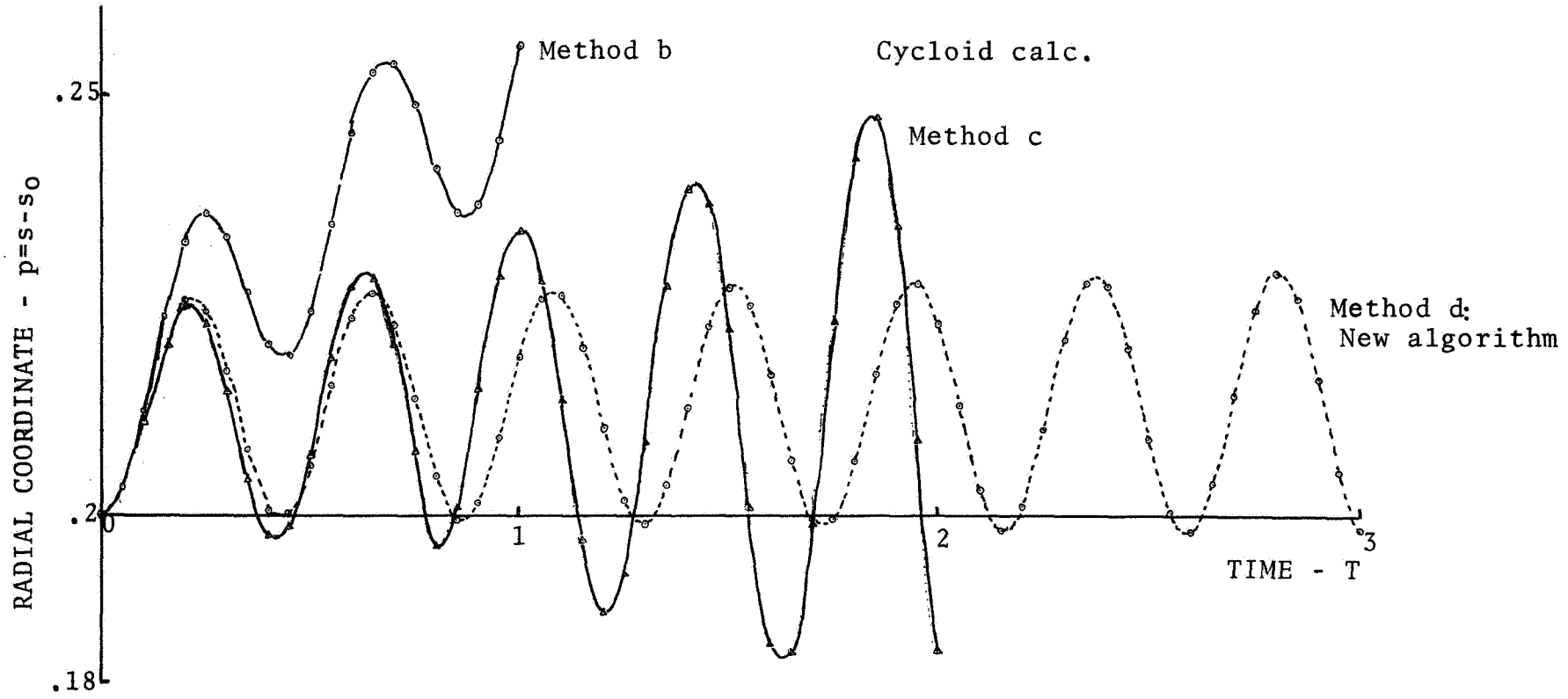

Figure 4.2. Test calculations of electron orbit in static 1/r field.

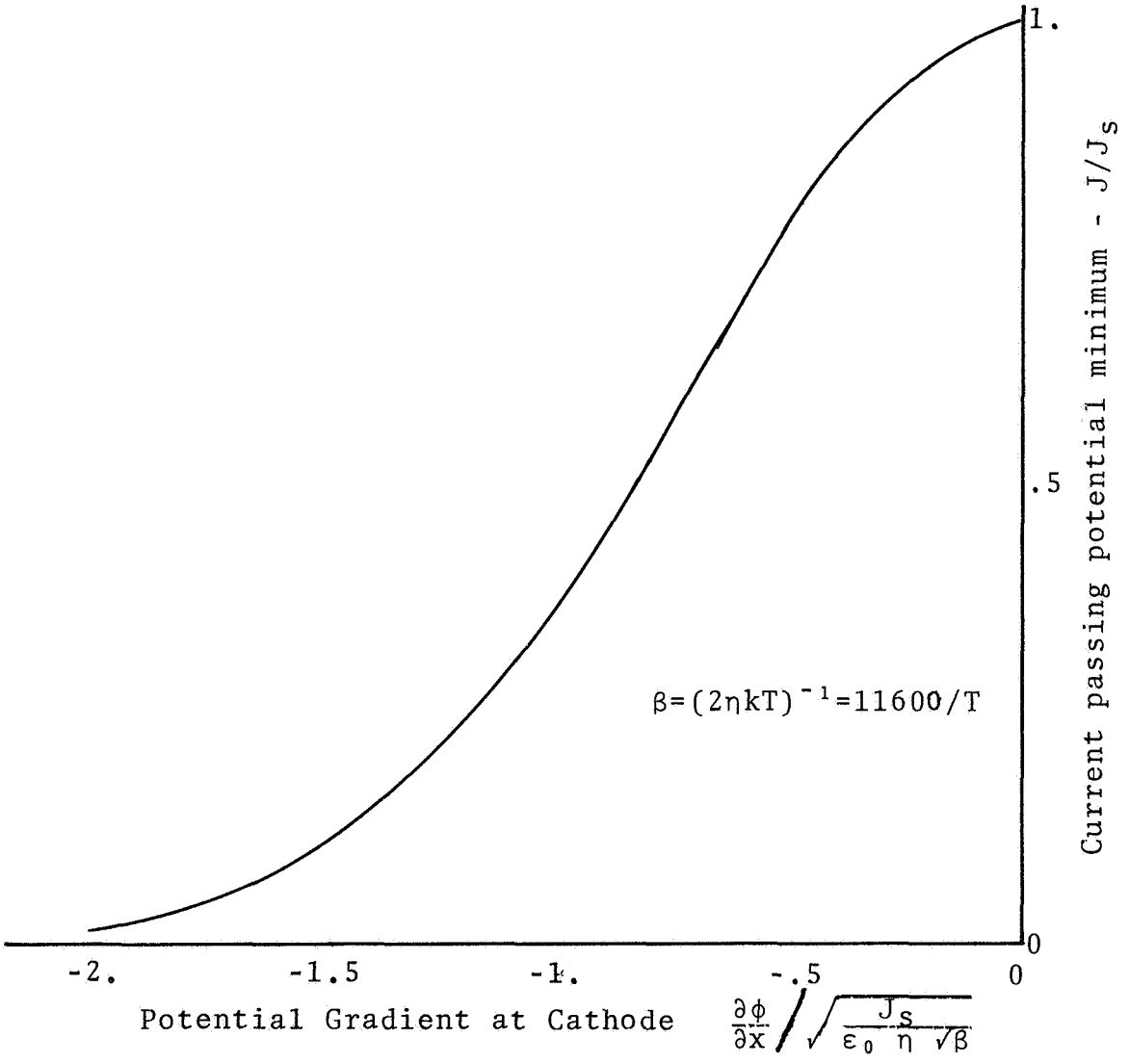

Figure 4.3. Net cathode emission as a function of cathode field.

apply in the present case (since velocities are so small as to result in no appreciable Lorentz force) to determine the net current passing the potential minimum. Actually, since the computer does not simulate the charge between cathode and potential minimum, the cathode gradient is modified by the amount of missing charge.

4.2.6 Beam Injection

The injected beam is represented by a set of NK charge elements--as few as 5, as many as 10 or 20--equally spaced on the same injection circle. They all have the same injection velocity. While the injected stream is thus monoenergetic, the stream resulting from space-charge forces after a few time steps nevertheless has a finite width and energy spread. It would be desirable to inject a stream with velocity spread, but this has not yet been done. This process is done in the subroutine MARGE, listed in Appendix A.9. MARGE also merges the injected or emitted electron into the total charge array, "cleans out" injected particles after their transit through the interaction space, and prints out results of the time step. It then advances time and returns control to the space-charge force evaluation routine.

4.2.7 Waveform Analysis

At intervals in the simulation, a Fourier analysis is performed on all electrode potentials and induced charge waveforms. The results are of interest in themselves and also as an indication of steady state. Dc, fundamental, second and third harmonics are calculated.

The analysis is a rather simple-minded one in which the waveforms are multiplied by trigonometric functions and integrated using Simpson's rule. The integrations are extended over the rf cycle just completed, however, since it would obviously be incorrect to include the transient. The one-cycle integration range also gives a good indication of departure (fluctuation) from steady state.

4.2.8 Graphic Output

Miscellaneous programs are also listed in Appendix A. They serve various housekeeping chores and are of no special interest scientifically; the listing is for the sake of completeness.

The graphic output program deserves special mention, however, because of its value in providing a quick check on the operation of the program and for valuable insight into the interaction itself. A specimen of the display of the Amplitron's electronic ensemble is shown in Figure 4.4; that for the injected beam amplifier, in Figure 4.5. The annular interaction space of the injected beam device is so slender that the polar plot is impractical. The annulus is therefore split into its four quadrants, each of which is plotted in Cartesian r-θ coordinates.

These plots can be of even greater use if viewed sequentially, as in a motion picture.

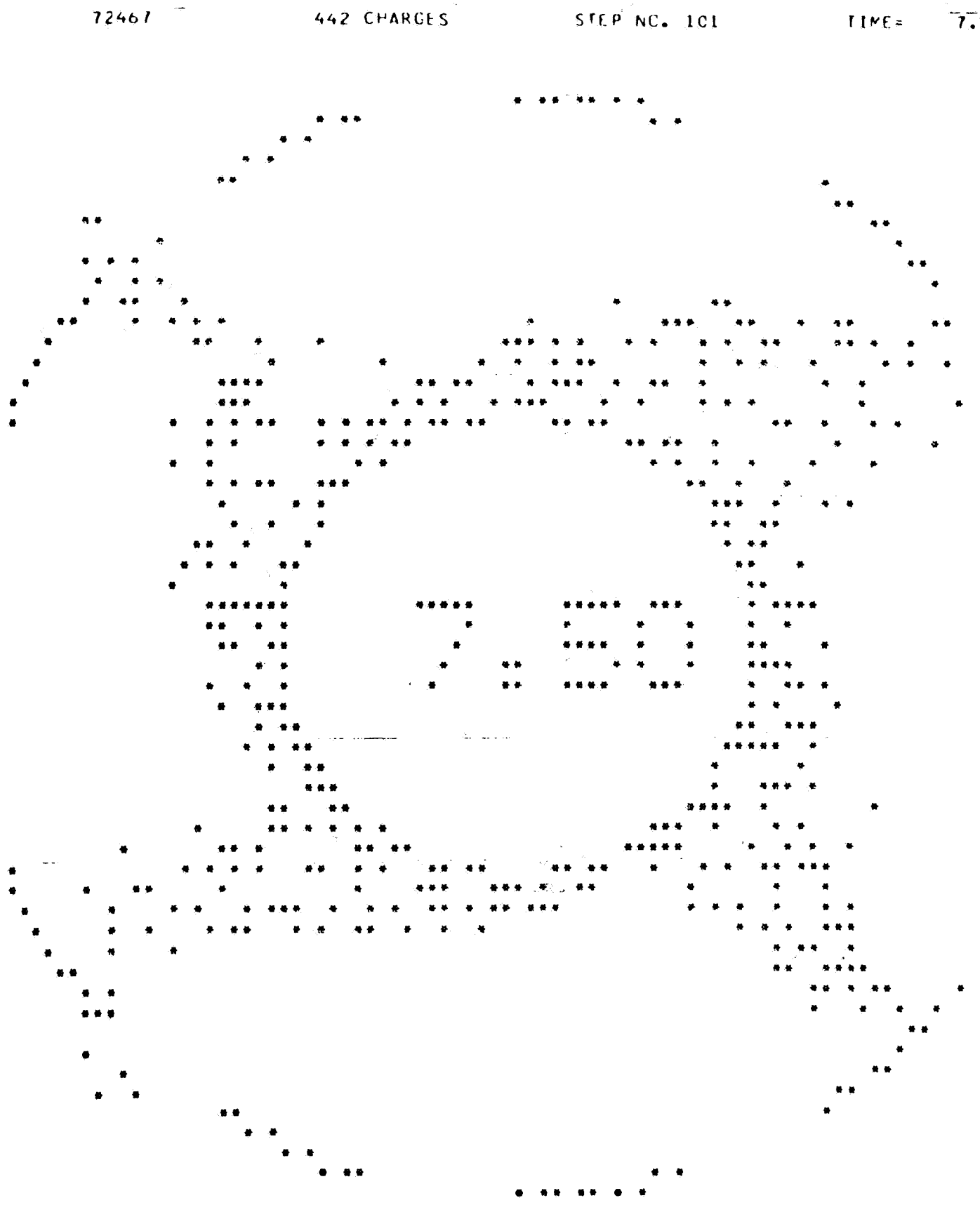

Figure 4.4. Specimen of Graphic Display for Amplitron Calculation.

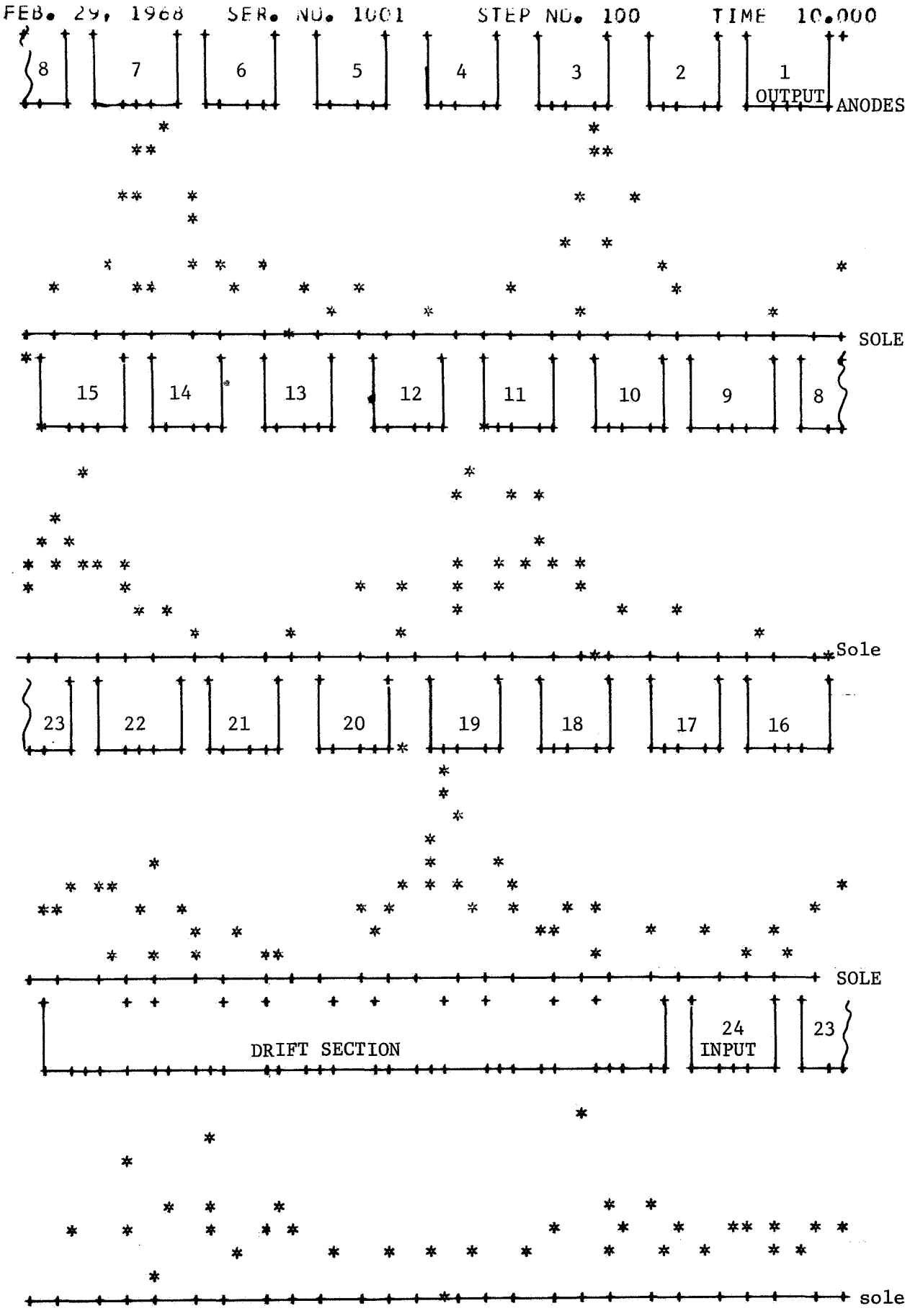

Figure 4.5. Specimen of graphic computer output.

When the Amplitron plots are to be interpreted, it should be noted that the star characters represent varying amounts of charge, depending on cathode emission. In the injected beam amplifier, however, these marks generally represent equal charges. The exception occurs when two charges are too close together to be resolved by the printer.

4.3 The Running of a Computation

4.3.1 Input Data

The principal variables which are entered into the computer are described here.

SZ	s_o, the ratio of anode diameter to sole (cathode) diameter;
THM	Azimuth beyond which the space-charge force between two electrons is negligibly small;
GAP	Fraction of anode pitch taken by intervane gap;
THMP	Azimuth (degrees) beyond which electron is not affected by an electrode's field;
NE	Number of anode sectors;
HT	Time step, fraction of period at reference frequency, HT = $\nu_o h_t$;
G	$.5(\omega_c k_o/\omega)$;
GG	$\omega_c/2\nu_o$; Magnetic field parameter;
PS	Particle average diameter, normalized to anode radius;
TMAX	Ending time for the calculations;
VDC	Dc anode voltage, normalized to V_o;
NG	Number of active anode segments;
VDD	Dc voltage(s) on drift anode segment(s)
CNST	Charge (normalized) emitted at each cathode site;
NK	Number of cathode sites. Normalized emission current = CNST*NK/HT;
PIN	Location, relative to sole (cathode) {Normalized};
PDIN	Radial
THDIN	Azimuthal } velocity of injection;
TLIFE	Transit time through interaction, rf cycles;
CA,CB,CC	A: Self parameter,
GA,GB,GC	Network elements {Normalized} B: Mutual to adjacent node,
ΓA,ΓB,ΓC	C: Mutual to alternate node;
CIN1,COUT1, CIN2,COUT2	Current sources feeding lines 1 or 2 at input or output ends;
G1,C1,GL1	G, C, of load (including matching elements) on line 1;
G2,C2,GL2	Ditto, for line 2;
FREQ	Frequency {Normalized}.

4.3.2 Computer Output

4.3.2.1 Graphic Display

The computer prints out a graphic representation of the anodes, the sole, (as + characters), and the electrons (rod charges) as * characters. There is a problem of resolution here, and one star (*) may

represent more than one electron. In the Amplitron calculations, not all stars represent the same amount of charge; in the injected beam device, they generally do. The graphic display comes at controllable intervals, but comes once each step within the last 2 cycles of the end.

4.3.2.2 Anode Electrode Data

Each time step the computer prints out the following data for each anode electrode:

Number; RF Inst. potential; induced charge; induced current (the difference from the previous induced charge); amount of charge collected; energy of bombardment. The total induced charge, total anode collection current and total anode bombardment energy are printed on another line. Similarly, the potential, collection charge and bombardment energy for the sole are printed. The injection charge and current are also printed.

If particles are removed from the interaction on account of having passed through it axially, the collector statistics are printed: amount of each charge element, its radial location, velocity components and kinetic energy. Within the last cycle of a computer run, these data are also punched for use in possible further computations.

The computer also prints out the value of the autocorrelation function

$$ACF = \sum_{t_j} Q(t)\ Q(t-\tau)$$

computed for the previous rf cycle, where Q is the induced charge at the electrode #1. This quantity is unity for a steady-state, and is used to determine whether that condition has arrived.

4.3.2.3 Further Manipulation and Interpretation of the Computer Output

It is first of all a good idea to plot the variation with time of some such key quantity as the Fourier amplitude of the output voltage. This generally shows slow variation for the first few rf cycles after a parameter is changed. It then begins to vary rapidly and over the space of a few cycles exhibits a wild oscillatory transient oscillation. After a total of about $2k_o$ cycles the oscillatory transient begins to disappear, and the Fourier amplitude approaches some steady state. There is usually some fluctuation about this level, however, and it may be so severe as to obscure the steady level or render it impossible to determine accurately.

In those cases where steady state failed to appear with reasonable certainty, considerable study was made to determine the cause. In some cases the root was not found, but a detailed Fourier analysis covering many cycles disclosed a reasonably precise value for the spectral component at the signal frequency. This is but one of many possible statistical approaches to the use of the computer output. Another is

simply to take the average value of the Fourier fundamental amplitude as determined by examining the plot. The use of such averaging methods is to be avoided, however.

Further analysis of the computer output consists in summing the collection of charge and bombardment energies for the various electrodes over the space of one cycle after steady state is attained. These figures yield the convection currents and bombardment powers associated with the several anodes, the anode as a whole, the sole and the collector. In the case of the collector, it is assumed that electrons are intercepted at the radial locations at which they emerge from the interaction region, without further acceleration or deceleration. This might be accomplished, for example, by use of a collector having infinitely many segments, each at the dc potential corresponding to its radius.

The dc input power to the device is thus given by the sums of the anode dc input power, $V_b I_b$, and the collector dc input power, in $V_c Q_c$ or $\langle V_c \rangle I_c$. The usefully generated rf power is the difference between the output power, $V_1^2 G_1/2$, and the input power, $C_{out1}{}^2/2G_1$. These are fundamental frequency values. The efficiency is calculated as the ratio of this usefully generated power to the dc input power. For the purposes of establishing an energy balance, account must also be made of harmonic power (negligible here) and the fundamental power transmitted to the input source by virtue of the so-called "hot mismatch." The latter is also negligible in these devices.

5. Amplitron Calculations

5.1 Parameters

The first Amplitron calculations were intended to simulate the type QKS-1300 medium power Amplitron, a tube developed by Raytheon Company. The interaction space parameters, as furnished by the manufacturer, are listed in Table 5.1.

Table 5.1 QKS-1300 Amplitron Parameters

Anode diameter	d_a	.184	inch
Cathode diameter	d_c	.078	inch
Axial length	h	.210	inch
No. of anodes	NE	11	
Anode vane width	w	.032	inch
Operation:			
Frequency	ν_0	2282.5	GHz
Magnetic field	B	2100	gauss
Anode voltage	V_b	1800	volts
Anode current	I_b	18	ma.
Mode number	k_0	4	

The network is as shown in Figure 3.2(a). Its characteristic impedance is approximately 120 ohms; the interaction (coupling) impedance is not known.

Preliminary calculations were made with computer network parameters from previous Amplitron research which provide the proper phase constant, viz. 49.0909...degrees per cell. The characteristic impedance of this network, however, was high (1480 ohms), and the rf input power level was also high (3.17 P_o). These exaggerations provide for strong rf fields with which to start the computations quickly; they can be relaxed once a large-signal configuration is obtained.

5.2 Results

The calculations were run initially with a time step of .1 cycle. After reaching steady state the time interval was reduced to .05 cycle and further calculations were made for refinement. The space-charge configuration is shown in Figure 4.4. The computed output voltage waveforms were used to compute total rf output power from the simple average of $V^2(T)G$. The results are shown in Table 5.2.

Table 5.2 Results of Amplitron Calculations Nos. 7/19/67 & 7/24/67

Time interval	.1	.05	
Anode current, I_b	210	337	ma.
Dc input power	310	500	watts
Rf output power	291	450	watts
Gain	8.3	10.2	db
Efficiency	86.	83.	percent.

The dc anode currents are greater than in the actual Amplitron by an order of magnitude; the rf output powers are correspondingly high. This is the result of computation with high impedance and high rf input power. This magnitude of impedance probably cannot be realized in a real tube, nor could the cathode emission be obtained.

It was noted that the energy balance in this calculation was poor; the total dc and rf input power does not account quantitatively for the total rf output power and the anode bombardment rate. This is at least in part caused by errors in the trajectory calculations, which are aggravated by the smallness of the cathode and by the relatively high cyclotron frequency.

5.3 Termination of Amplitron Computations

Shortly after the preliminary calculations reported above, notice was received that the Amplitron was no longer of interest for the particular application requiring its numerical analysis. The Amplitron computations were therefore terminated and alaysis of the injected beam forward-wave amplifier commenced.

6. Injected Beam Forward-Wave Amplifier Calculations

The calculations made for the injected beam forward wave amplifier had the immediate objective of providing information relative to a

proposed design (subsequently revised) for tube development on the one hand, and the more remote objective of exploring the device operation and optimizing the configuration.

6.1 Parameters

The two designs mentioned above were similar in many respects; calculations were made with many parameters unchanged as, for example, the sole-to-anode diameter ratio and the network constants. The parameters used in the calculations are listed in the table below. In the table, single values denote unchanged parameters. Multiple values denote that a range was covered. Values corresponding to the first design are underlined once; those for the second design are double underlined.

Table 6.1 Injected Beam Forward-Wave Parameters

Anode/sole diameter ratio		1.22
Interaction height	h	1.
Vane gap-to-pitch ratio	GAP	.328
Total number of anodes	NE	28, <u>30</u>, <u><u>64</u></u>
Number of active anodes	NG	<u>24</u>, 27, 30, <u><u>52</u></u>
Phase constant at ν_0	θ_{c_0}	90 ^{o}/cell
Network attenuation		0, <u>.17</u>, 1.35, 2.7 db
Coupling impedance at ν_0	K_0	80, 160, <u>200</u> ohms

Table 6.2 Operating Parameters

Magnetic Field:	
Relative cyclotron frequency	5.5
Dc anode voltage, V_o	<u>12.5-27.8</u>
Injected beam current, I_k	.8-5.
Axial transit time, cycles	2-7.5
Rf input power, P_{in}	.2-5.
Frequency	.9-1.0

These parameters are normalized. For reference, the two amplifier designs have the following scaling parameters:

Table 6.3 Scaling of Proposed Designs

		First	Second	
ν_0	Frequency	800	800	MHz
k_0	Mode number	7.5	16	
V_0	Voltage	625	945	volts
I_0	Current	.695	1.05	amperes
P_0	Power	434	1000	watts
R_0	Impedance	900	900	ohms
B_0	Magnetic field	233	109	gauss

The value of anode-sole diameter ratio renders the interaction space essentially linear. Accordingly, the graphic display was revised to

provide better resolution; typical output is shown in Figure 4.5.

This magnetic field is high for the frequency involved, i.e., the cyclotron frequency is high relative to the signal frequency. Fortunately, the trajectory computation difficulty it poses had been solved as described in Section 4.2.4.

The number of anode segments and wavelengths is much larger for this amplifier than for the Amplitron calculations for which the program was originally developed. Computer storage requirements are increased because of the greater number of electrodes and also because the simulation requires a niminum number of electrons per wavelength, and there are more of these. Fortunately, the new computer has adequate capacity. The execution time is also affected, however, and this is more serious than storage problems. The time required for each time interval increases as the square of the mode number, k_o, because more electrons are involved. In addition, more rf time is required for the entire calculation; this is proportional to the mode number. The execution time thus is roughly proportional to the cube of the mode number. Again, it is fortunate that the new computer (IBM 360/65) is much faster than the older one (IBM 7040) and has a more powerful central processor which affords a further increase in speed.

6.2 Results

6.2.1 Preliminary Calculations

Because it can accommodate no more than 20 electrodes, the original program written for the Amplitron was used for preliminary calculations with a network which simulated the actual one rather imperfectly. It contained 15 active cells, rather than the required 24, each of which had phase shift of $3\pi/4$, rather than $\pi/2$. This network model thus had the same total electric length (all at reference frequency) as in the design.

Steady state failed to appear in these calculations. A sizeable variation of the output amplitude occurred at a slow rate, ás shown in Figure 6.1. This appears to be an amplitude modulation of the carrier input signal. The frequency of the upper side band indicated that this was in fact a band-edge phenomenon--an oscillation or sustained transient. It is attributed to the placement of the input signal frequency high in the pass band of the network in order to obtain the desired phase rate, as reference to Figure 3.3(b) will show. The band edge is actually only 8.3 percent higher than the signal frequency. Subsequent use of network models having lower phase rates, especially those containing dissipative elements, were free from such large oscillatory transients.

Tests were made to determine the effects of such computational parameters as time interval and number of emission sites. It is well to maintain a balanced relation between these two: the time interval governs the number of electrons emitted per cycle from one site; the number of cathode sites governs the number of particles emitted per wave-

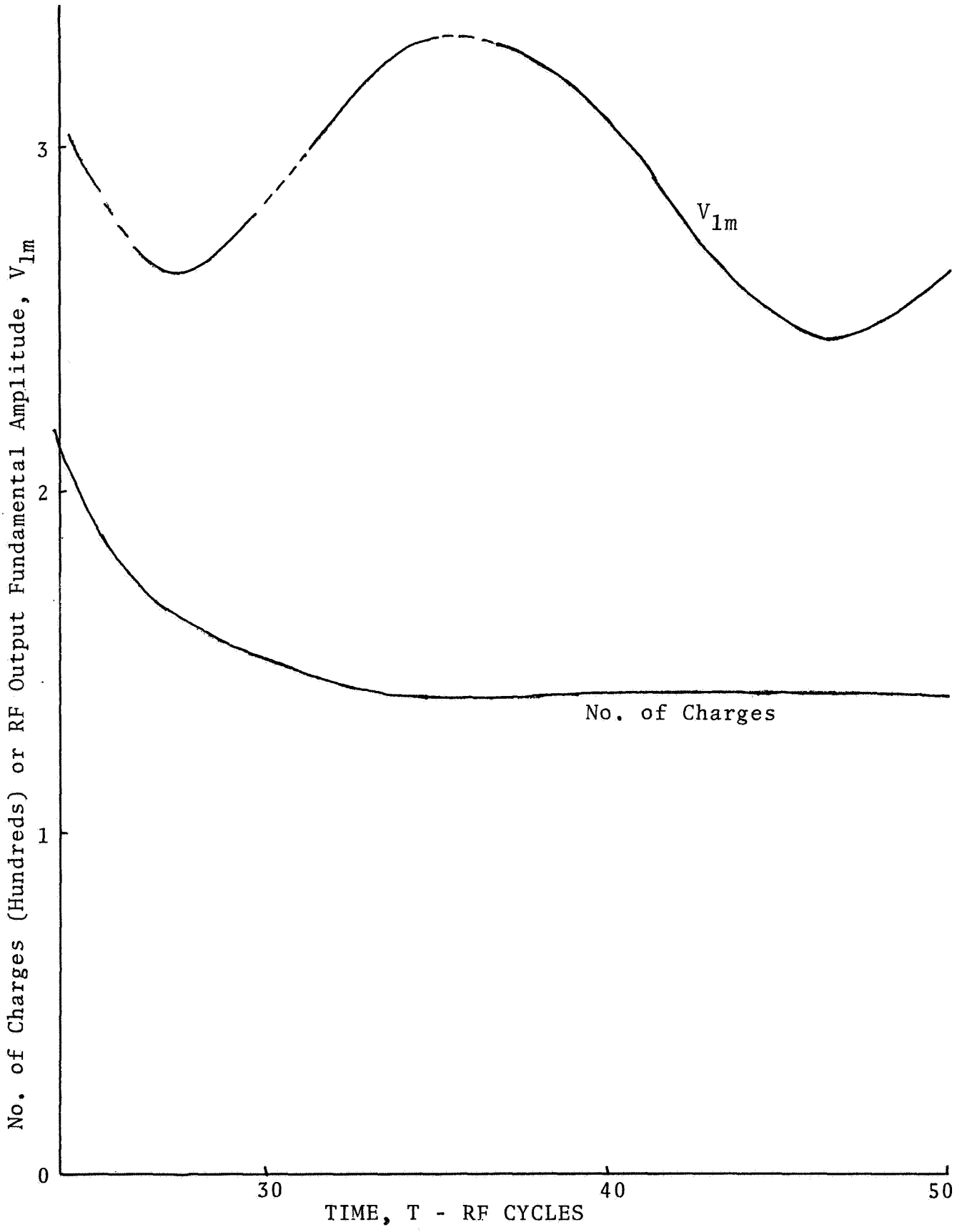

Figure 6.1. Extension of CFA calculation #010268:
Failure to Reach Steady State

length at each time. Together, they control the total number of electrons. It was generally found that a time interval of .1 cycle and one emission site per wavelength describe the stream fairly well. Better precision would on occasion be needed; it would be more expensive.

6.2.2 Demodulation & Feedback Through the Stream

It became apparent in the preliminary stage that considerable rf current was being induced in the anode segments of the drift region. When this stream reaches the input region of the rf delay line, there is a strong signal fed back into the electron stream-network system, affecting the performance of the amplifier.

Information relative to the actual device was lacking at the time, hence preliminary computer experiments were made with schemes for artificially removing the stream modulation in the stream as it passes through the drift region. This consists in replacing reentering electrons with newly-injected ones in the drift region. Although artificial in the sense that the energy balance is destroyed for those electrons, computations were made which showed that the rf stream feedback was indeed reduced. It was not eliminated completely, however, because although the velocity modulation and the radial displacement modulation were eliminated, the azimuthal modulation was not. This is inevitably tied in with the fact that an electron is present at some azimuthal position and the computer has no information as to where it would have been had there been no rf signal. Even if it did, and the electron were moved to such a location, the fact that some electrons reentered and some did not (because of their rf interaction in "favorable phase") would furnish a density modulation of the reentering stream.

Details of the actual device demodulation system were finally obtained. This consists of a variation with azimuth of the dc electric field in the drift region. It is simulated in the computer rather readily by assignment of different dc voltages to the several segments of the drift portion of the anode. Computations made with this computer model, which represents a physically realizable scheme, have a validity concerning energy balance and efficiency that the others do not. The collector statistics, i.e., the information as to where electrons are to be collected and at what bombardment energied, are no longer subject to the errors of the artificial scheme. The results still showed, however, that the rf stream current persists, although it is reduced to about the same degree as observed in the artificial scheme, viz., a reduction of about 15 db in current-squared.

6.2.3 Instabilities at High Gain

The previous, preliminary calculations had been made with relatively high rf input power and therefore resulted in low gain (c. 6-10 db). The course of the calculation program was thus to reduce the input power to attain the gain level of approximately 20 db reported for experimental tubes. As this was being done, further failure of the calculations to reach steady state were noted. Figure 6.2 shows such behavior. Considerable effort was made to determine its cause and to eliminate it; this

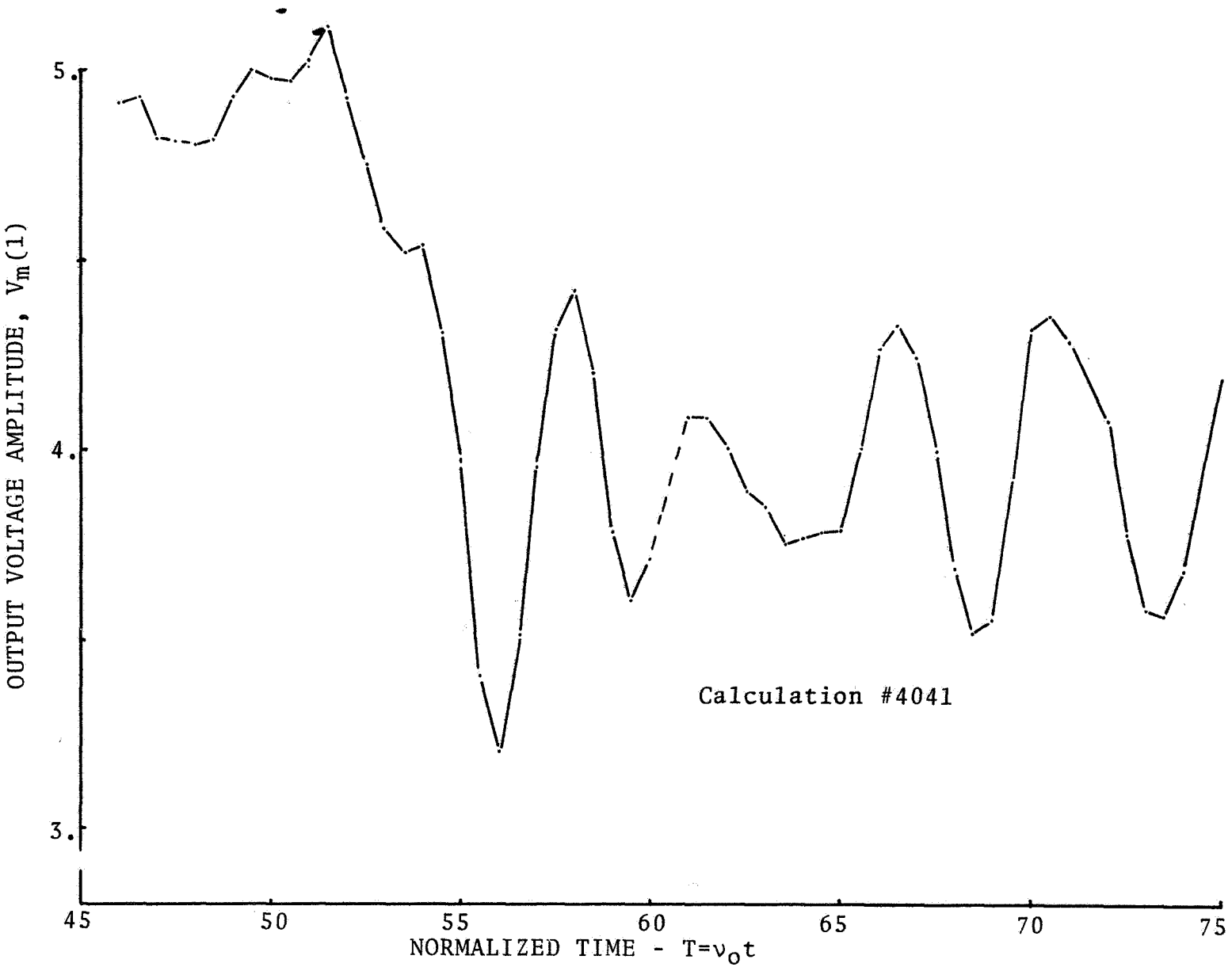

Figure 6.2 Example of Instability.

has not been completely successful.

The apparent a-m of the output signal does not appear in this case to be related to the band-edge.

It was thought at first that a computational instability might be involved. The time interval, HT, and the number of emission points, NK, were varied. Halving HT or doubling NK results in doubling the number of electrons in the problem. This increase in precision had no noticeable effect on the instability. Indeed, the variations in output were remarkably alike, indic ating that the stream was well represented to begin with. Moreover, halving the time step has the additional effect of improving the accuracy of the trajectory calculations and also of the network calculations. It was concluded that the computer program was not seriously involved.

On the possibility that the apparent instability might be a manifestation of some kind of plasma or cyclotron wave instability, calculations were made without computing space-charge forces. This showed the same degree of fluctuation as those with space-charge taken into account. Neglect of space-charge forces, incidentally, appears as a distortion of the spoke configuration, as shown in Figure 6.3.

The calculations were also run with increased dc anode voltage. Such a parameter change would alter the degree of traveling-wave interaction and hence change the nature of any instability related to the principal mode of interaction. In this computer experiment, no appreciable change was seen with a 5% increase in dc anode voltage as compared with the original dc anode voltage, which was the Hartree voltage.

The oscillations were observed both with and without the dc voltage taper in the drift section.

The network was in one computer experiment deliberately mismatched with a resistive load having a reflection coefficient of 1/3. at both ends. As seen in Figure 6.4, a standing-wave pattern appears internally at the wavelength dictated by the network characteristic, and the input signal level is greatly increased by the presence of internal network feedback, while the output level remains much the same. It is concluded that network mismatch is not related to the instability of concern here.

Calculations were in one case run for a much longer period than previously, with the result shown in Figure 6.5. The variation suggests presence of a signal at about 30% higher and lower frequencies relative to the signal. Fourier analysis of the waveform obtained from the computer resulted in the spectrum shown in Figure 6.6. This indeed verifies the existence of a component at 1.3 ν_o, which is of the same order of magnitude as the second harmonic. There is no particular significance, however, to this frequency in terms of network properties. (The band edge is at $\sqrt{2}\ \nu_o$.)

From all the above evidence, it began to appear that the long period (c. 16 cycles) of the rapid oscillations was related to the signal transit

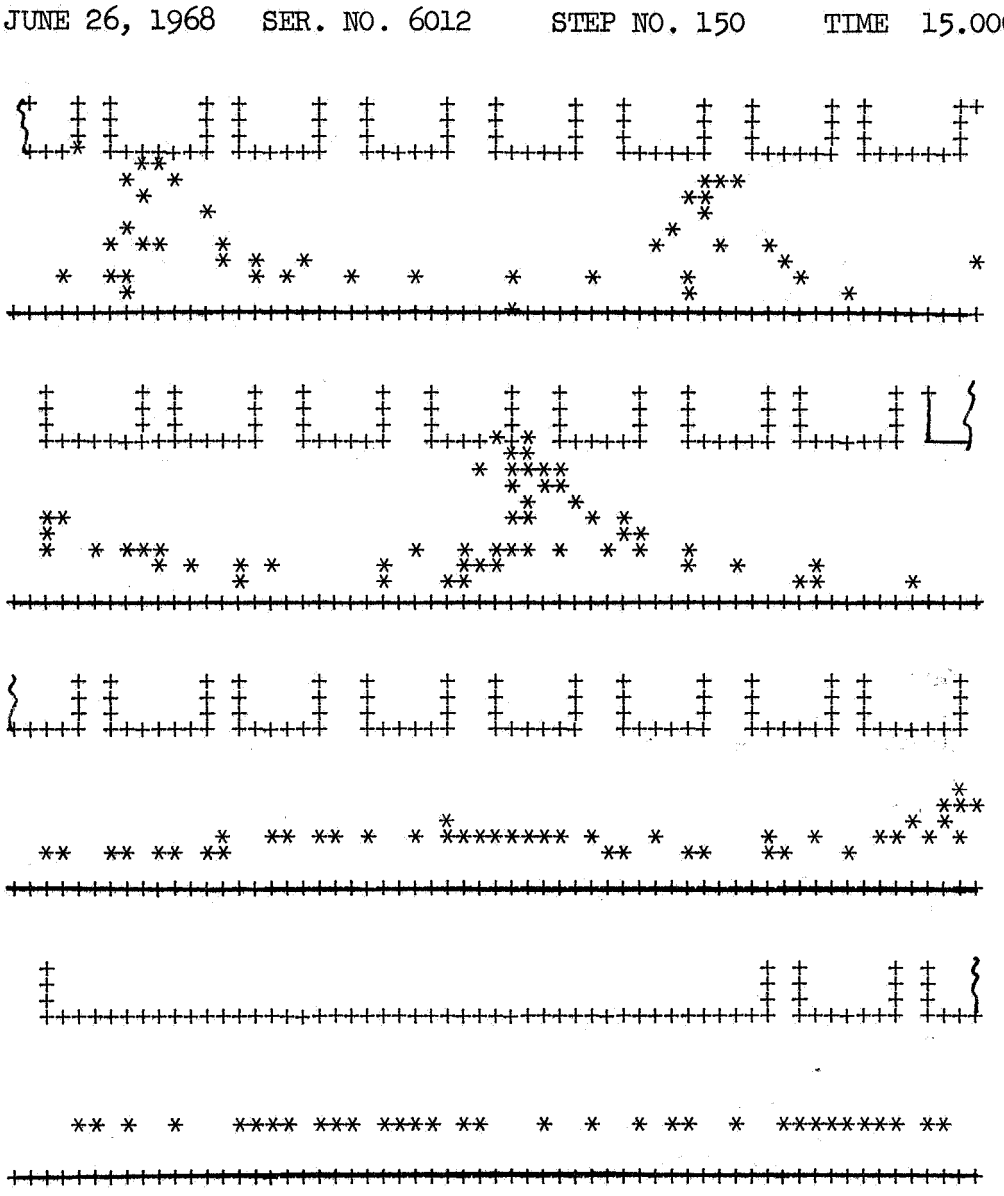

Figure 6.3 Calculation 6.12; Space-charge forces omitted; Artificial stream demodulation.

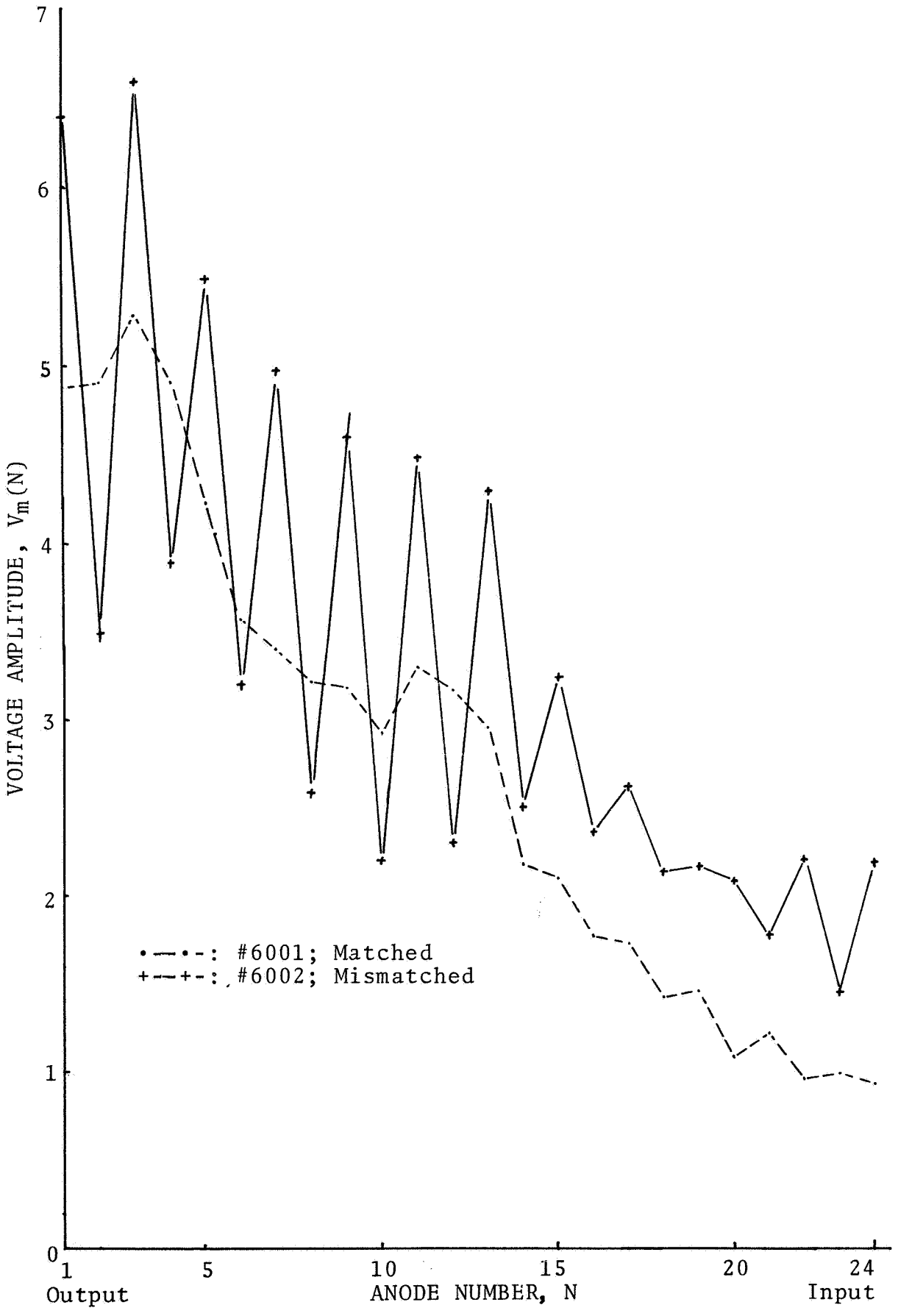

Figure 6.4 Standing-wave resulting from mismatch of Amplifier Reflection Coefficient: 1/3 at each end.

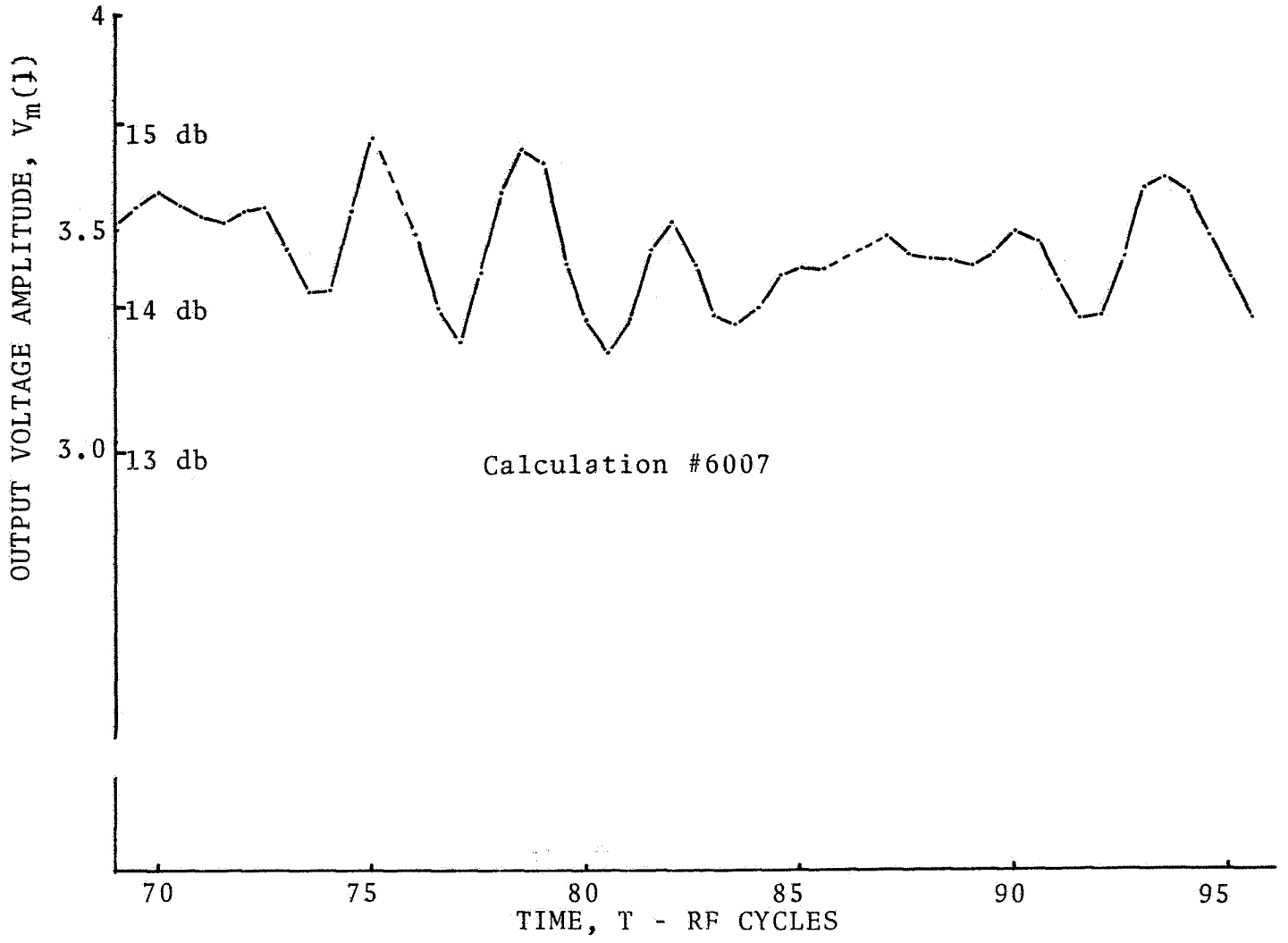

Figure 6.5 Calculation carried for an extended period.

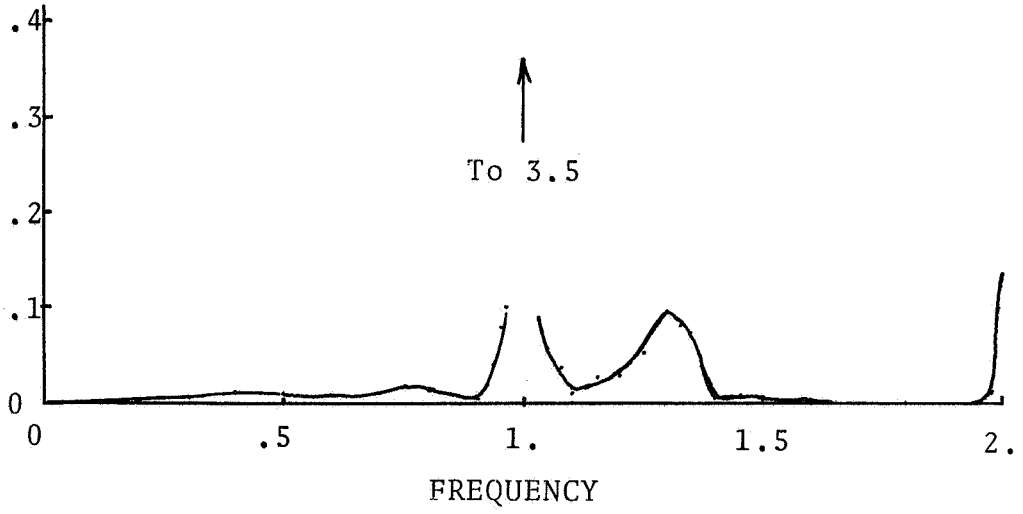

Figure 6.6 Spectrum analysis of output voltage waveform of run #6007, T=68 to T=93

time through the network (6 cycles) or to the total time required for synchronous electrons to circumnavigate the cathode (7.5 cycles when no drift section dc voltage taper is involved, approximately 8 cycles when the voltage variation was used). The long period thus appears to be about twice one of these transit times. What appears to be happening is that stream feedback allows a fluctuation in the output level to pass through to the input and excite a network transient; this consists of a ringing oscillation at band edge. The stream current that causes it propagates along with the stream, taking 6 cycles to pass through the network and somewhat longer to pass through the drift section (attenuated) where it then can re-excite a transient. The fact that the ringing has a period of about two transits around the loop is perhaps related to the phase of the feedback stream current.

Figure 6.7 shows the transition from a calculation without a drift voltage taper to one in which the dc voltage abruptly drops to 1/2 the Hartree level as the electron enters the drift region, and then linearly rises to full anode voltage. For the first 6 to 8 cycles the original output condition persists, as the changed feedback conditions (mostly phase) cause a new signal to be propagated from the input toward the output. Much the same situation would appear if the input signal had been changed rather than the drift parameters. After the new feedback signal arrives at the output, there is a rapid and large swing to a lower level and, with rapid ringing, a slow, saw-tooth-like transient to a new steady state. The period of this saw-tooth is 15 cycles, indicative of the feedback path involved in electron reentrance. It appears, however, that it takes much longer for the steady state (or semblance thereof) to arrive than had previously been realized.

As attention was focused on stream feedback as the root of the instability, computer experiments were run to study the role of the drift region and the phasing and attenuation in it. This has the further objective of studying the effects of length of network and drift spaces on the amplifier performance. More will be said on this subject in Section 6.3, but the effect on the appearance of transient oscillations will be discussed here. The length of the active section (NG) was first varied in steps at the expense of the length of drift space; the results are shown in Figure 6.8. The level at the start is that for the designed case (NG=24, NE=30). After some rather violent transients, the Fourier amplitude is seen to settle down rather well. This is attributed to the difference produced by changing the feedback properties of the drift region relative to the entire signal path. It is somewhat difficult to specify the feedback more precisely because the phase shift depends on electron stream parameters, including the rf level.

Additional evidence of the role of feedback is presented in Figure 6.9, which pertains to a reduction in the electrical length of the circumference from 7.5 wavelengths to 7.0. This allows comparison in relative terms primarily. It shows that the 7.0 wavelength system has higher gain--probably because of the different feedback phase, but is also less stable.

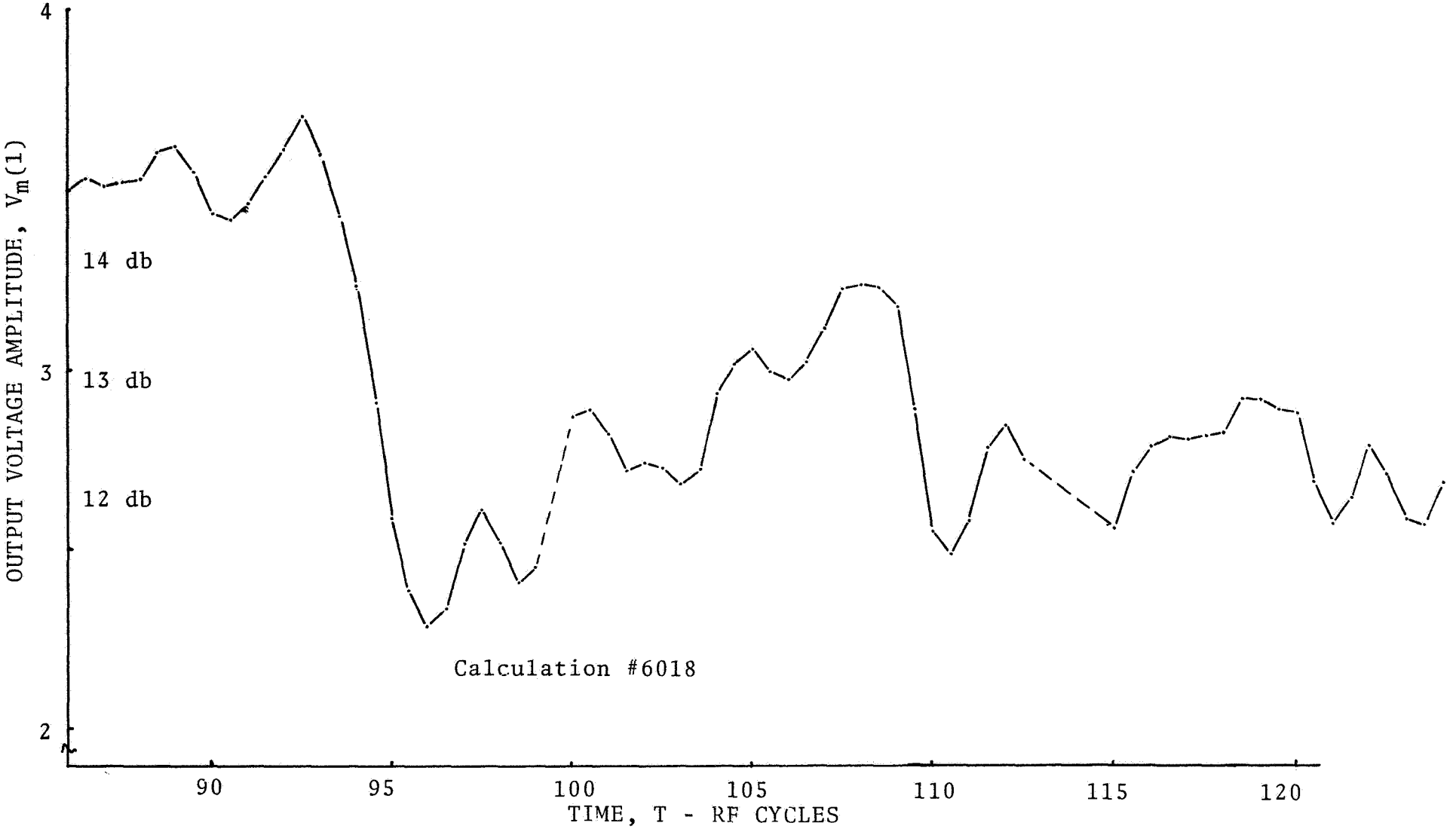

Figure 6.7 Transition from Uniform DC Drift Potential to Tapered Drift Potential

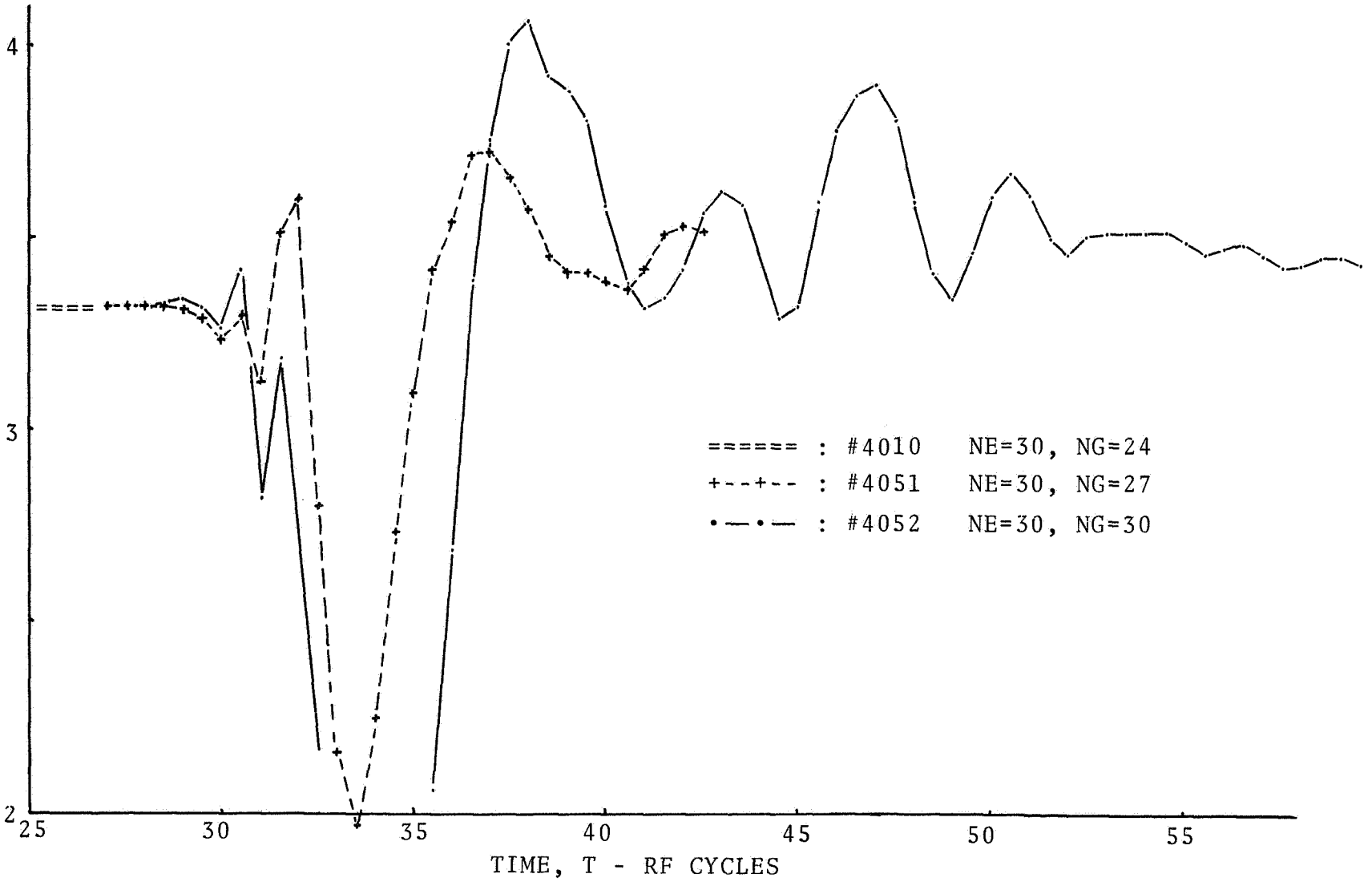

Figure 6.8 Variation of Length of Drift and Active Sections.

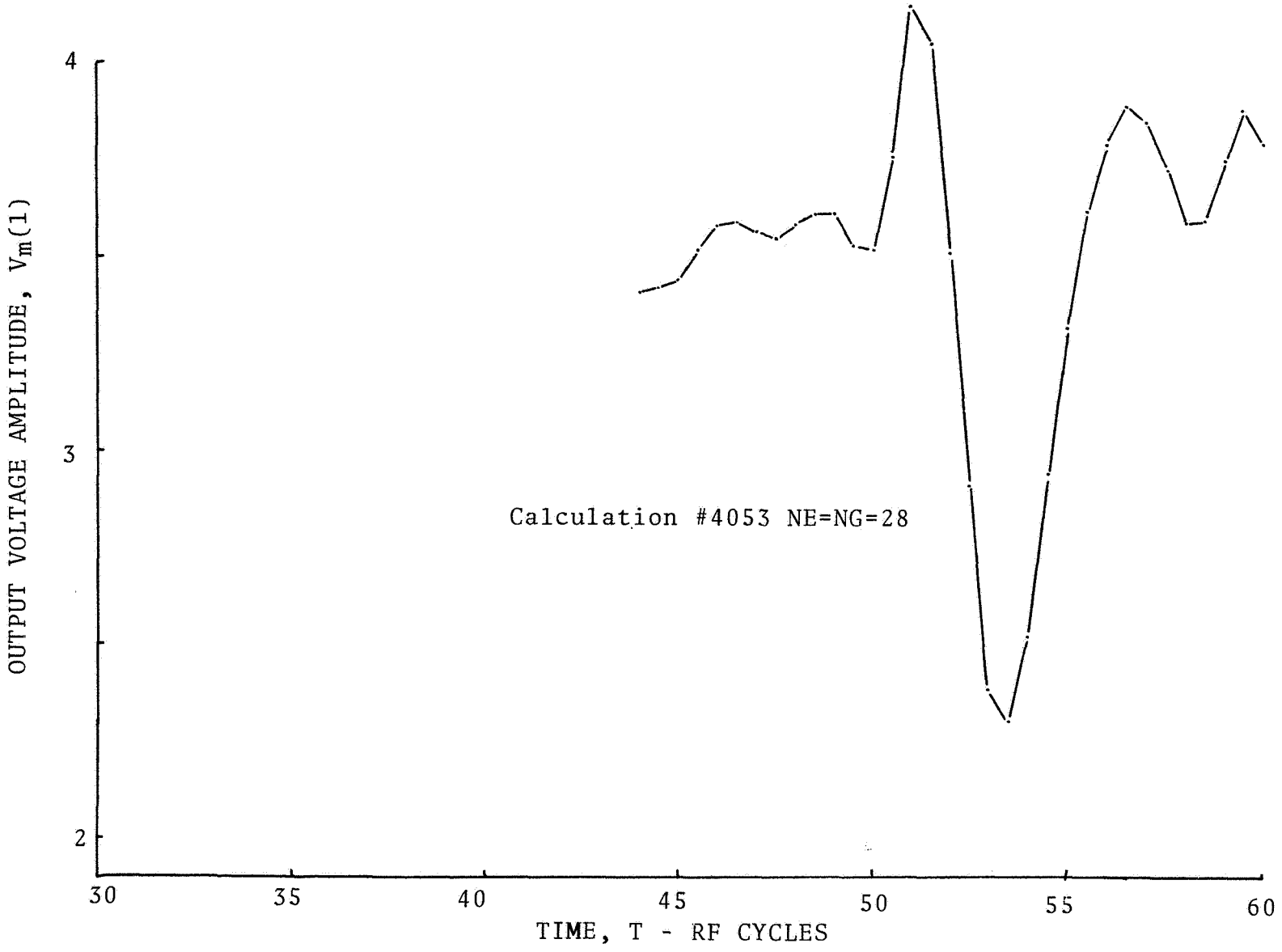

Figure 6.9 Drift section removed (NG=NE). Total circumference reduced to 7 wavelengths. Compare with #4052 in Figure 6.

Finally, Figure 6.10 shows two calculations which differ in that by accident a potential barrier was placed in the drift space practically eliminating the reentrance of the stream. This appears to eliminate the large oscillations that appear in the usual reentrant stream case.

The feedback is also related to the particle lifetime: if the electrons make very rapid transits through the interaction space, relative to the time required for them to pass through the drift region, then the stream feedback will disappear. Some computer experimentation was done with reduction of the electron lifetime parameter, but the results are inconclusive because of the simultaneous reduction in gain that occurs.

The overall assessment of this series of calculations is that a combination of transients occurs, involving the ringing imposed by the network itself, and also feedback through the stream. It is generally necessary to protract the calculation through about $2k_o$ cycles before steady state can be reached or perceived. Random fluctuations in the steady state may still occur, and in some cases the transient may be so violent that steady state may never be seen.

6.3 Amplifier Performance at Moderate Gain

Because considerable effort was devoted to study of the instability (Section 6.2.3) and also because of the changing type and design of amplifier to be studied, complete data on any one design were not obtained. The study had to be limited in scope to obtaining a better understanding of the operation of the injected beam amplifier rather than optimizing it in all respects.

It was finally possible to obtain a reasonably certain steady state at high gain in some instances. One of these is described here; it had the parameters listed in Table 6.4. The reentering stream is artificially demodulated.

Table 6.4 Calculation #6007: Parameters & Results

Anode voltage	12.5 (Hartree)
Injected current	1.67
Axial transit time	7.5 cycles
Number of anodes (tot.)	30
Number of active anodes	24
Frequency ν/ν_o	1.
Coupling impedance	160 ohms
Network loss	0
Rf input power	.5
Rf output power	13.4
Gain	14.3 db

Figures 6.11, 6.12, and 6.13 show the space-charge configurations at successive times. Anode collection takes place only on the 13 highest level electrodes. Substantial penetration of the intervane gaps occurs only for the half-dozen highest level gaps.

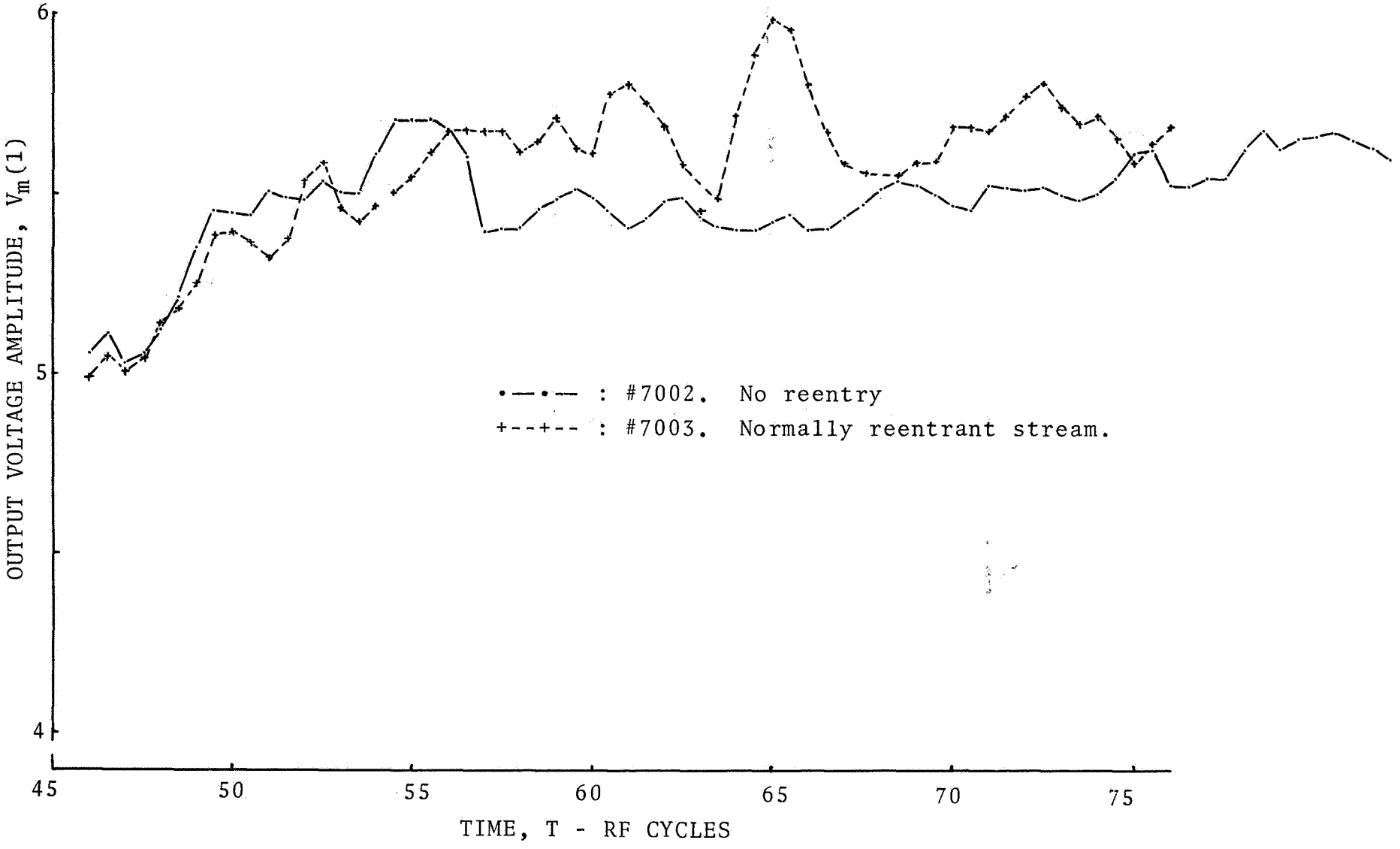

Figure 6.10 Comparison of calculations made with and without stream reentrance.

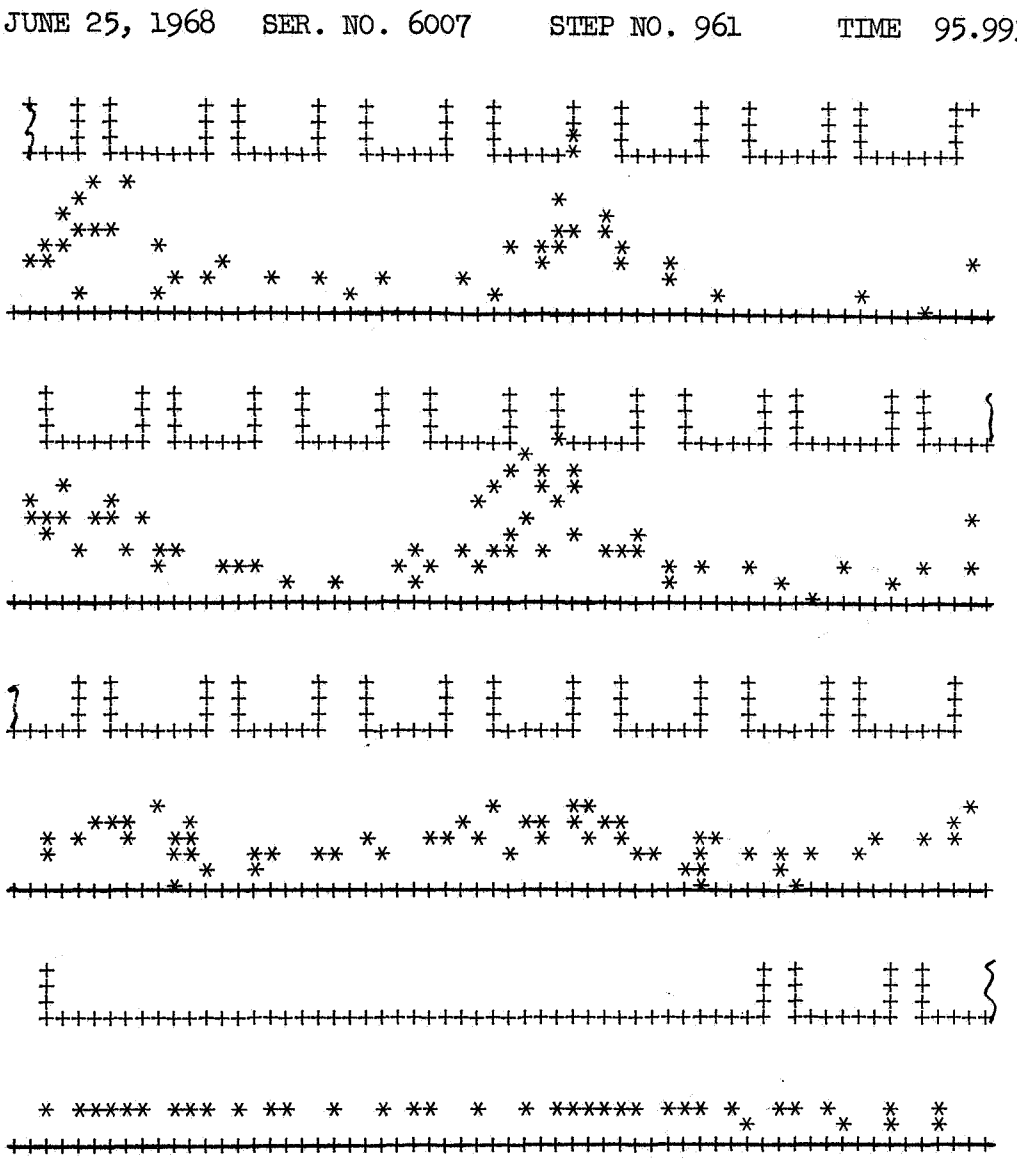

Figure 6.11 Calculation #6007: Configuration at T = 96.0

JUNE 25, 1968 SER. NO. 6007 STEP NO. 966 TIME 96.493

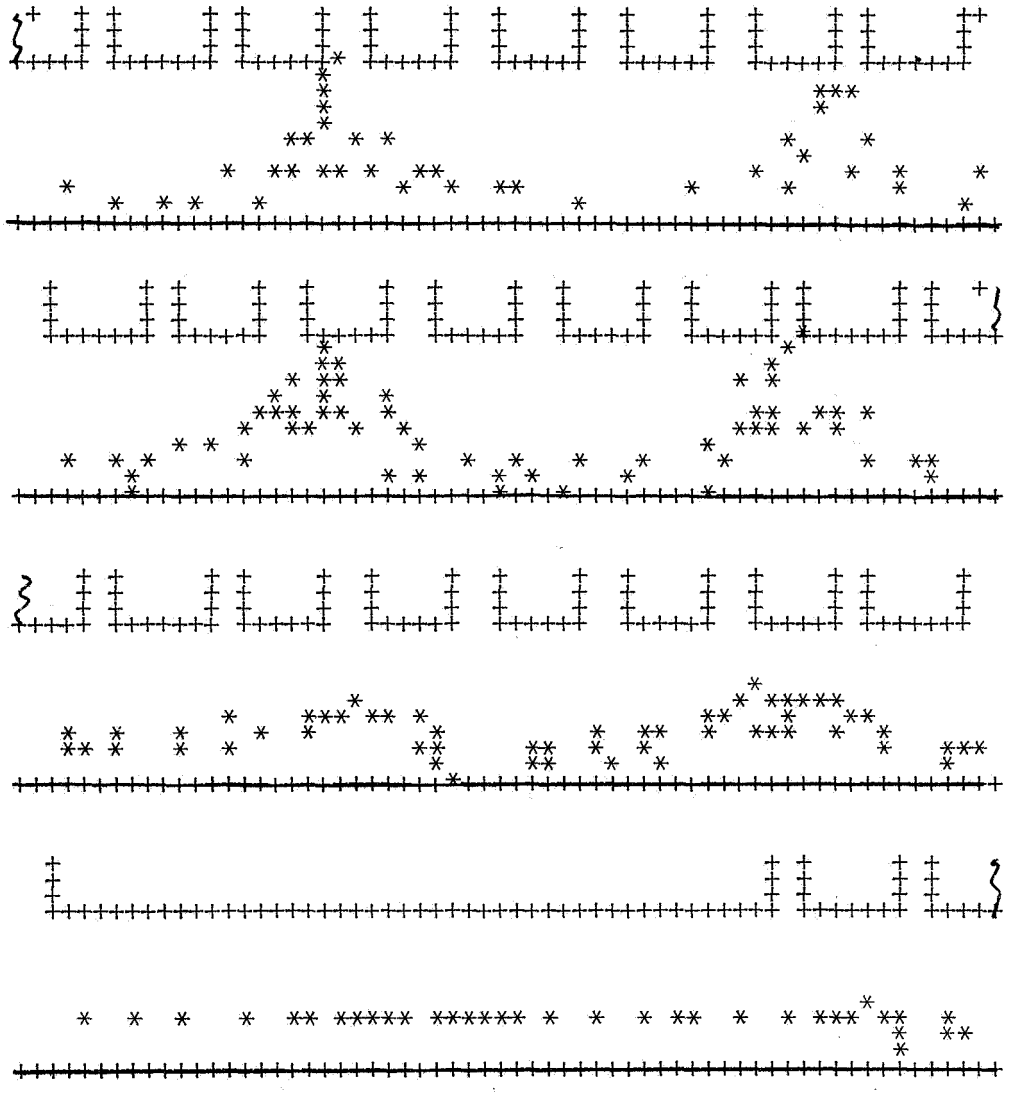

Figure 6.12 Calculation #6007: Configuration at T = 96.5

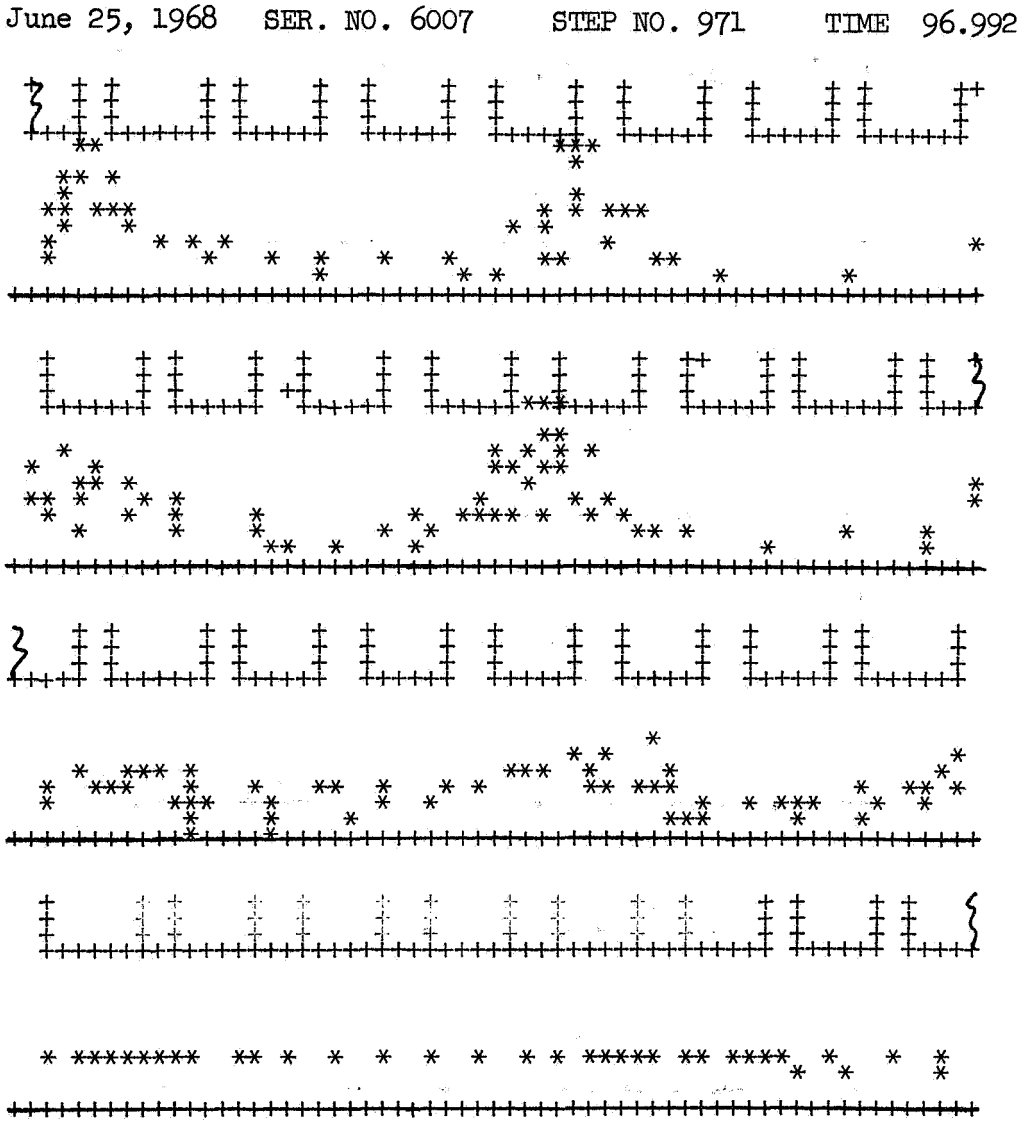

Figure 6.13 Calculation #6007: Configuration at T = 97.0

Figure 6.14 shows the internal rf voltage and rf induced current distribution on the network. Severe standing waves as shown in Figure 6.4 are absent here, indicating absence of appreciable mismatch. Further evidence of this is the fact that the input electrode, #24, is close to that of the incident signal. There does, however, appear some voltage disturbance having a slow space-variation. This is a symptom of the instability discussed in Section 6.2.3; the disturbance propagates and appears as an oscillation of the output signal amplitude.

Figure 6.15 is an histogram of the collector data. These are sketchy; averaging over several cycles would improve them. There appears to be a grouping of collected particles at low potentials. This must be viewed with caution, however, as it is probably exaggerated by the artificial demodulation process.

6.4 Effect of Parameters on Operation

It has not been possible to cover the entire range of parameters thoroughly. The discussion below is necessarily incomplete, particularly with respect to high gain conditions.

6.4.1 Dc Anode Voltage

Operation as a function of dc anode voltage is of interest because of the effect of electron stream velocity--and hence on the traveling-wave interaction--and also because of effects on emission from cathodes (magnetron & Amplitron).

The dc anode voltage was increased from the Hartree level to 10% above it at an early stage in the calculations. There was practically no effect on gain or power output at the 6 db gain level obtained at the time. The amplifier was close to saturation, and small-signal gain conditions were absent. The increase in dc anode voltage, 1.25 V_o, was in this case somewhat less than the peak input voltage, which was 1.78 V_o. It is possible that variations of the dc anode voltage have more effect at lower power levels.

The principal changes noted with the increase in anode voltage were reduction in efficiency (because the dc input power increased without increase in rf output) and a small change in output phase. This phase-pushing due to dc anode voltage was approximately -1.3^o per 1% increase in the anode voltage.

6.4.2 Dc Injected Current

Increasing the injected current provides greater stream current, other factors remaining constant. This increases the gain and correspondingly shortens the small-signal region, lengthening the saturated region (or causing one to appear if at the verge of saturation). Figure 6.16 shows this.

The stronger rf fields shorten the transit time to the anode for favorably interacting electrons, however, tending to provide an offsetting

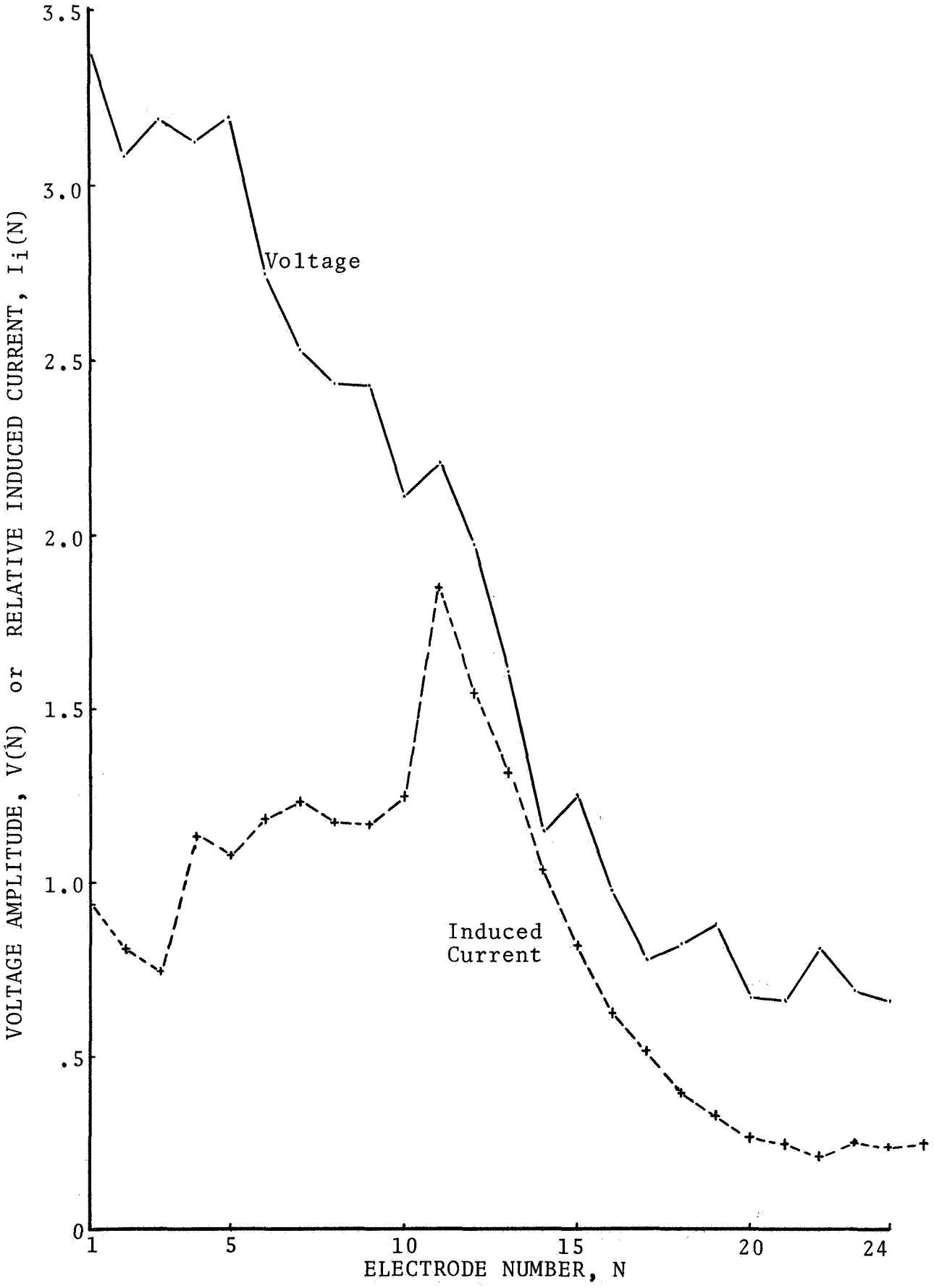

Figure 6.14 Distribution of Current and Voltage on Network Calculation #6007, T = 97.0

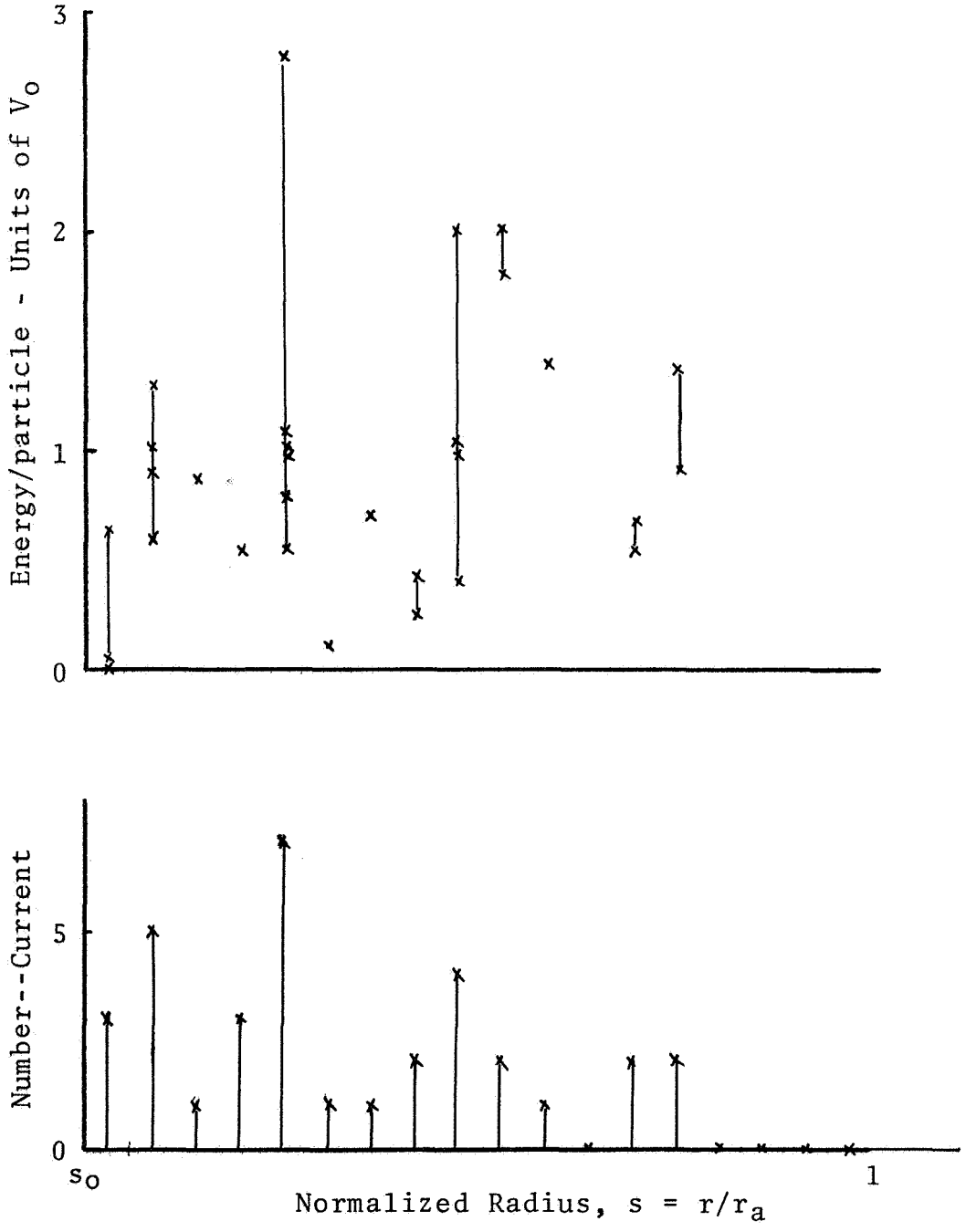

Figure 6.15 Calculation #6007: Collector Histogram

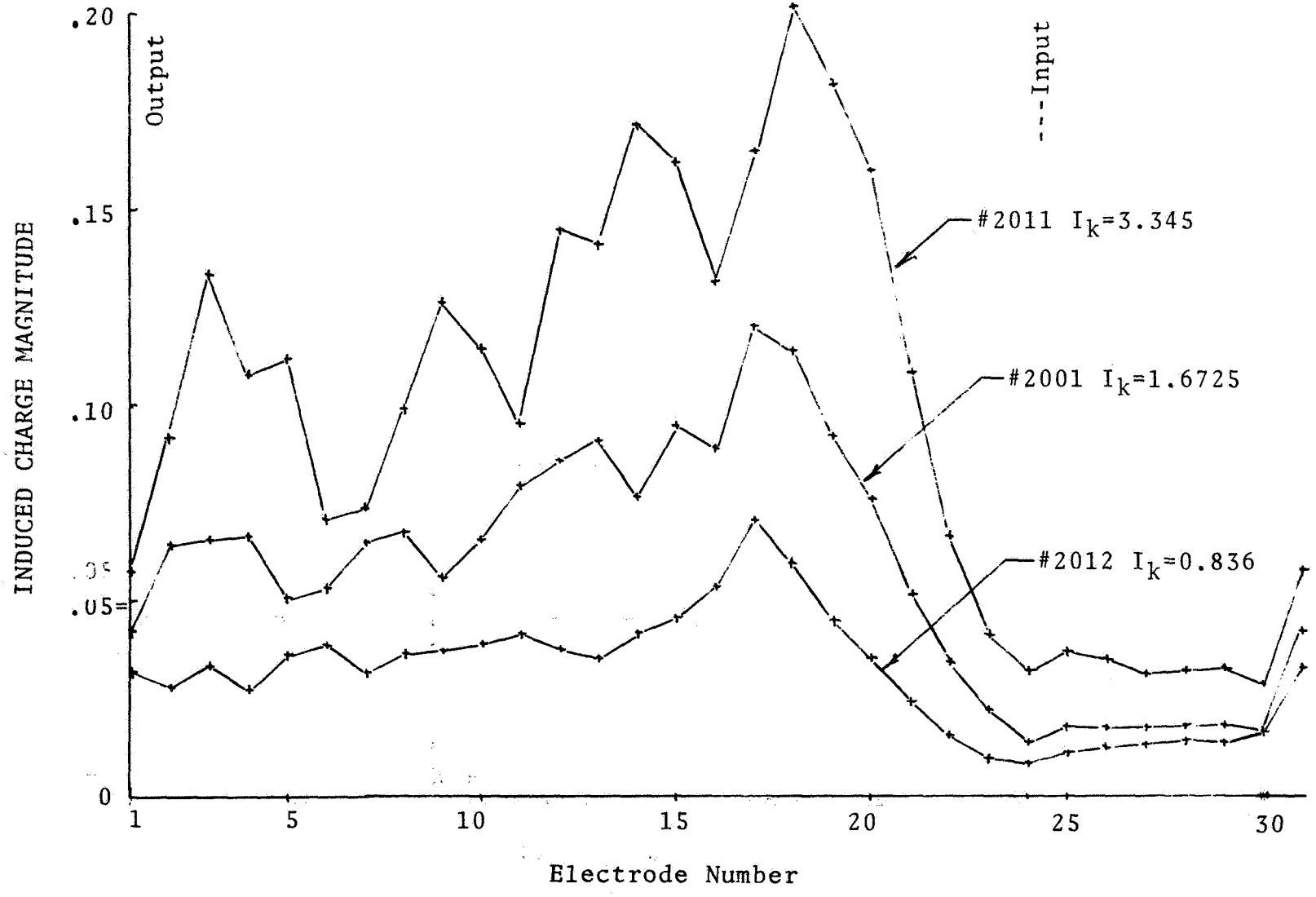

Figure 6.16 RF current distribution as function of Injected Current

reduction in the total stream current. Furthermore, the unfavorably focused electrons gain more energy from the stronger rf fields, and sole current is larger. Another factor complicating the efficiency picture is the fact that because the large-signal region is longer, the efficiency is higher. The plot of computed efficiency is shown in Figure 6.17. This plot, even more importantly, shows that the output signal is linearly related to the injected current.

Use can be made of the relation shown between rf output and injected current by using in conjunction with it the relation between the rf level and the injection current, as reported experimentally. This information is not known here. The actual injected current, to the extent that it is controlled by the rf fields extending from the network toward the cathode, is probably sorted by the process. It thus would appear to be similar to provision of a prebunched beam in a traveling-wave device. There are many unknown factors involved, some of them raising questions as to the adequacy of the two-dimensional model used here.

The computations showed a phase-pushing due to injected current variation of $+0.3^{o}/I_{o}$.

6.4.3 Rf Input Power Level

The rf power input was reduced to take the amplifier from the saturation region of its operation toward the linear region. Figure 6.18 shows the network rf current distribution as the power level was reduced from 3.5 to .2. The disappearance of the saturated region within the interaction is clear. The input-output relation for the amplifier is shown in Figure 6.19. In these calculations progressive instability was encountered as the input power level was reduced. This is probably because of the feedback problem noted in Section 6.2.3.

In one trial calculation the rf level was reduced to about 20 db below the output levels heretofore observed. This level is about the level of voltage induced by the reentering rf stream current. The calculation was started from empty interaction space, with the result shown in Figure 6.20. Large-signal conditions appear rather quickly in spite of the small input signal and the amplifier--probably because of stream feedback--behaves as an injection-controlled (locked) oscillator.

6.4.4 Rf Impedance Level

Most of the injected beam forward-wave amplifier calculations were made for a characteristic impedance at reference frequency equal to 400 ohms; this corresponds to an interaction (coupling) impedance, $EE^{*}/2\beta^{2}P$, of 160 ohms at the anode surface. A few calculations were made for the higher design value of 200 ohms. The results are compared in Table 6.5.

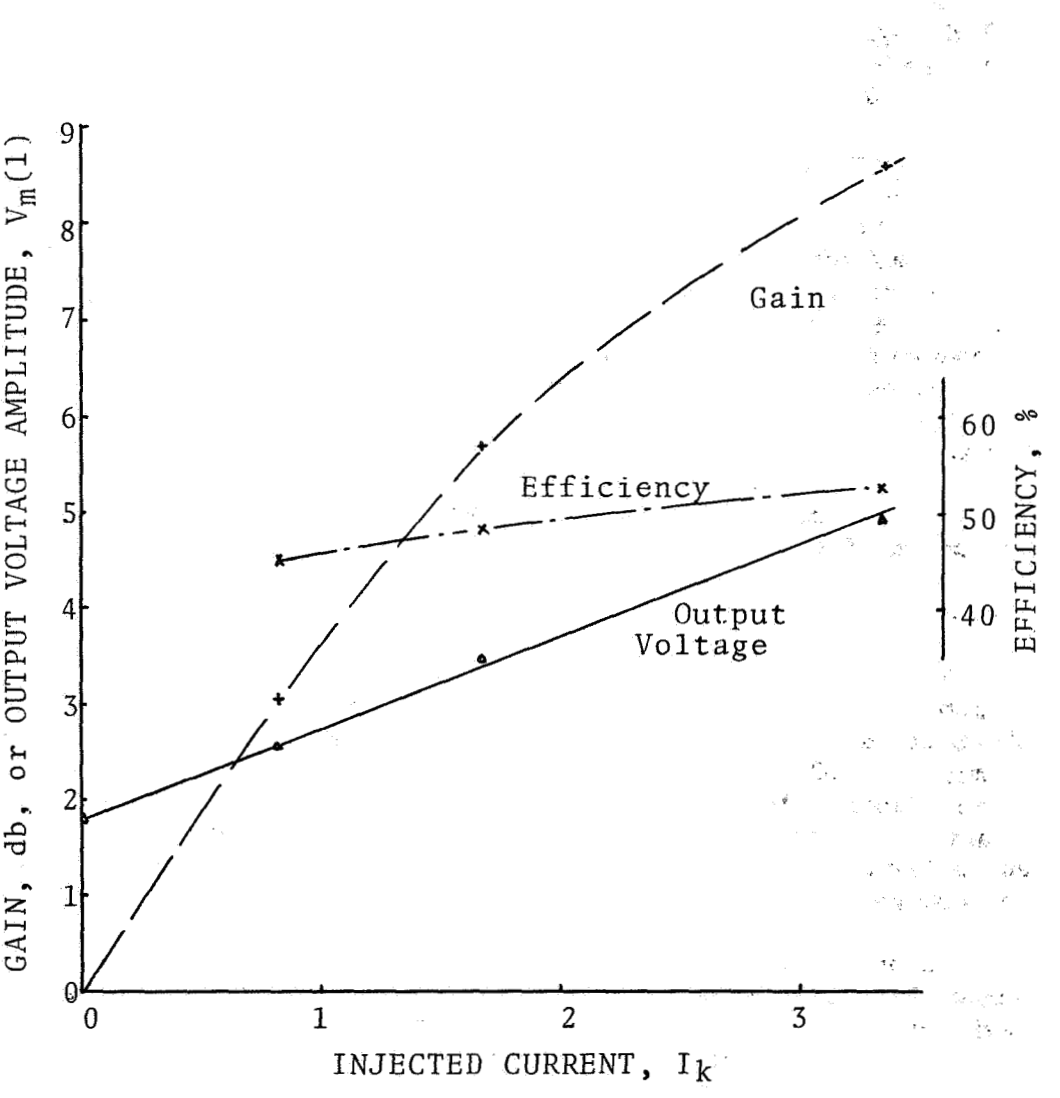

Figure 6.17 Effect of Injected Current.

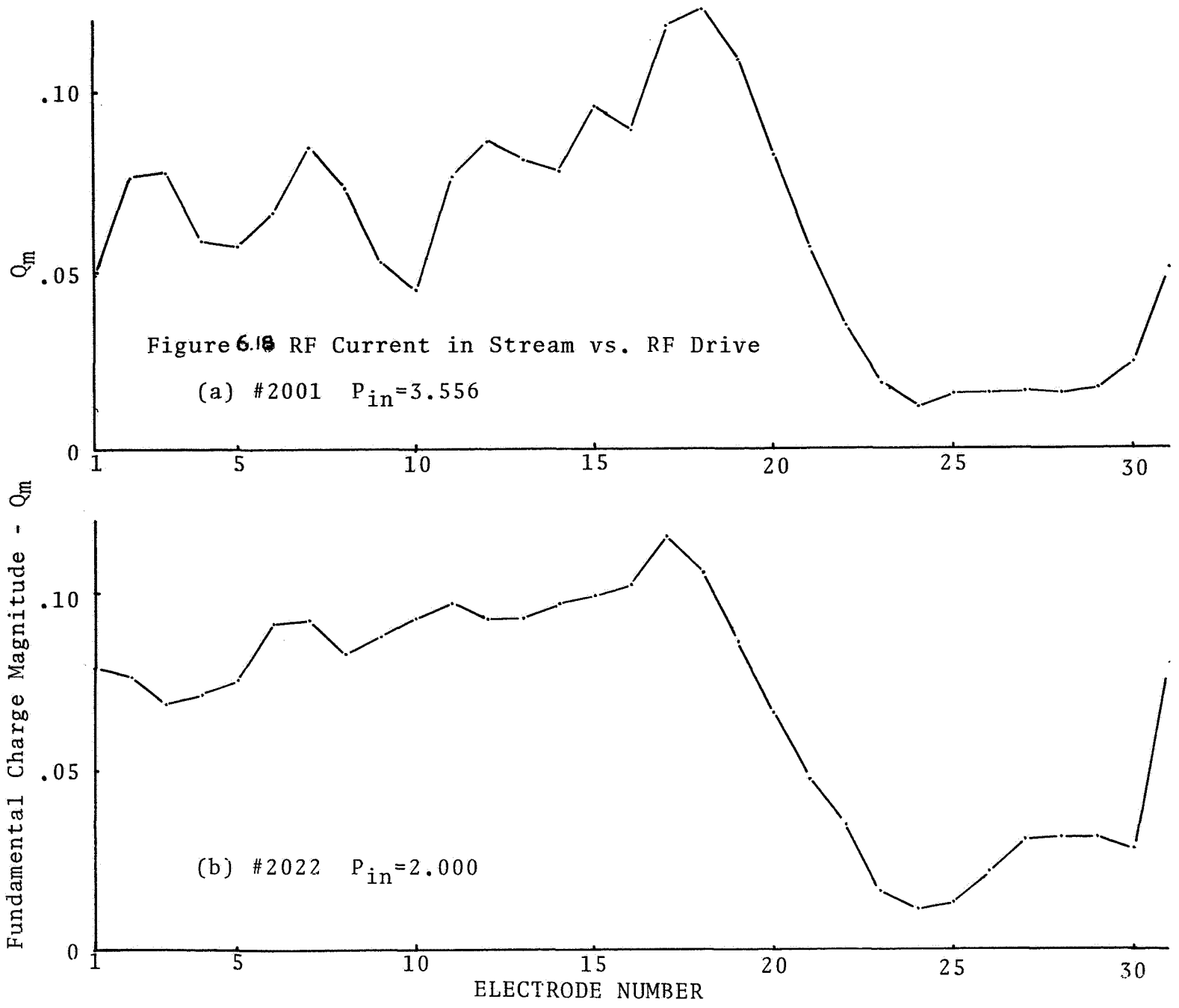

Figure 6.18 RF Current in Stream vs. RF Drive

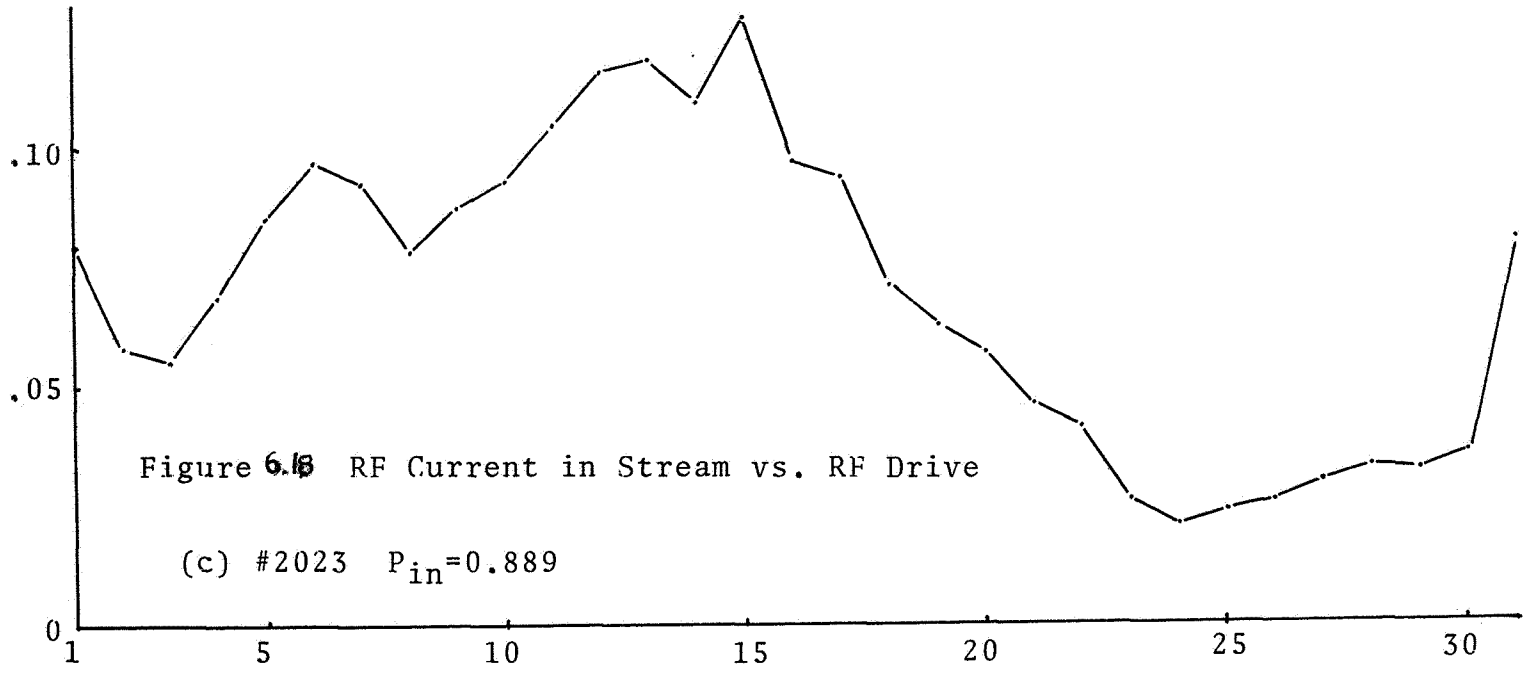

Figure 6.8 RF Current in Stream vs. RF Drive

(c) #2023 P_{in}=0.889

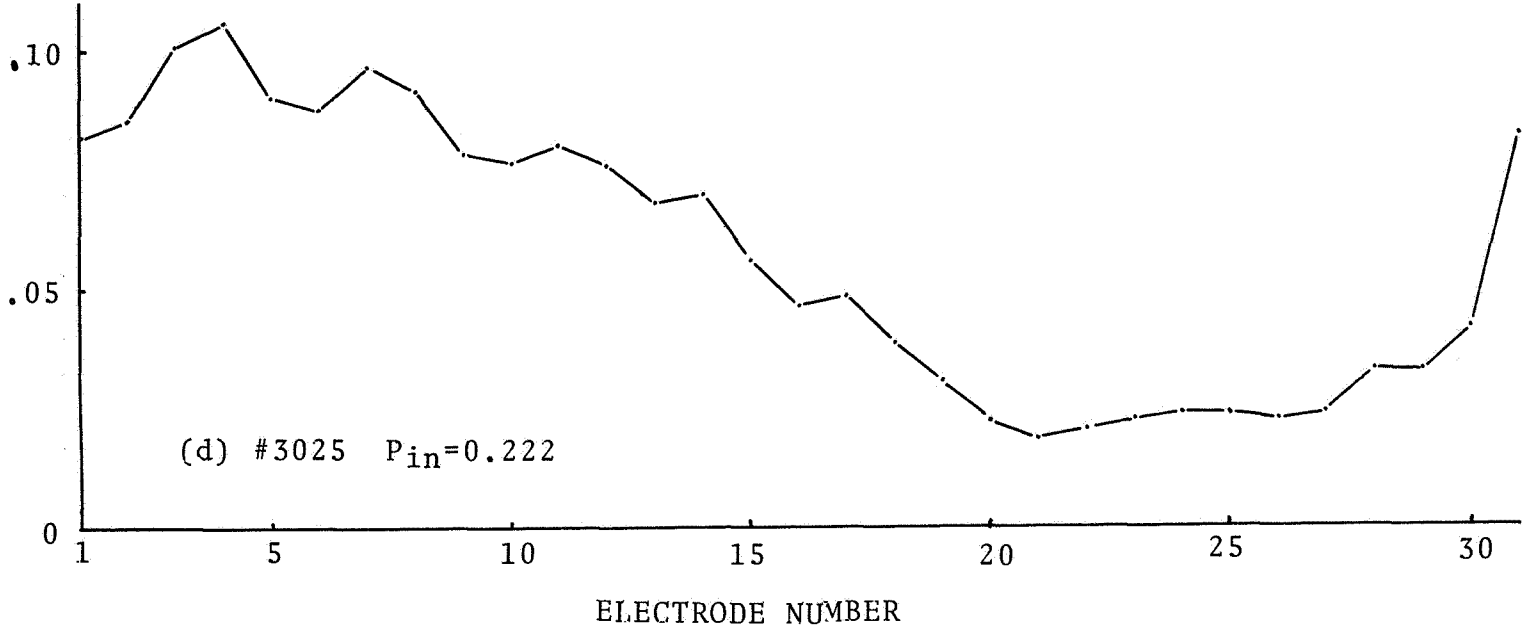

(d) #3025 P_{in}=0.222

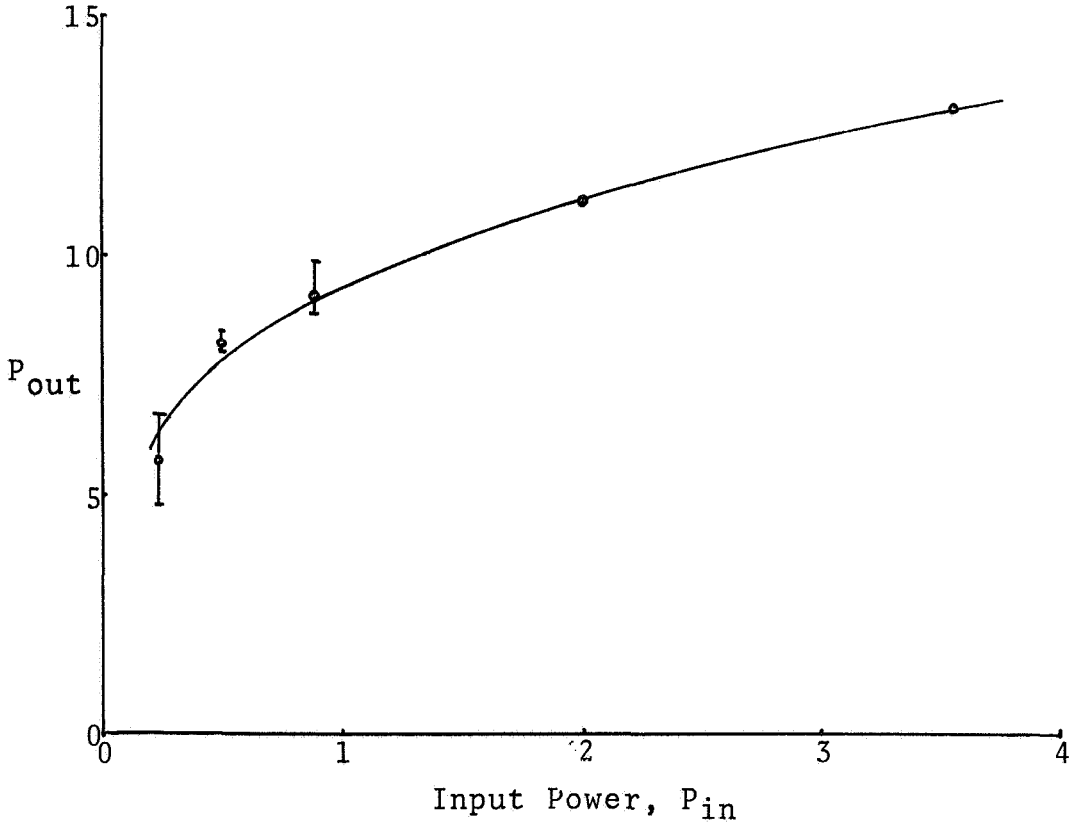

Figure 6.19 Power Transfer Characteristic. 2000-3000 Series Calculations; I_k = 1.67.

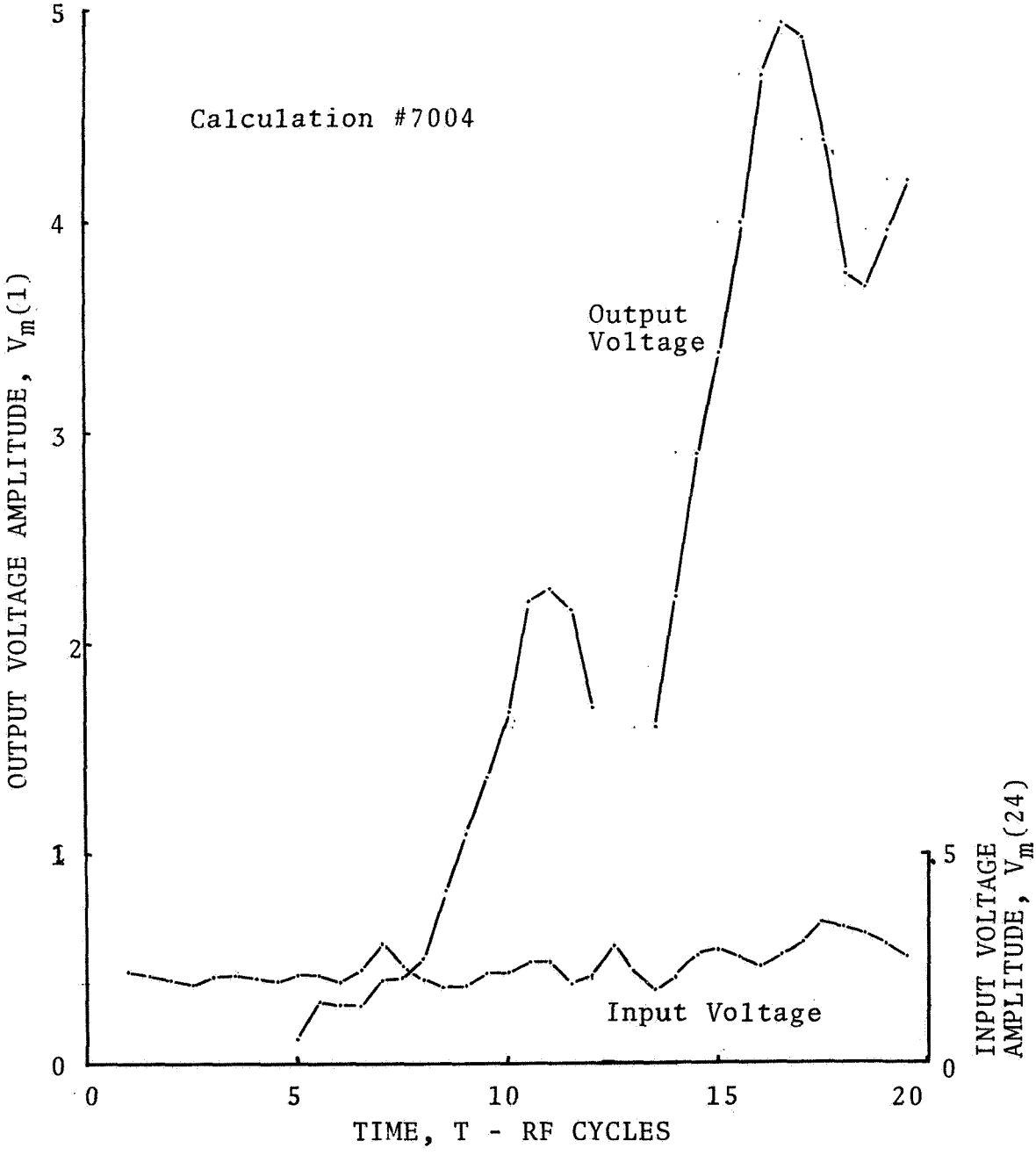

Figure 6.20 Start-up transient with very small rf input signal

Table 6.5 Effect of Network Impedance

Run No.	4012	7003	
Characteristic impedance	400	500	ohms
Coupling impedance	160	200	ohms
Injected current	3.75	3.75	
Anode current	2.50		
Rf input			
Rf output			
Gain	7.9	8.9	db

The higher network impedance results in higher circuit fields, tending to overcome space-charge debunching effects; it is therefore advantageous. No optimum impedance level was observed. Such an optimum probably does exist, however, since excessive transverse velocities would result, and this would indicate high anode bombardment and lowered efficiency. It probably would be tolerated only if there were no better way to get higher power.

6.5 Second Design of the Injected Beam Amplifier

As in the design of magnetrons and other crossed-field devices, there exists some degree (not excessive) of freedom in meeting the objectives. Use of scaling techniques is common. By suitable choice of dimensions and mode number, the scaling voltage can be varied over a considerable range. Similarly, the scaling current can be varied so that the device can be a low impedance one or high. This is especially useful when one encounters space-charge effects that limit performance, as by dc current limits or spurious oscillations or noise. It is the function of the analysis to determine these limits, of course, and the limits are most generally stated in normalized terms as has been done in this report.

The second design of the injected beam amplifier raises the anode voltage and lowers the current level. The mode number was increased from 7.5 to 16; this reduces the azimuthal electron velocity and hence reduces the scaling magnetic field, B_o (cf Table 6.3). For a given applied magnetic field, then, the synchronous (Hartree) voltage is much higher (esp. when normalized) and higher efficiency is indicated. In this design a depressed sole is used; this should make it virtually impossible for electron interception there.

The computer program was again rewritten to allow for the larger number of electrodes. It was used both with artificial and with physical demodulation of the reentering stream; some results are shown in Table 6.6.

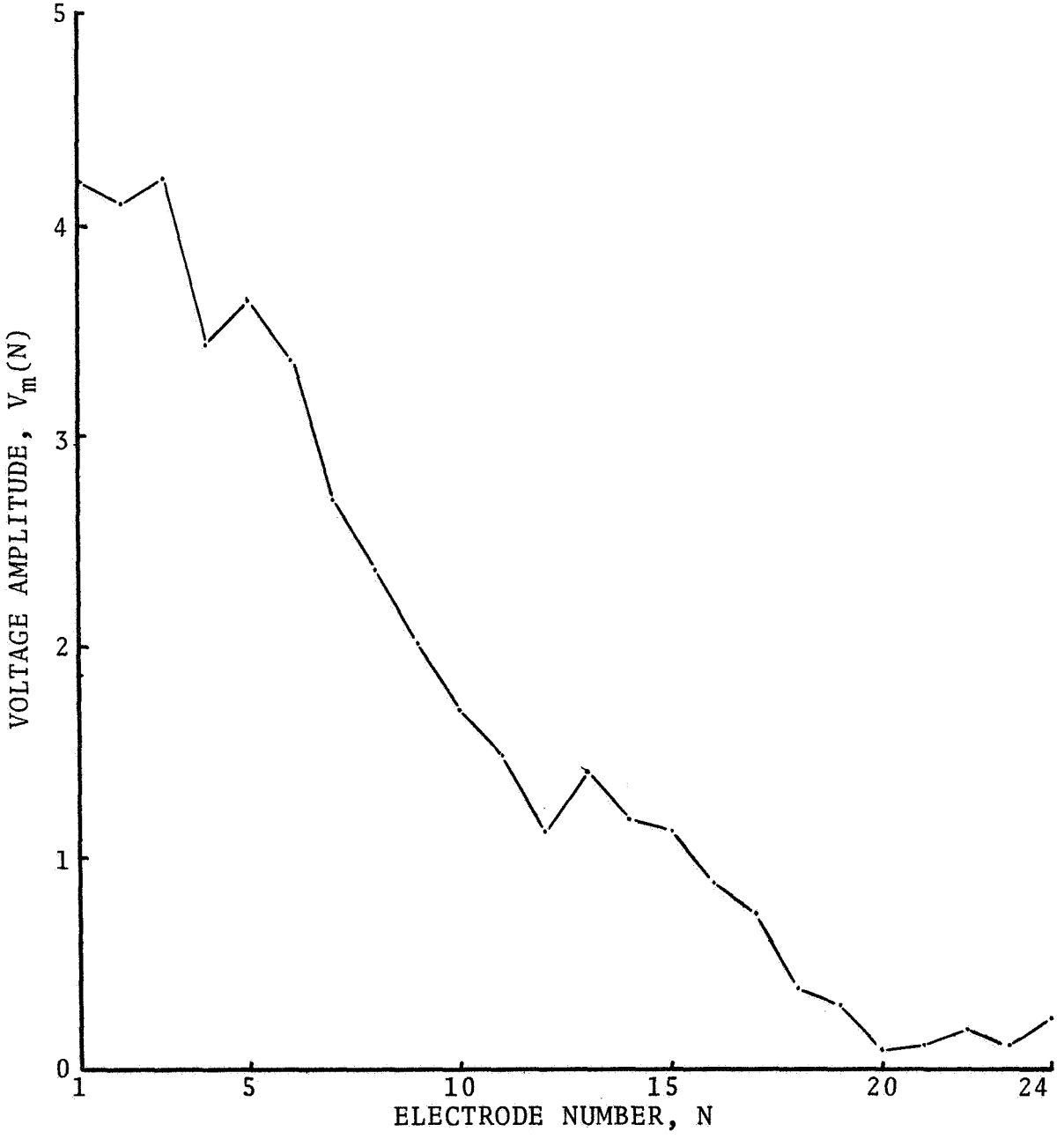

Figure 6.21 Calculation #7004: Internal voltage distribution
T = 19.5

Table 6.6 Calculations with High Mode Number (Second Design)

Run No.	5000	5010	5011	
Anode voltage	27.8	27.8	27.8	(Hartree)
Injected current	1.67	1.67	1.67	
Axial transit	10	10	10	cycles
# of anodes	64	64	64	
# active anodes	52	52	52	
Coupling impedance		160	160	ohms
Network loss	.7	.7	.7	db
Rf input power	3.6	3.6	2.0	
Ef output power	24.9	22.8	21.8	
Gain	8.46	8.08	10.4	db

The charge configurations are shown in Figures 6.22, 6.23, and 6.24.

These calculations appear to be relatively free of the instability that was so troublesome in calculations of the first design. This is considered to be the result of better demodulation in the drift region, which is longer and which allows electrons to move transversely toward the sole. The efficiency figures obtained are suspect; poor energy balance was encountered. The calculations should be made with a smaller time interval; this is costly because of the high mode number.

7. CONCLUSIONS OF PART I.

7.1 Conclusions

Computer results for relatively low gain operation (6 to 12db) of the injected beam forward-wave amplifier were obtained. They show that gain can be increased by increase of injected current and/or rf impedance level. Stream feedback is important in regard to high gain, but moderate gain can be obtained for a wide range of feedback conditions.

Some calculations were carried through for higher gain conditions, but these were restricted by appearance of instabilities in the computations. After considerable effort, it was concluded that the instability was caused by stream feedback. Means for eliminating the feedback both in the electron tube and the computer model of it are needed.

7.2 Recommendations

Further study of the amplifier is needed to answer the questions left unanswered here, viz., questions as to the effects of varying the magnetic field, the frequency, on the amplifier performance. More thorough exploration of the range of variable than has been possible in the present limited program.

More basic questions need to be answered concerning this new amplifier. Typical are: how does the rf field influence the injection current and the axial transit velocity? What are the precise details of the drift region? the collector? the network? Any future work should be done by those in a position to obtain this information. It is not

JUNE 28, 1968 SER. NO. 5010 STEP NO. 408 TIME 40.797

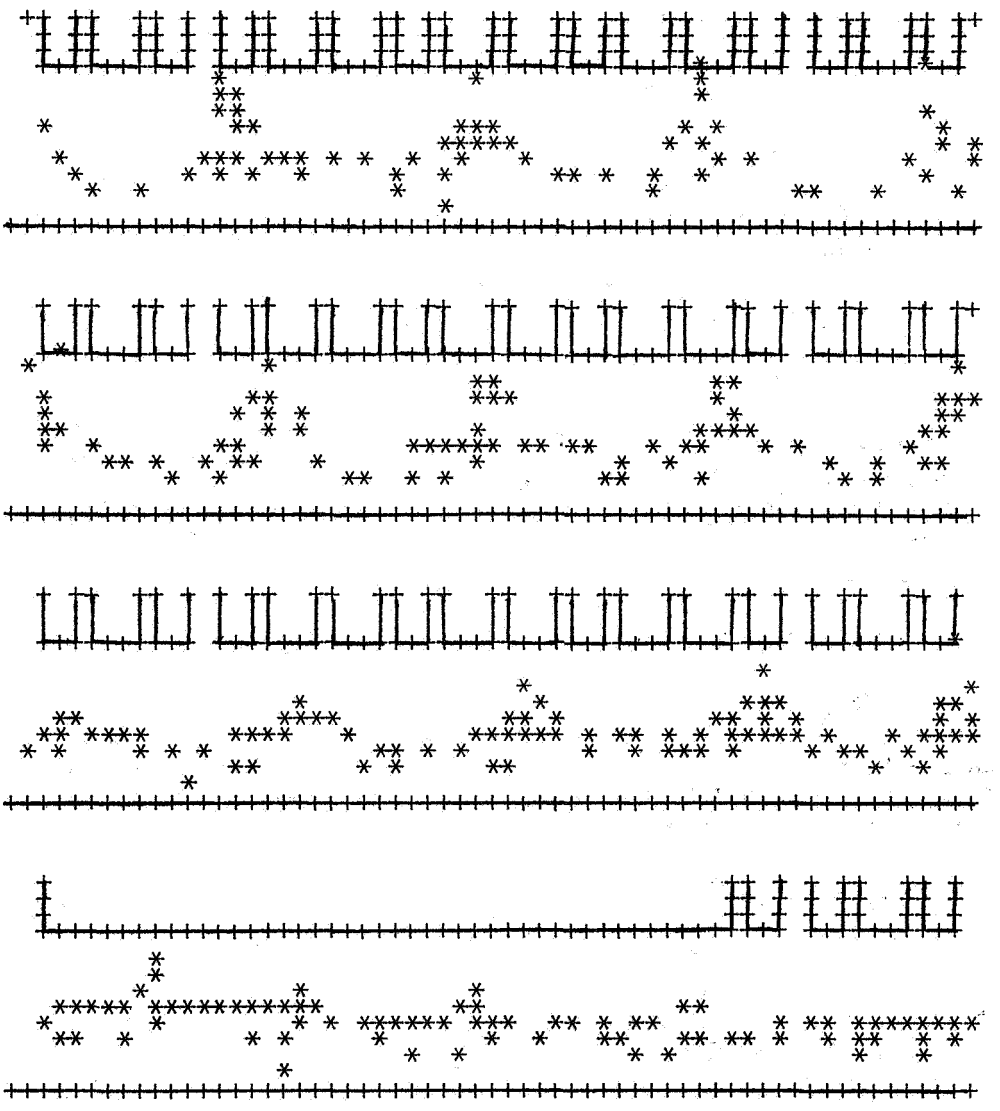

Figure 6.22 Calculation #5010: Configuration at T = 40.8

JUNE 28, 1968 SER. NO. 5010 STEP NO. 412 TIME 41.197

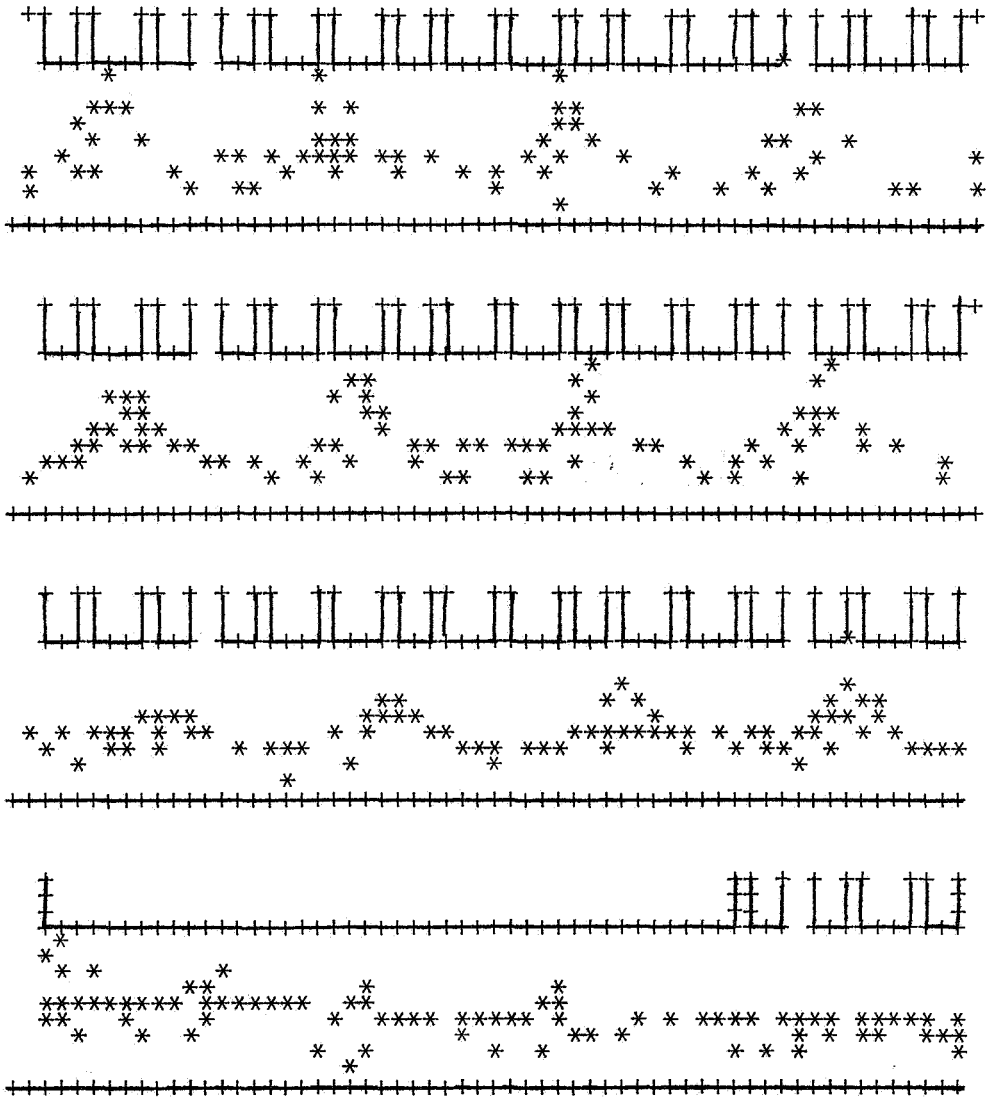

Figure 6.23 Calculation #5010: Configuration at T = 41.2

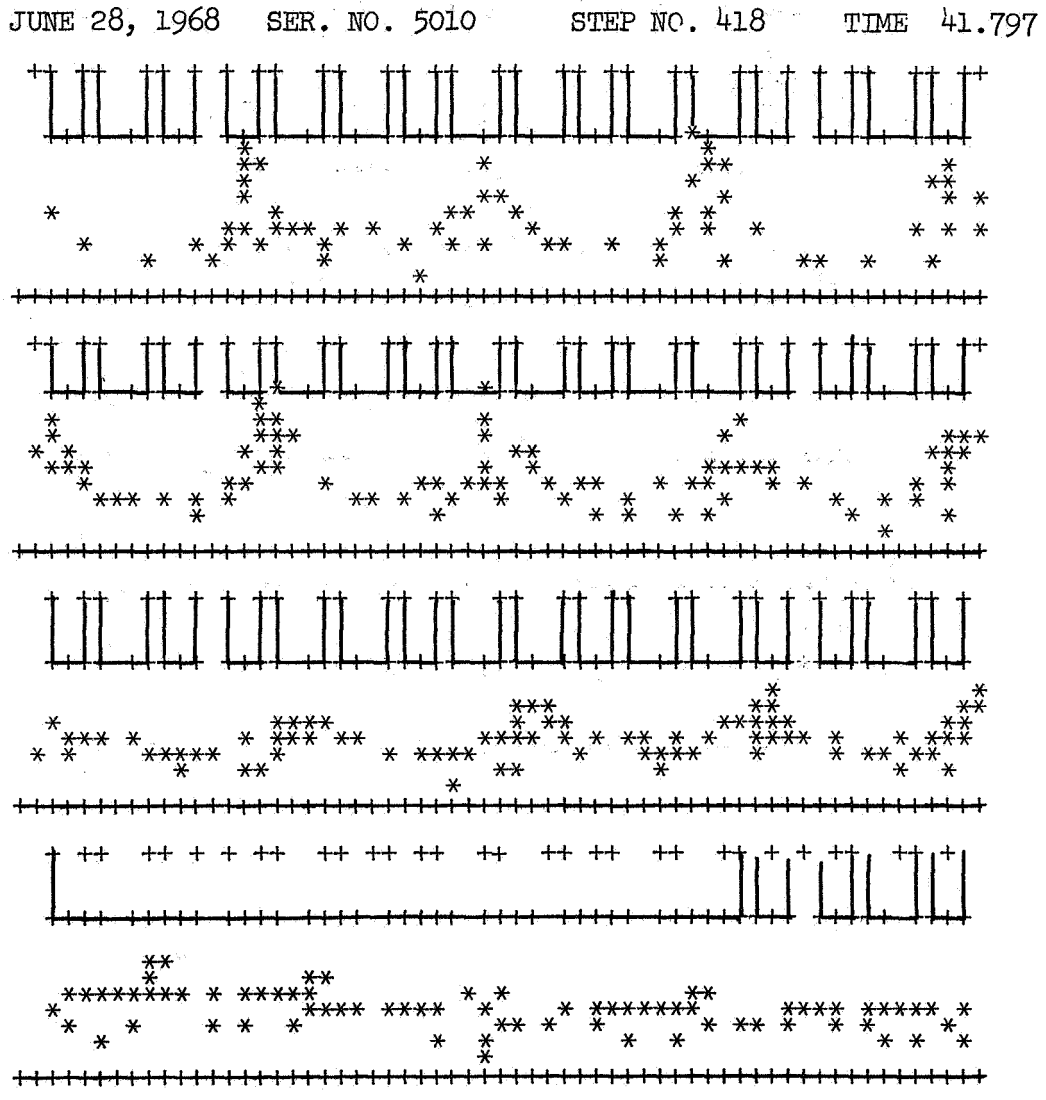

Figure 6.24 Calculation #5010: Configuration at T = 41.8

realistic to expect useful results from isolated analysts. E.g., the computer at best will only tell one what happens when certain parameters have certain values. They do not generally tell one what values are the best ones to use; this information can best come from the experimentalist.

It may also be possible that the transient/simulation method may not work under conditions of severe space charge, as difficulty has repeatedly been had in the magnetron situation. Perhaps some other computational technique should be used, e.g., those used by Rowe et al. at the University of Michigan.

PART II. AMPLITRON NOISE MEASUREMENTS

8. INTRODUCTION

This part of the research program is to evaluate the noise characteristics of a commercially available Amplitron, the Raytheon type QKS-1300. Two such tubes (nos. 156 and 185) were supplied by NASA. This tube has an output power rating of 25 watts.

Sources of noise in amplifiers fall into two classes: (1) those of a controllable nature, and (2) the uncontrollable ones. The former includes power supply ripple, microphonics and outside interference. A well-designed system takes the necessary precautions against these sources and is limited only by economics. Further discussion of these sources will not be made.

The uncontrollable sources are largely traceable to the cathode and its random emission of electrons with random velocities. Cathode flicker noise and partition noise also appear in microwave tubes. These components of noise are usually very broad band, whereas the controllable ones are usually characterized by frequencies related to the frequencies characteristic of the ripple or other disturbing forces. When resolved into a-m and f-m components, a correlation between the a-m and f-m components often exists.

The purpose of this research, however, is not to investigate the sources of the noise, but to measure it.

9. MEASUREMENTS

9.1 Scope

Since the Amplitron is to be used as a transmitter device rather than, say, a local oscillator, the noise must be measured over a wide range of frequency from several tens of megahertz from the carrier to as close to the carrier as possible--on the order of a few kHz. To define the noise adequately, a resolution into a-m and f-m noise is required.

9.2 Measurement Techniques

The noise measuring system must be capable of measuring very low level signals (the noise) in the presence of a very strong one (the carrier). While it is possible to reject a strong signal with a preselector, (which is not readily available, anyway), the selectivity required of such a device to discern noise within a few KHz of the carrier is impossible to attain. An alternative scheme is required to prevent the carrier signal from entering the measuring system lest it "swamp" the noise to be measured.

The method used here consists of use of the bridge arrangement shown in Figure 9.1. In this arrangement, the input signal of the amplifier is balanced against the output signal in amplitude and phase

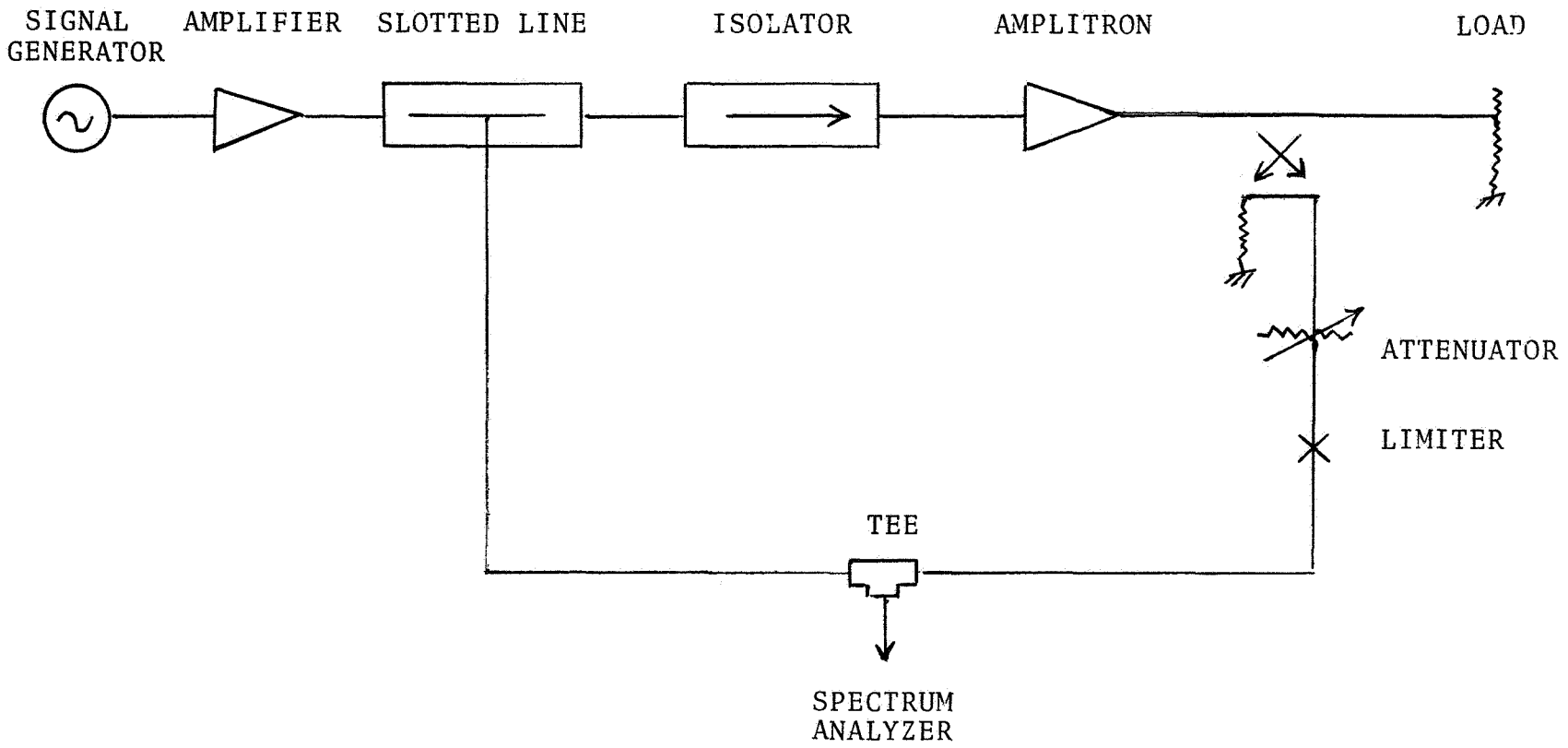

Figure 9.1. Amplitron noise measuring bridge system.

so that the carrier signal is nulled. The only signal remaining to be measured by the detector is the noise and other spurious signals generated within the amplifier under test. In the present case, the phase adjustment is made by variation of the probe position in the slotted line in the input arm. The amplitude adjustment for balance is made in the attenuator connected to the branch which samples the output arm, itself connected to a high power load.

Among the difficulties of this technique is the fact that the probe must be sufficiently deep to couple appreciably so that the noise signal fed into the detector may be large enough to be observed. On the other hand, the degree of coupling must not be so large that a signal be fed back into the input line from the output line or so deep that serious mismatch be caused in the input line. These measurements were made without any apparent difficulty from these factors.

Measurements are made with the system as shown, and also with a limiter placed in the output arm signal path. The former measurement yields the total noise measurement; the latter, only the f-m part. The a-m noise power density is determined by differencing the two.

The noise measured by the detector after carrier cancellation is rendered in absolute terms by a calibration procedure in which a known power level from a signal generator is passed directly into the detector (a Tektronix type 1L20 spectrum analyzer) having sufficient bandwidth to accept the signal.

The noise power spectral density measurement is limited by the presence of the residual carrier and the prospect of its passing into the spectrum analyzer. The frequency "jitter" of the input signal was at best $\pm$ 3 kHz; the spectrum analyzer bandwidth was adjustable in steps downward to 1 kHz. Thus, the noise measurements can be considered useful to within approximately $\pm$ 4 kHz. of the carrier.

9.3 Results

9.3.1 Preliminary Measurements on Serial No. 185

It was originally planned to perform complete measurements on two Amplitrons. The first tube tested (#185) failed, however. It exhibited spurious oscillations when operated, and on cold test showed a large internal reflection. Permanent damage had apparently occurred. Generally, it was observed that most of the noise is within a few kHz of the carrier frequency. Over a broad spectrum of several MHZ about the carrier--mostly described by the pass band of the Amplitron network--there was some "white" noise. This noise was strongly dependent on cathode temperature; even small changes in heater current produced severe changes in this background noise level.

9.3.2 Measurements on Serial No. 156

Noise in the second of the two Amplitrons was also dependent on heater power, hence on cathode temperature. Figure 9.2 shows the total

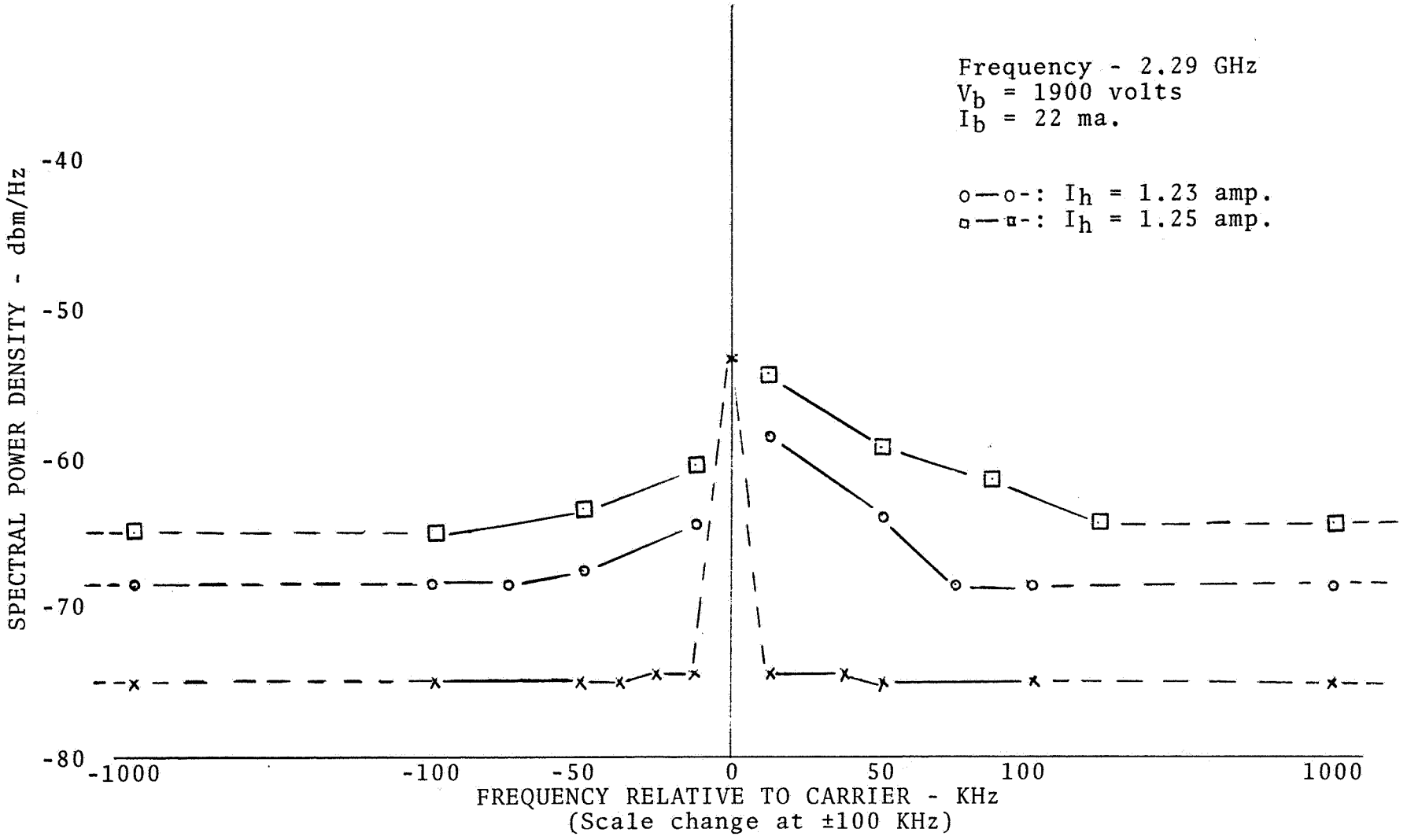

Figure 9.2 Effect of Heater Current on Noise

noise spectrum density when the Amplitron is operated under rated operating conditions with the optimum heater current, I_h=1.23 dc amperes, and with a slightly different heater current. It should be noted that the plotted frequency scale changes at 100 KHZ for the sake of convenience. Beyond 100 KHz from the carrier, the noise is essentially "white." For reference, the measurement was repeated with the Amplitron "cold"; the results shown indicate the limits of measurement reliability. Clearly, the noise in excess of -75 dbm/Hz can be discerned at frequencies at least 10 KHz from the carrier.

It is perhaps premature to draw significant conclusions from the heater power dependence of the noise, since the tubes tested were both known to have thermal peculiarities, having been rejected by the manufacturer on this account.

Measurements were also made with normal rf drive power and with very small drive. The results are shown in Figure 9.3. The fact that no peaking of noise occurred at the carrier frequency probably means that the Amplitron was not locked to the drive signal. In this case, the noise observed is probably all thermal noise from the cathode, with no carrier-associated noise (which would have strong f-m components as well as a-m). The large noise level in the $\pm$ 50 KHz band around the carrier appears when the drive level is raised to normal levels.

Insertion of the limiter in the bridge as shown in Figure 9.1 produced the results shown in Figures 9.4 and 9.5. It would appear from Figure 9.4 that the noise measurement is seriously upset near the carrier frequency, and that the measurement with the Amplitron operating consequently has little meaning. It is thought likely that the limiter itself is a source of considerable noise.

9.4 Conclusions

The carrier cancellation system using a slotted line proved usable for measurement of the total noise power density of the two Amplitrons tested. The noise power density was measured at frequencies to within 10 KHz of the carrier; the results are given principally in Figure 9.2. They show that the noise level is -68 dbm/Hz for frequencies more than 75 KHz from the carrier, rising to approximately -58 dbm/Hz at 10 KHz from the carrier. There is slight asymmetry in the spectrum.

Measurement of the purely f-m component of the noise was not possible because of system defects which are thought to be limiter noise.

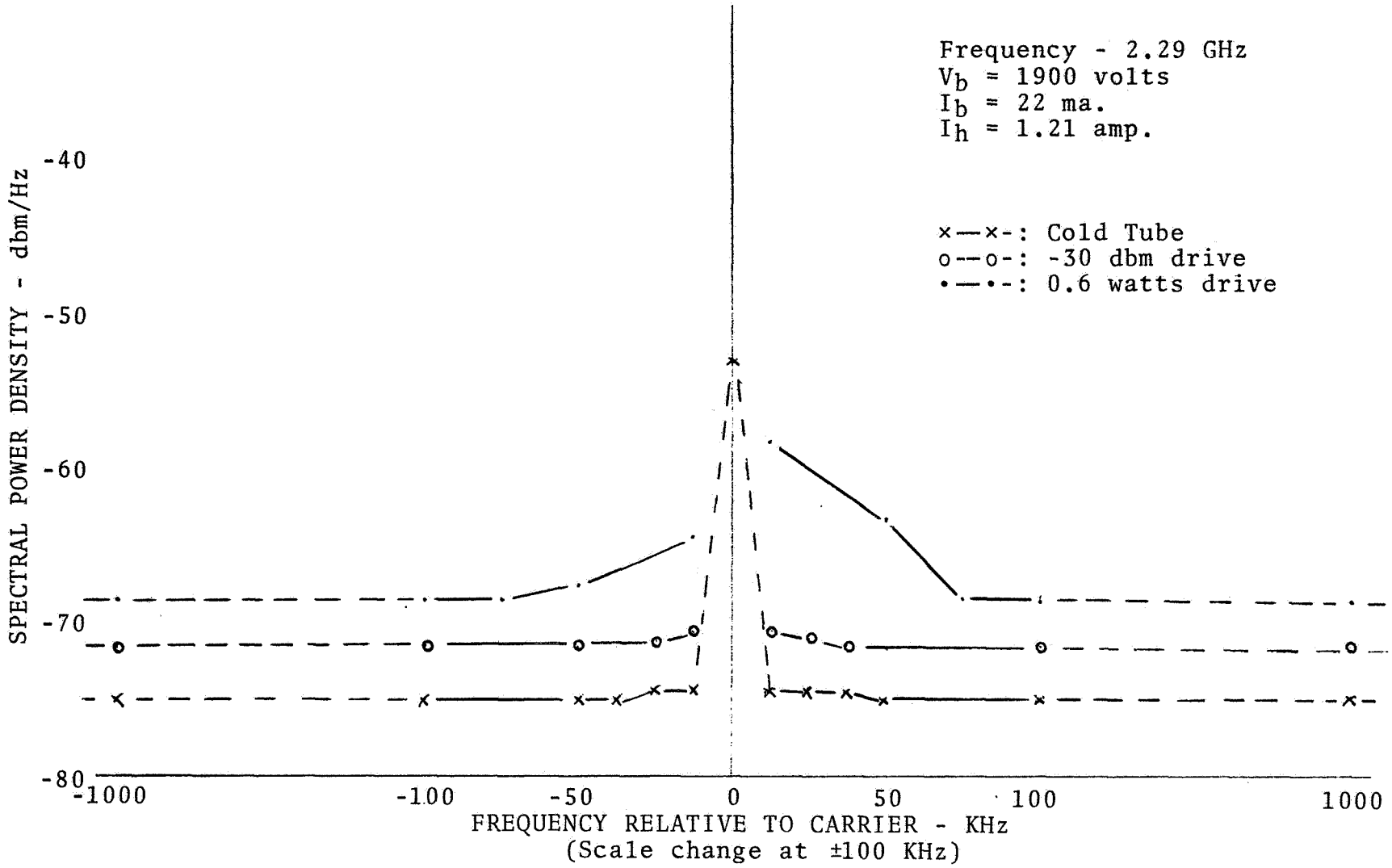

Figure 9.3. Noise power as a function of rf drive power.

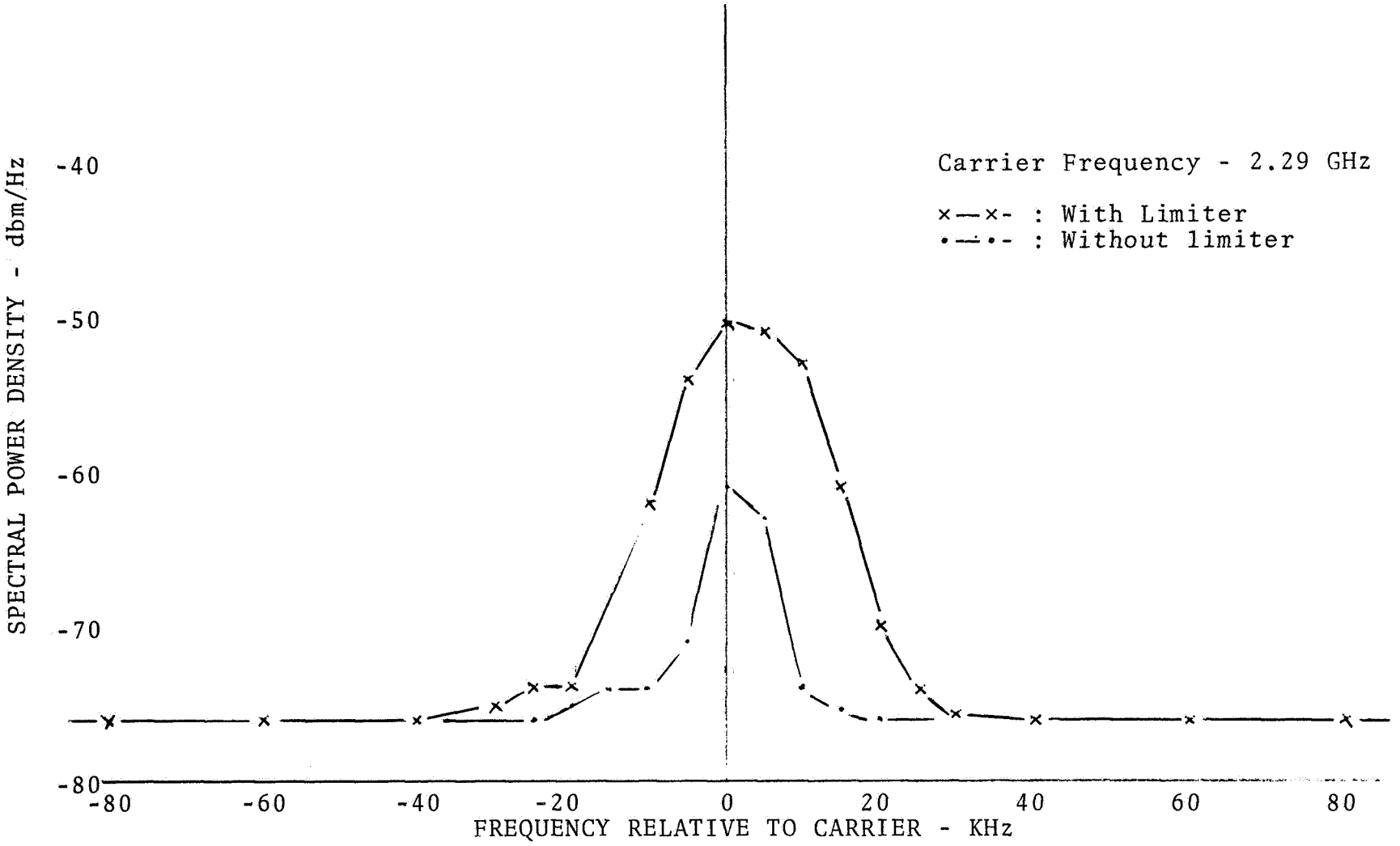

Figure 9.4. F-M Noise power density measurement: "Cold" Tube

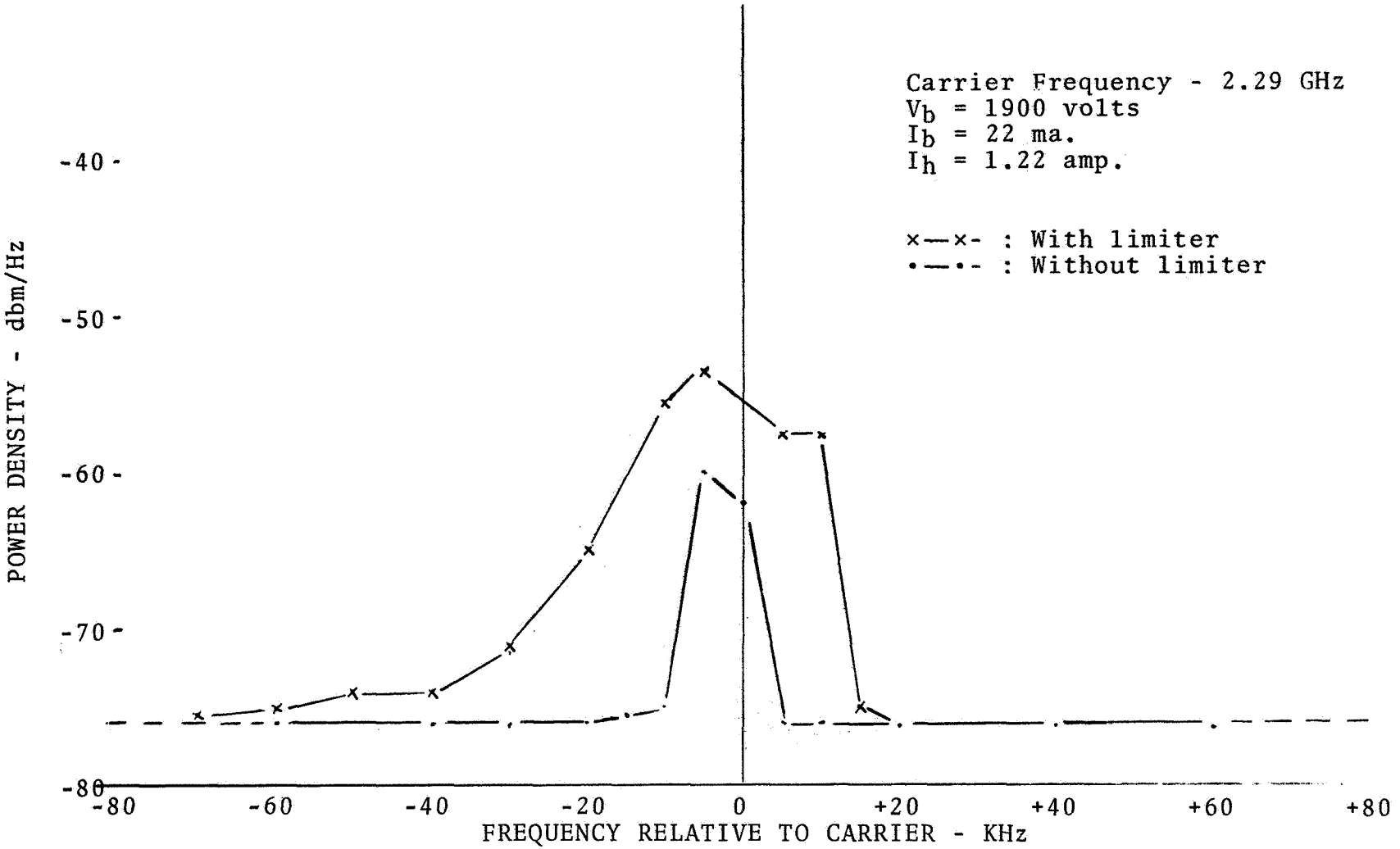

Figure 9.5. F-M Noise power density measurement: Operating Tube

APPENDIX A. COMPUTER PROGRAM LISTING

Appendix A.1 Listing of Control Program

```
C       CONTROL PROGRAM
C       JUNE 26
        COMMON/PROB/JP,SZ,THM,MM,NM,PS,NE,GAP,THMP,MMP,NMP,ND,NKD,
       1VDC,NG,VOR,CA,CB,CC,GAMA,GAMB,GAMC,GA,GB,GC,C1,C2,GAM1,GAM2,G1,G2,
       2CIN1,CIN2,COUT1,COUT2,FREQ,THTC,
       3HT,G,GG,TMAX,NK,KM,LNWT,EMIN,CSAT,CNST,UTHERM,PIN,POIN,THDIN,TAU
       4,KDIS,TD
        COMMON/CHARGE/IM
        COMMON/STATUS/TIME,STEPN,M4,QPP,ACG,XX,LG,CCAT,JT,QA,QB
        COMMON/CONSTS/ALP,DA,DB,DC,DD,DAG,DBG,DCG,DDG,WA,MMM,HS,NMM,HTH,PS
       1S,MMPM,HSP,NMPM,HTHP,PI,TPI,MPI,MA,MB,MC,MD,ICH,HHT,  GU,THCR ,GAM
       2P,GAMM,GV,GQ,GAMN,OMEGA,THS,PMT,GBT,GTHS,PMAX,FNS,AB,AC,AA,TP,TPT,
       3DUM
        DIMENSION ICH(15)
        INTEGER STEPN
 10     CALL RESET(L)
        CALL INPUT
 1      CALL RESET(M4)
        CALL SETTIM(JT ,ACF)
        CALL TIMEGN(L,ICH(1))
        K=0
 4      CALL RESET(L)
 61     CALL SPACH
        CALL TIMEGN(L,ICH(2))
 3      CALL RESET(L)
 62     CALL CKT
        CALL TIMEGN(L,ICH(3))
 41     CALL RESET(L)
        K=K+1
        IF(MOD(K,KDIS).EQ.1.OR.TIME.GE.TD)CALL DISPLA
        CALL TIMEGN(L,ICH(4))
        CALL TIMLFT(J,ACF)
 63     CALL RESET(L)
 40     IF(J.LT.ICH(12))GO TO 300
        CALL FIVE
 53     CALL TIMEGN(L,ICH(5))
 64     CALL RESET(L)
        CALL PSIPR
        CALL TIMEGN(L,ICH(6))
        CALL TIMLFT(J,ACF)
        IF(J.LT.ICH(13)) GO TO 300
 65     CALL RESET(L)
        IF(K.NE.1) GO TO 410
 52     CALL KATE
 410    CALL TIMEGN(L,ICH(7))
          IF(K.EQ.KM) K=0
        CALL TIMLFT(J,ACF)
        IF(J.LT.ICH(14)) GO TO 300
 66     CALL RESET(L)
        CALL NEWT
```

```
      CALL TIMEGN(L,ICH(8))
      CALL TIMLFT(J,ACF)
      IF (J.LT.ICH(15)) GO TO 300
30    CALL RESET(L)
      CALL ANAL
      CALL MARGE
      IF(TIME.GT.TMAX)GO TO 10
      CALL TIMEGN(L,ICH(9))
      GO TO 41
300   MA=3
      CALL MARGE
      GO TO 10
      END
```

Appendix A.1.1 Timing Subroutine (IBM 360 Assembler Language)

```
          TITLE 'TIMER'
*         CALL RESET(L)
*         CALL TIMEGN(L,M)
*         CALL SETTIM (L,TMAX)
*         CALL TIMLFT(J,TMAX)
          ENTRY RESET,TIMEGN,SETTIM,TIMLFT
          BALR  10,0
          USING *,10
RESET     SAVE  (14,12)
          L     12,0(1)
          TIME  BIN
          ST    0,0(12)
          RETURN (14,12)
TIMEGN    SAVE  (14,12)
          LR    11,1
          L     12,0(1)
          L     11,4(11)
          TIME  BIN
          S     0,0(12)
          ST    0,0(11)
        RETURN (14,12)
SETTIM    SAVE  (14,12)
          L     12,0(1)
          LR    11,1
          L     11,4(11)
          TIME  BIN
          A     0,0(12)
          ST    0,0(11)
        RETURN (14,12)
TIMLFT    SAVE  (14,12)
          L     12,0(1)
          LR    11,1
          L     11,4(11)
          TIME  BIN
          LCR   0,0
          A     0,0(11)
          ST    0,0(12)
        RETURN (14,12)
          END
```

Appendix A.1.2

```
         TITLE 'DATE SUBROUTINE'
         ENTRY DATE
DATE     SAVE  (14,12)
         BALR  5,0
         USING *,5
         L     9,0(1)
         L     10,4(1)
         L     11,8(1)
         TIME
         L     2,=X'0000000F'
         NR    2,1
         L     3,=X'0000FFFF'
         NR    3,1
         SRA   1,16
         SLA   1,4
         AR    1,2
         ST    3,B+4
         SR    6,6
         ST    6,B
         ST    6,D
         CVB   3,B
         ST    3,B+4
         ST    1,D+4
         CVB   1,D
         ST    1,B
         LA    2,4
AGN      L     3,MEND(2)
TST      C     3,B+4
         BNL   OUT
         A     2,=F'4'
         B     AGN
OUT      L     4,B+4
         S     4,MEND-4(2)
         ST    4,0(10)
         SRA   2,2
         ST    2,0(9)
         L     2,B
         ST    2,0(11)
         RETURN (14,12)
B        DS    D
D        DS    D
MEND     DC    13F'0,31,60,91,121,152,182,213,244,274,305,335,366'
         END
```

Appendix A.2 Input Program

```
      SUBROUTINE INP1
C     JUNE 20
      COMMON/PROB/JP,SZ,THM,MM,NM,PS,NE,GAP,THMP,MMP,NMP,ND,NKD,
     1VDC,NG,VDR,CA,CB,CC,GAMA,GAMB,GAMC,GA,GB,GC,C1,C2,GAM1,GAM2,G1,G2,
     2CIN1,CIN2,COUT1,COUT2,FREQ,THTC,
     3HT,G,GG,TMAX,NK,KM,LNWT,EMIN,CSAT,CNST,UTHERM,PIN,PDIN,THDIN,TAU
     4,KDIS,TD
      COMMON/STATUS/TIME,STEPN,M4,QPP,ACF,XX,LG,CCAT,JT,QA,QB
      DIMENSION QA(100),QB(100)
      COMMON/CHARGE/IM,C,P,TH,UY,UX,ER,ETH,ERS,ETHS
      DIMENSION C(600),P(600),TH(600),UX(600),UY (600),ER(600),ETH(600),
     1ERS(600),ETHS(600)
      COMMON/CONSTS/ALP,DA,DB,DC,DD,DAG,DBG,DCG,DDG,WA,MMM,HS,NMM,HTH,PS
     1S,MMPM,HSP,NMPM,HTHP,PI,TPI,MPI,MA,MB,MC,MD,ICH,HHT,  GU,THCR ,GAM
     2P,GAMM,GV,GQ,GAMN,OMEGA,THS,PMT,GBT,GTHS,PMAX,FNS,AB,AC,AA,TP,TPT,
     3DDT
      DIMENSION ICH(15)
      COMMON/NETWRK/VF,VF,VI,QE,QP,M
      DIMENSION VF(80),VF(80),VI(80),QE(80),QP(80)
      DIMENSION M(6400),LL(80),PP(80)
      DIMENSION VDD(80)
      REAL M
      DIMENSION MN(12)
      DATA MN/'JAN.FEB.MAR.APR. MAYJUNEJULYAUG.SEP.OCT.NOV.DEC.'/
      DIMENSION ERA(2),ERB(2),ERC(2),ERD(2),ERE(2),ERF(2),ERG(2),ERH(2)
      EQUIVALENCE (ERA,JP),(ERB,TIME),(ERC,VE),(ERD,IM),(ERE,F),
     1(ERF,PSI),(ERG,ALP),(ERH,CAN),(LNWT,ME)
      INTEGER STEPN
      ENTRY INPUT
      DO 1001 I=1,54
 1001 ERA(I)=0.
      DO 1002 I=1,209
 1002 ERB(I)=0.
      DO 1003 I=1,6800
 1003 ERC(I)=0.
      DO 1004 I=1,5401
 1004 ERD(I)=0.
      DO 1007 I=1,  62
 1007 ERG(I)=0.
  113 FORMAT('1  JOB RUN ON ',A4,I3,', 19',I2//)
      CALL DATE(JMN,JDA,JYR)
      PRINT 113,MN(JMN),JDA,JYR
      READ 111,JP,JT
      PRINT111,JP,JT
      READ 111,MC,MQ
      PRINT111,MC,MQ
      READ 111,ME,MF
      PRINT111,ME,MF
      IF(MC.EQ.1) GO TO 210
      READ 110,SZ,THM,MM,NM,ICH(15)
```

```
      PRINT110,SZ,THM,MM,NM,ICH(15)
110   FORMAT(2E15.4,3I10)
      READ 110,GAP,THMP,MMP,NMP,NE
      PRINT110,GAP,THMP,MMP,NMP,NE
      READ 111,ND,NKD
      PRINT111,ND,NKD
      READ 111,ICH(12),ICH(13)
      PRINT111,ICH(12),ICH(13)
      READ 112,HT,G,GG,TMAX
      PRINT112,HT,G,GG,TMAX
      READ 112,UTHERM,EMIN,CONST,PS
      PRINT112,UTHERM,EMIN,CONST,PS
      READ 120,VDC,NG
      PRINT120,VDC,NG
      NGP=NG+1
      READ 112,(VDD(I),I=NGP,NE)
      PRINT112,(VDD(I),I=NGP,NE)
111   FORMAT(2I10)
112   FORMAT(  4E18.3)
120   FORMAT(E20.6,I15)
121   FORMAT(  5E14.7)
      READ 120,CNST,NK
      PRINT120,CNST,NK
      EQUIVALENCE (TAU,TLIFE)
      READ 121,PIN,PDIN,THDIN,TLIFE
      PRINT121,PIN,PDIN,THDIN,TLIFE
      READ 111,KM,KDIS
      PRINT111,KM,KDIS
      READ 121,CA,CB,CC,GAMA,GAMB,GAMC,GA,GB,GC
      PRINT121,CA,CB,CC,GAMA,GAMB,GAMC,GA,GB,GC
      READ 121,CIN1,G1,C1,GL1,COUT1
      PRINT121,CIN1,G1,C1,GL1,COUT1
      READ 121,CIN2,G2,C2,GL2,COUT2
      PRINT121,CIN2,G2,C2,GL2,COUT2
      READ 121,FREQ,THTC
      PRINT121,FREQ,THTC
      READ 111,JPR
      PRINT111,JPR
      IF(MC.NE.2) GO TO 75
      READ  120,TIME,JPL
      PRINT 120,TIME,JPL
      READ 120,TIME,IM
      PRINT120,TIME,IM
621   FORMAT(20A4)
      READ 621,(C(I),P(I),TH(I),UY(I),UX (I),I=1,IM)
      PRINT121,(C(I),P(I),TH(I),UY(I),UX (I),I=1,IM)
      READ  621,(QE(J) ,J=1,NE)
      PRINT 121,(QE(J) ,J=1,NE)
      READ  621,(QP(J) ,J=1,NE)
      PRINT 121,(QP(J) ,J=1,NE)
```

```
      READ  621,(VE(J)  ,J=1,NE)
      PRINT 121,(VE(J)  ,J=1,NE)
      READ  621,(VF(J)  ,J=1,NE)
      PRINT 121,(VF(J)  ,J=1,NE)
      READ  621,(VI(J)  ,J=1,NE)
      PRINT 121,(VI(J)  ,J=1,NE)
      READ  120,XX,LG,CCAT,STEPN
      PRINT 120,XX,LG,CCAT,STEPN
      READ  621,(QA(K),K=1,LG)
      PRINT 121,(QA(K),K=1,LG)
      READ  621,(QB(K),K=1,LG)
75    PI=3.141593
      THCR=   PI/FLOAT(NK)
      IF(MQ.NE.0)MD=1
      IF(MQ.EQ.0)MD=2
      NMM=NM-1
      FMMM=FLOAT(MM-1)
      FNMM=NMM
      MMPM=MMP-1
      NMPM=NMP-1
      FMMPM=MMPM
      FNMPM=NMPM
      HS=(1.-SZ)/FMMM
      THM=PI*THM/180.
      THMP=THMP*PI/180.
      HTH=THM/FNMM
      TPI=PI+PI
      DDT=TPI/FLOAT(NE)
      HSP=(1.-SZ)/FMMPM
      WA=-FLOAT(NK)/SZ
      HTHP=THMP/FNMPM
      PSS=PS*PS
      TD=TMAX-2.
      ALP=2.*GG*HT
      DB=ALP
      DA=.5*ALP**2
      DD=(ALP**3)/6.
      DC=(ALP**4)/24.
      DDG=DD*G
      DAG=DA*G
      DBG=DB*G
      HHT=.5*HT
      HA=     HT*HHT/3.
      GAM1=GL1+GAMA+GAMC +GAMB
      GAM2=GL2+GAMA+GAMC +GAMB+GAMB
      GAMN=GAMA+GAMC+GAMC+GAMB+GAMB
      H=-GAMC*HA-CC -GC*HHT
      D=CA+CB+C1          +GAM1*HA +CC+(G1+GA+GB+GC)*HHT
      E=-CB -GAMB*HA-GB*HHT
      F=CA+CB+CB+C2         +GAM2*HA +CC +(G2+GA+2.*GB+GC)*HHT
```

```
      A=CA+CB+CR+GAMN*HA   +CC+CC  +(GA+2.*GB+2.*GC)*HHT
      NET=NG-2
      DO 2101 J=1,NET
      N1=J+NG*(J-1)
      N2=N1+1
      N3=N1+NG
      N4=N1+2
      N5=N3+NG
      M(N1)=A
      M(N2)=E
      M(N3)=E
      M(N4)=H
2101  M(N5)=H
      M(1)=D
      N1=NG**2
      N2=2+NG
      N3=NG-1+NG*(NG-2)
      N4=N3+1
      N5=N1-1
      M(N1)=D
      M(N2)=F
      M(N3)=F
      M(N4)=F
      M(N5)=F
      CALL MINV(M,NG,DELTA,LL,PP)
      GAMM=-GAMC
      GAMP=-GAMB
      GU=G1+GAM1*HHT+GA+GB+GC
      GV=G2+GAM2*HHT+GA+2.*GB+GC
      GQ=GAMN*HHT+GA+2.*GB+2.*GC
      GB=-GAMB*HHT-GB
      GC   =-GAMC*HHT-GC
      DO 76 N=NGP,NE
      VF(N)=VDD(N)-VDC
76    VE(N)=VDD(N)
210   RETURN
      END
```

Appendix A.2.1

```
      SUBROUTINE MINV(A,N,D,L,M)
      DIMENSION A(1),L(1),M(1)
3     D=1.
      NK=-N
      DO 80 K=1,N
      NK=NK+N
      L(K)=K
      M(K)=K
      KK=NK+K
      BIGA=A(KK)
      DO 20 J=K,N
      IZ=N*(J-1)
      DO 20 I=K,N
      IJ=IZ+I
10    IF(ABS(BIGA)-ABS(A(IJ)))15,20,20
15    BIGA=A(IJ)
      L(K)=I
      M(K)=J
20    CONTINUE
      J=L(K)
      IF(J-K)35,35,25
25    KI=K-N
      DO 30 I=1,N
      KI=KI+N
      HOLD=-A(KI)
      JI=KI-K+J
      A(KI)=A(JI)
30    A(JI)=HOLD
35    I=M(K)
      IF(I-K)45,45,38
38    JP=N*(I-1)
      DO 40 J=1,N
      JK=NK+J
      JI=JP+J
      HOLD=-A(JK)
      A(JK)=A(JI)
40    A(JI)=HOLD
45    IF(BIGA)48,46,48
46    D=0.
      RETURN
48    DO 55 I=1,N
      IF(I-K)50,55,50
50    IK=NK+I
      A(IK)=A(IK)/(-BIGA)
55    CONTINUE
      DO 65 I=1,N
      IK=NK+I
      IJ=I-N
      DO 65 J=1,N
      IJ=IJ+N
```

```
      IF(I-K)60,65,60
60    IF(J-K)62,65,62
62    KJ=IJ-I+K
      A(IJ)=A(IK)*A(KJ)+A(IJ)
65    CONTINUE
      KJ=K-N
      DO 75 J=1,N
      KJ=KJ+N
      IF(J-K)70,75,70
70    A(KJ)=A(KJ)/BIGA
75    CONTINUE
      D=D*BIGA
      A(KK)=1./BIGA
80    CONTINUE
      K=N
100   K=K-1
      IF(K)150,150,105
105   I=L(K)
      IF(I-K)120,120,108
108   JQ=N*(K-1)
      JR=N*(I-1)
      DO 110 J=1,N
      JK=JQ+J
      HOLD=A(JK)
      JI=JR+J
      A(JK)=-A(JI)
110   A(JI)=HOLD
120   J=M(K)
      IF(J-K)100,100,125
125   KI=K-N
      DO 130 I=1,N
      KI=KI+N
      HOLD=A(KI)
      JI=KI-K+J
      A(KI)=-A(JI)
130   A(JI)=HOLD
      GO TO 100
150   RETURN
      END
```

Appendix A.3 Space-Charge Green's Function

```
      SUBROUTINE SPACH
      COMMON/PROB/JP,SZ,THM,MM,NM,PS,NE,GAP,THMP,MMP,NMP,ND,NKD,
     1VDC,NG,VDR,CA,CB,CC,GAMA,GAMB,GAMC,GA,GB,GC,C1,C2,GAM1,GAM2,G1,G2,
     2CIN1,CIN2,COUT1,COUT2,FREQ,THTC,
     3HT,G,GG,TMAX,NK,KM,LNWT,EMIN,CSAT,CNST,UTHERM,PIN,PDIN,THDIN,TAU
     4,KDIS,TD
      COMMON/SPCHEN/E
        DIMENSION BK(100),E(18,18,18),ED(5832)
      COMMON/CONSTS/ALP,DA,DB,DC,DD,DAG,DBG,DCG,DDG,WA,MMM,HS,NMM,HTH,PS
     1S,MMPM,HSP,NMPM,HTHP,PI,TPI,MPI,MA,MB,MC,MD,ICH,HHT,  GU,THCR ,GAM
     2P,GAMM,GV,GQ,GAMN,OMEGA,THS,PMT,GBT,GTHS,PMAX,ENS,AB,AC,AA,TP,TPT,
     3DUM
      DIMENSION ICH(15)
      IF(MA.EQ.1)GO TO 220
      D=ALOG(SZ)
      CDT=COS(HTH)
      SDT=SIN(HTH)
      Q=SZ-HS
      DO 166 M=1,MM
      Q=Q+HS
      BB=ALOG(Q)
      S=SZ-HS
60    DO 166 L=1,M
      S=S+HS
      CG=ALOG(S)
90    BZ=BB*(CG/D-1.)
85    BZP=BZ/1000.
      SZK=1.
      SK=1.
      QK=1.
      EK=0.
      DO 100 K=1,100
      EK=EK+1.
      SK=SK*S
      QK=QK*Q
      SZK=SZK*SZ
      IF(SZK.GE.1.E-04)GO TO 902
901   E=1.
      GO TO 91
902   E=1.-SZK*SZK
91    EP=(QK-1./QK)/E
93    GP=0.
      IF(SK.LT.10000.*SZK)
     1GP=(SZK/SK)*SZK
98    BK(K)=EP*(GP-SK)/EK
99    IF(BK(K).GE.BZP)GO TO 100
101   KA=K
      GO TO 140
100   CONTINUE
      KA=100
140   CT=CDT
      ST=-SDT
```

```
      DO 165 N=1,NM
      TE=CT*CDT-ST*SDT
      ST=CT*SDT+ST*CDT
      CT=TE
      B=0.
      CKT=1.
      SKT=0.
      DO 160 K=1,KA
      CL=CKT*CT-SKT*ST
      SKT=CKT*ST+SKT*CT
      CKT=CL
  160 B=B+BK(K)*CKT
      B=B+BZ
      F(M,L,N)=B
  163 F(L,M,N)=B
  165 CONTINUE
  166 CONTINUE
      MA=1
      GO TO (200,220),MD
      EQUIVALENCE(F,FD)
  200 CALL PDUMP(FD(1),FD( 5832),5)
  220 RETURN
      END
```

Appendix A.4 Anode Green's Function

```
C       CALCULATION OF CIRCUIT POTENTIAL FUNCTION
        SUBROUTINE CKT
        COMMON/PROB/JP,SZ,THM,MM,NM,PS,NE,GAP,THMP,MMP,NMP,ND,NKD,
       3DU
        COMMON/STATUS/TIME,STEPN,M4,QPP,ACF,XX,LG,CCAT,JT,QA,QB
        COMMON/CKTFCN/PSI
        DIMENSION PSI(2500)
       3,VS(100),VB(100),V(50,50)
        EQUIVALENCE(V,PSI)
        COMMON/CONSTS/ALP,DA,DB,DC,DD,DAG,DBG,DCG,DDG,WA,MMM,HS,NMM,HTH,PS
       1S,MMPM,HSP,NMPM,HTHP,PI,TPI,MPI,MA,MB,MC,MD,ICH,HHT,  GU,THCR ,GAM
       2P,GAMM,GV,GQ,GAMN,OMEGA,THS,PMT,GBT,GTHS,PMAX,ENS,AB,AC,AA,TP,TPT,
       3DUM
        DIMENSION ICH(15)
        IF(MB.EQ.1) GO TO 220
        SZSQ=SZ*SZ
        EN=NE
        CN=-1./(EN*ALOG(SZ))
        DELTHB=PI/EN
        DELGP=GAP*DELTHB
        THB=0.
        GP=0.
        DO 30 K=1,100
        GP=GP+DELGP
        THB=THB+DELTHB
        VK=(SIN (GP)/GP)*(SIN (THB)/THB)
 30     VB(K)=(VK+VK)/EN
        S=SZ
        DO 45 N=1,NMP
 45     V(1,N)=0.
        DO 100 M=2,MMP
        S=S+HSP
        VSZ=CN*ALOG(S/SZ)
        V(M,1)=VSZ
        SZTK=1.
        SK=1.
        DO 50 K=1,100
        SK=SK*S
        SZTK=SZTK*SZSQ
        E=1.-SZTK
        R=(SK-SZTK/SK)/E
        VS(K)=VB(K)*R
        V(M,1)=V(M,1)+VS(K)
        IF(R.GE..005)GO TO 50
 46     KA=K
        GO TO 55
 50     CONTINUE
        KA=100
 55     DO 70 N=2,NMP
```

```
      AH=FLOAT (N-1)*HTHP
      SDTH=SIN (AH)
      SKTH=0.
      CDTH=COS (AH)
      CKTH=1.
      VSTH=0.
      DO 60 K=1,KA
      TE=SKTH*CDTH+CKTH*SDTH
      CKTH=CKTH*CDTH-SKTH*SDTH
      SKTH=TE
60    VSTH=VSTH+VS(K)*CKTH
70    V(M,N)=VSTH+VSZ
100   CONTINUE
      MB=1
      GO TO (250,220),MD
250     CALL PDUMP(V,V(50,50),5)
220   RETURN
       END
```

Appendix A.5 Graphic Display

```
 SUBROUTINE DISPLA
 COMMON/PROB/JP,SZ,THM,MM,NM,PS,NE,GAP,THMP,MMP,NMP,ND,NKD,
1VDC,NG,VDR,CA,CB,CC,GAMA,GAMB,GAMC,GA,GB,GC,C1,C2,GAM1,GAM2,G1,G2,
2CIN1,CIN2,COUT1,COUT2,FREQ,THTC,
3HT,G,GG,TMAX,NK,KM,LNWT,EMIN,CSAT,CNST,UTHERM,PIN,PDIN,THDIN,TAU
4,KDIS,TD
 COMMON/CONSTS/ALP,DA,DB,DC,DD,DAG,DBG,DCG,DDG,WA,MMM,HS,NMM,HTH,PS
1S,MMPM,HSP,NMPM,HTHP,PI,TPI,MPI,MA,MB,MC,MD,ICH,HHT,  GU,THCR ,GAM
2P,GAMM,GV,GQ,GAMN,OMEGA,THS,PMT,GBT,GTHS,PMAX,FNS,AB,AC,AA,TP,TPT,
3MDD
 DIMENSION ICH(15)
 COMMON/CHARGE/IM,C,P,TH,UY,UX,ER,ETH,ERS,ETHS
 DIMENSION C(600),P(600),TH(600),UX(600),UY (600),ER(600),ETH(600),
1ERS(600),ETHS(600)
 COMMON/STATUS/TIME,STEPN,M4,QPP,ACF,XX,LG,CCAT,JT,QA,QB
 DIMENSION JFMT(3)
 DATA JFMT/'(1X,0000A1)'/
 DIMENSION IA(4),NC(4),W(8300),XX(600),YY(600),X(500),Y(500)
1,LDIX(250),DIX(63)
 DATA DIX/' *** *   **   **   * ***   *   **    *    *   ***  ***
1   * *** *    ***** ***     *  **     * ***    *   **  * * *****
2 * ******    ****     *****  *** *    **** *   * *** *****    *
3*   *   *    *** *   * *** *   * ***  *** *   * ****    * *** '/,
4DECPT/'*'/,BLANK/' '/,PLUS/'+'/
5,NC/37,44,53,60/,JM/0/
 DIMENSION MN(12)
 DATA MN/'JAN.FEB.MAR.APR. MAYJUNEJULYAUG.SEP.OCT.NOV.DEC.'/
 INTEGER STEPN
 LOGICAL*1 LBLANK,LDIX,LDECPT,W,LPLUS,LSTAR
 EQUIVALENCE (BLANK,LBLANK),(DIX,LDIX),(DECPT,LDECPT,LSTAR)
1,(PLUS,LPLUS)
 IF(JM.GT.0 )GO TO 10
 JM=61
 NH=61
 IX=MOD(NH,10)
 IY=MOD(NH,100)/10
 IZ=MOD(NH,1000)/100
 JFMT(2)=JFMT(2)+IX+256*IY+65536*IZ
 NV=14
 NHNV=NH*NV
 NHP=4*NHNV
 NH=NH-1
 CALL DATE(JMN,JDA,JYR)
 X(1)=0.
 Y(1)=1.05-SZ
 X(2)=PI/2.
 Y(2)=Y(1)
 X(3)=X(2)+PI
 Y(3)=0.
 X(4)=TPI
```

```
      Y(4)=0.
      J=5
      FA=NE
      FB=ND
      ARC=PI/FA
      FR=1.-GAP
      DTH=FR*ARC/FB
      CD=DTH
      DO 210 L=1,NE
      Z=L+L-1
      THC=Z*ARC
      CC=THC
      CQ=CC
      CB=CC
      X (J)=CQ
      Y(J)=1.-SZ
      J=J+1
      DO 200 N=1,ND
      CQ=CQ+CD
      CB=CB-CD
      X(J)=CQ
      Y(J)=1.-SZ
      J=J+1
      X(J)=CB
      Y(J)=1.-SZ
200   J=J+1
      PP=1.     -SZ
      PP=PP+.05
      X (J)=CB
      Y(J)=PP
      J=J+1
      X(J)=CQ
      Y(J)=PP
210   J=J+1
      FC=50.
      DTK=PI/FC
      SF=0.
      DO 300 M=1,100
      X(J)=SF
      Y(J)=0.
      J=J+1
300   SF=SF+DTK
10    DO 60 I=1,NHP
60    W(I)=LBLANK
      DO 450 N=1,4
      JW=1+(N-1)*NHNV
      HLFT=FLOAT(N)*PI/2.
      HRT=HLFT-PI/2.
      CALL PLOTS(J-1,NH,NV,HLFT,HRT,1.05001-SZ,0.,X,Y,LPLUS,W(JW))
 450  CALL PLOTS(IM,NH,NV,HLFT,HRT,1.05001-SZ,0.,TH,P,LSTAR,W(JW))
```

```
      PRINT 1,MN(JMN),JDA,JYR,JP,STEPN,TIME
1     FORMAT(1H1,A4,I3,4H, 19,I2,3X,8HSER. NO.  ,I5,5X,8HSTEP NO. ,I4,
     15X,5HTIME' ,F7.3)
      PRINT JFMT,(W(I),I=1,NHP)
550   RETURN
      END
```

Appendix A.5.1

```
      SUBROUTINE PLOTS(NP,NH,NV,HLFT,HRT,VTOP,VBOT,H,V,CHAR,W)
      DIMENSION H(1),V(1),W(1)
      LOGICAL*1 CHAR,W
      HR=HRT-HLFT
      VR=VBOT-VTOP
      NHP=NH+1
      DO 600 N=1,NP
      RV=(V(N)-VTOP)/VR
      IF(RV.LT.0..OR.PV.GT.1.) GO TO 600
      J=PV*FLOAT(NV-1)+1.5
      RH=(H(N)-HLFT)/HR
      IF(RH.LT.0..OR.RH.GT.1.) GO TO 600
      K=RH*FLOAT(NH-1)+2.5
      NB=K+NHP*(J-1)
      W(NB)= CHAR
600   CONTINUE
       RETURN
      END
```

Appendix A.6 Space-Charge Field Calculation

```
      SUBROUTINE FIVE
      COMMON/STATUS/TIME,STEPN,M4,QPP,ACF,XX,LG,CCAT,JT,QA,QB
      COMMON/CONSTS/ALP,DA,DB,DC,DD,DAG,DBG,DCG,DDG,WA,MMM,HS,NMM,HT
     1S,MMPM,HSP,NMPM,HTHP,PI,TPI,MPI,MA,MB,MC,MD
      COMMON/CHARGE/IM,C,P,TH,UY,UX,ER,ETH,ERS,ETHS
      DIMENSION C(600),P(600),TH(600),UX(600),UY (600),ER(600),ETH(6
     1ERS(600),ETHS(600)
      COMMON/SPCHFN/F
      DIMENSION F(2)
      CALL COOL(F)
      GO TO (10,20),MD
10    CALL PDUMP(TIME,TIME,5,IM,IM,4,C,C(IM),5,P,P(IM),5,ERS,ERS(IM),
     1ETHS(1),ETHS(IM),5)
20    RETURN
      END
```

Appendix A.6.1

```
          TITLE 'COOL10 FOR 360 SYSTEM'
*               REGISTER                        CONTENTS
*               0                               =4
*               1                               4*IM-4
*               2                               4*(I-1)
*               3                               4*(J-1)
*               4                               L
*               5                               N
*               6                               M
*         7     BASE REG. FOR CHARGE
*         8     BASE REG. FOR CHARGE            +4096
*         9     BASE REG. FOR EPS
*               10                              A(F(L,M,N))-3372
*               11                              18*M
*               13                              324*N
*         14    BASE REG. FOR ETHS
*         15    BASE REG. FOR COOL
        ENTRY COOL
COOL    SAVE    (14,12),,COOL
        BALR  15,0
        USING *,15
          USING CHARGE,7,8
          L     7,CHAD
          L     8,CHAD
          A     8,=F'4096'
          L     9,CAD
          L     14,172(9)
          ST    14,THCR
          L     14,44(9)
          ST    14,HS
          L     14,52(9)
          ST    14,HTH
          L     14,56(9)
          ST    14,PSS
          L     14,36(9)
          ST    14,WA
          L     9,PRAD
          L     14,4(9)
          ST    14,SZ
          L     14,12(9)
          ST    14,MM
          L     9,CHAD
          A     9,=F'16804'
          USING FRS,9
          LR    14,9
          A     14,=F'2400'
          USING ETHS,14
          L     1,0(1)
          S     1,=X'80000000'
          S     1,=F'3372'
```

```
          ST     1,AD
        ST     13,TS
        LE     0,MUN
        DE     0,HS
        STE    0,MRHS
          LPER   0,0
        STE    0,RHS
        LE     2,MUN
        DE     2,HTH
        STE    2,MRHTH
          LPER   2,2
        STE    2,RHTH
        LE     6,HTH
        ME     6,=E'16.'
        STE    6,THMX
        LA      0,4
        L      1,IM
        SLA    1,2
        SR     1,0
        SR     2,2
AA        C       0,C(2)
          BH     EA
        SER    4,4
        STE    4,ERS(2)
        STE    4,ETHS(2)
        LE     4,P(2)
        ME       4,RHS
          LER    2,4
        AU     4,CON
        STE    4,TF
          LH     4,TF+2
          AE     4,=E'0.'
          SER    2,4
        A      4,WUN
          C      4,MM
          BNL    EA
          C      4,WUN
          BH     ACC
          A      4,WUN
          AE     2,MUN
ACC       STE    2,FL
        SR     3,3
AC        C      14,C(3)
          BH     EC
ED      LE     0,TH(3)
        SE     0,TH(2)
EE      CE     0,MPI
        BNH    EQQ
YC      CE     0,PI
        BH     YB
```

```
EQ      STE    0,DTH
        LDER   0,0
        CE      0,THMX
        BNL    EC
          ME     0,RHTH
          LER    2,0
        AU     0,CON
        STE    0,TF
          LH     5,TF+2
          AE     0,=E'0.'
          SER    2,0
        A      5,WUN
          STE    2,FTH
        LE     6,P(3)
          ME     6,RHS
          LER    4,6
        AU     6,CON
        STE    6,TF
          LH     6,TF+2
        A      6,WUN
          AE     6,=E'0.'
          SER    4,6
          C      6,MM
          BNL    EC
YA        STE    4,FM
FJ        C      5,TOO
          BL      EF
          BE     EGH
FGG     C      6,WUN
          BE     FG
FBB       LA     13,324
        MR     12,5
        LA     11,18
        MR     10,6
        AR     11,13
        LR     10,11
        AR     10,4                    L+18 M+ 324 N
        SLA    10,2
          A      10,AD
EM        LE     2,3300(10)
          AE     2,0700(10)
          SE     2,3292(10)
          SE     2,0708(10)
          HER    2,2
          HER    2,2
          LER    0,2
          ME     0,FL
          LE     6,3368(10)
          AE     6,0632(10)
          SE     6,0776(10)
```

```
         SE     6,3224(10)
         HER    6,6
         HER    6,6
         ME     6,FM
         AER    0,6                      GB FM + GC FL
         LE     6,3296(10)
         SE     6,0704(10)
         HER    6,6
         AER    0,6                      E + GB FM + GC FL
         LE     4,2000(10)
         AER    4,4
         LE     6,3296(10)
         AE     6,0704(10)
EMM      SER    6,4                      TFA
         ME     6,FTH
         AER    0,6                      E+GB*FM+GC*FL+TFA*FTH
         ME     0,C(3)
         ME     0,MRHTH
         C      0,DTH
         BH     NX
         LCER   0,0
NX       AE     0,ETHS(2)
         STE    0,ETHS(2)
         ME     2,FTH                    GC*FTH
         LE     0,2004(10)
         AE     0,1996(10)
         SER    0,4
         ME     0,FL
         AER    0,2
         LE     6,2076(10)
         AE     6,1924(10)
         SE     6,1932(10)
         SE     6,2068(10)
         HER    6,6
         HER    6,6
         ME     6,FM
         AER    0,6                      GA*FM+GC*FTH+TBB*FL
         LE     6,2004(10)
         SE     6,1996(10)
         HER    6,6                      A
         AER    0,6                      A+GA*FM+GC*FTH+TBB*FL
         ME     0,MRHS
ECL      ME     0,C(3)
         AE     0,ERS(2)
         STE    0,ERS(2)
EC       BXLE   3,0,AC
EA       BXLE   2,0,AA
         L      13,TS
         RETURN (14,12)
EF       CR     2,3
```

```
            BE      EC
            LR      11,4
            SR      11,6
            C       11,WUN
            BH      EB
            C       11,MIN
            BNL     UF
EB          SER     0,0
            C       6,WUN
            BE      EGG
            SER     2,2
            LA      13,324
            MR      12,5
            LA      11,18
            MR      10,6
            AR      11,13
            LR      10,11
            AR      10,4
            SLA     10,2
            A       10,AD
            LE      4,2000(10)
            AER     4,4
            LE      6,3296(10)
            AER     6,6
            B       EMM
EQQ         AE      0,TPI
            B       EQ
YB          SE      0,TPI
            B       EQ
UF          C       4,WUN
            BNE     CL
UEP         LE      0,P(2)
            CE      0,P(3)
            BH      EC
SH          LE      0,WA
            B       ECL
CL          B       EN
EN          LE      0,P(3)
            LER     2,0
            AE      0,SZ
            LER     6,0
            ME      0,DTH
            MER     0,0
            SE      2,P(2)
            LER     4,0
            MER     2,2
            AER     0,2
            CE      0,PSS
            BH      NXX
            LE      0,PSS
```

```
NXX     LE    2,P(2)
        SE    2,P(3)
        DER   2,0
        ME    2,C(3)
        AE    2,ERS(2)
        STE   2,ERS(2)
        LCER  2,6
        DER   2,0
        ME    2,DTH
        MER   2,6
        ME    2,C(3)
        AE    2,ETHS(2)
        STE   2,ETHS(2)
        B     EC
EG      LE    0,DTH
        LPER  0,0
        CE    0,THCR
        BL    UFP
        B     EC
EGH     LR    11,4
        SR    11,6
        LPR   11,11
        C     11,WUN
        BH    EGG
        A     5,WUN
        LE    2,FTH
        SE    2,FUN
        STE   2,FTH
        B     EGG
MUN     DC    E'-1.'
MS      DC    X'00FFFFFF'
CON     DC    X'46000000'
WUN     DC    F'1'
TOO     DC    F'2'
MIN     DC    F'-1'
MPI     DC    E'-3.141593'
AD      DC    F'0'
TS      DC    F'0'
THMX    DC    F'0'
MRHS    DC    F'0'
RHS     DC    F'0'
MRHTH   DC    F'0'
RHTH    DC    F'0'
AL      DC    F'0'
TF      DC    F'0'
TFL     DC    F'0'
DTH     DC    F'0'
FTH     DC    F'0'
FM      DC    F'0'
FL      DC    F'0'
```

```
FUN       DC    E'1.'
THCR      DS    E
HS        DS    E
HTH       DS    E
PSS       DS    E
WA        DS    E
PI        DC    E'3.141593'
TPI       DC    E'6.283186'
SZ        DS    E
MM        DS    E
CHAD      DC    V(CHARGE)
CAD       DC    V(CONSTS)
PRAD      DC    V(PROB)
CHARGE    DSECT
TM        DS    E
C         DS  600E
P         DS  600E
TH        DS  600E
PD        DS  600E
THD       DS  600E
EE        DS  600E
ETH       DS  600E
EPS       DS  600E
ETHS      DS  600E
CONSTS    DSECT
PROB      DSECT
          END
```

```
      SUBROUTINE PSIPR
      COMMON/STATUS/TIME,STEPN,M4,QPP,ACF,XX,LG,CCAT,JT,QA,QB
      DIMENSION QA(100),QB(100)
      COMMON/CHARGE/IM,C,P,TH,UY,UX,ER,ETH,ERS,ETHS
      DIMENSION C(600),P(600),TH(600),UX(600),UY (600),ER(600),ETH(600),
     1ERS(600),ETHS(600)
      COMMON/CKTFCN/PSI
      DIMENSION PSI(50,50)
      COMMON/NETWRK/VE,VF,VI,QE,QP,M
      DIMENSION VE(80),VF(80),VI(80),QE(80),QP(80)
      DIMENSION M(6400),VR(80),W (80)
      COMMON/PROB/JP,SZ,THM,MM,NM,PS,NE,GAP,THMP,MMP,NMP,ND,NKD,
     1VDC,NG,VDR,CA,CB,CC,GAMA,GAMB,GAMC,GA,GB,GC,C1,C2,GAM1,GAM2,G1,G2,
     2CIN1,CIN2,COUT1,COUT2,FREQ,THTC,
     3HT,G,GG,TMAX,NK,KM,LNWT,EMIN,CSAT,CNST,UTHERM,PIN,PDIN,THDIN,TAU
     4,KDIS,TD
      COMMON/CONSTS/ALP,DA,DB,DC,DD,DAG,DBG,DCG,DDG,WA,MMM,HS,NMM,HTH,PS
     1S,MMPM,HSP,NMPM,HTHP,PI,TPI,MPI,MA,MB,MC,MD,ICH,HHT,  GU,THCR ,GAM
     2P,GAMM,GV,GQ,GAMN,OMEGA,THS,PMT,GBT,GTHS,PMAX,FNS,AB,AC,AA,TP,TPT,
     3DDT
      DIMENSION ICH(15)
      THS=TPI/FLOAT(NE)
      GTHS=GAP*THS
      IT=1
      DO 3 NA=1,NE
      QP(NA)=QE(NA)
3     QE(NA)=0.
501   DO 61 I=1,IM
      ER(I)=ERS(I)
      ETH(I)=ETHS(I)
      IF(C(I))61 ,61,610
610   AL=P(I)/HSP
      CALL FIXER (AL,FL,L)
5     IF(L-MMPM)7,6,630
630   SIG=TH(I)/THS
      ISE=SIG +.5
      FISE=ISE
      PSIP=(FISE-SIG   )/GAP+.5
      IY=ISE+1
      IF(IY.GT.NE) IY=1
      IZ=ISE
      IF(IZ.EQ.0) IZ=NE
      GO TO(640,660),IT
640   DQ=C(I)*PSIP
      QE(IZ)=QE(IZ)+DQ
      QE(IY)=QE(IY)+C(I)-DQ
      GO TO 61
660   ER(I)=0.
      ETH(I)=(VE(IY )-VE(IZ))/GTHS
      GO TO 61
```

```
    6 L=L-1
      FL=FL+1.
    7 DO 60 NA=1,NF
      LITE=0
 13   DTH= (FLOAT(NA-1)+.5)*DDT-TH(I)
 130  IF(DTH-PI)132,132,131
 131  DTH=DTH-TPI
      GO TO  130
 132  IF(DTH+PI) 133,133,139
 133  DTH=DTH+TPI
      GO TO 132
 139  IF(DTH)14,16,16
 14   LITE=2
 16   DDTH=ABS (DTH)
      AL=DDTH/HTHP
      CALL SIXER(AL,ETH,N)
 90   IF(N-NMPM)20,60,60
 20   B1=PSI(L,N)/2.
      B2=B1+PSI(L,N)
 922  B3=2.*PSI(L+1,N)
 923  B5=.5*PSI(L+2,N)
   33 A=B3-B5-B2
      B=B5-PSI(L+1,N)+B1
 924  B3=2.*PSI(L,N+1)
 925  B5=.5*PSI(L,N+2)
   35 C=B3-B5-B2
      D=B5-PSI(L,N+1)+B1
   40 GX=PSI(L+1,N+1)+PSI(L,N)-PSI(L+1,N)-PSI(L,N+1)
      GO TO (59,50),IT
 50   ER(I)=ER(I)+VE(NA)*(A+2.*B*FL+GX*ETH)/HSP
      GTH=(C+2.*D*ETH+GX*FL)/HTHP
 91    IF(         LITE.GE.1)GO TO 52
 51   ETH(I)=ETH(I)-VE(NA)*GTH
      GO TO 60
 52   ETH(I)=ETH(I)+VE(NA)*GTH
      GO TO 60
 59   QE(NA)=QE(NA)+C(I)*(PSI(L,N)+FL*(A+B*FL+GX*ETH)+(C+D*ETH)*ETH)
   60 CONTINUE
   61 CONTINUE
      GO TO(500,99),IT
 500  TPT=TPI*FREQ*(TIME-HHT)
      W(1)=CIN1*COS(TPT)+(QP(1)-QE(1))/HT-GU*VF(1)-GC*VF(3)-GAM1*VI(1)-
     1GAMM*VI(3)-GB*VF(2)-GAMP*VI(2)
      W(2)=CIN2*COS(TPT-THTC)+(QP(2)-QE(2))/HT-GV*VF(2)-GC*VF(4)
     1-GAM2*VI(2)-GAMM*VI(4)-GB*VF(3)-GAMP*(VI(1)+VI(3))-GB*VF(1)
      W(NG-1)=(QP(NG-1)-QE(NG-1))/HT-GV*VF(NG-1)-GC*VF(NG-3)-GAM2*VI(NG-
     11)-GAMM*VI(NG-3)-GB*VF(NG-2)-GAMP*VI(NG-2)-GB*VF(NG)-GAMP*VI(NG)
     2 +COUT2*COS(TPT-THTC)
      W(NG)=(QP(NG)-QE(NG))/HT-GU*VF(NG)-GC*VF(NG-2)-GAM1*VI(NG)-GAMM*
     1VI(NG-2)-GB*VF(NG-1)-GAMP*VI(NG-1) +COUT1*COS(TPT)
```

```
      NET=NG-2
      IF(NG.LT.5) GO TO 411
      DO 410 L=3,NET
410   W(L)=(QP(L)-QE(L))/HT-GQ*VF(L)-GC*(VF(L-2)+VF(L+2))-GAMN*VI(L)
     1-GAMM*(VI(L-2)+VI(L+2))-GB*(VF(L-1)+VF(L+1))-GAMP*(VI(L-1)+VI(L+1
     1)
411   CALL GMPRD(W,M,VR,1,NG,NG )
      DO 420 L=1,NG
      VI(L)=VI(L)+(VF(L)+VR(L)*HHT)*HT
      VF(L)=VF(L)+VR(L)*HT
420   VE(L)=VF(L)+VDC
      IT=2
      GO TO 501
99    GO TO (100,120),MD
100   CALL PDUMP(C    ,C(IM),5,P,P(IM),5,TH,TH(IM),5,ER,ER(IM),5,ETH,ETH(
     1IM),5,VE,VE(NE),5,QE,QE(NE),5)
120   RETURN
      END
```

Appendix A.7.1

```
          TITLE 'FIXER(AL,FL,L)'
          ENTRY FIXER
          BALR  15,0
          USING *,15
FIXER     SAVE  (14,12)
          STD   0,TK
          STD   2,TK+8
          STD   4,TK+16
          STD   6,TK+24
          L     9,0(1)
          LE    4,0(9)
          LER   6,4
          AU    6,CON
          STE   6,TE
          LH    6,TE+2
          A     6,WUN
          AE    6,=E'0.'
          SER   4,6
          L     9,4(1)
          STE   4,0(9)
          L     9,8(1)
          ST    6,0(9)
          LD    0,TK
          LD    2,TK+8
          LD    4,TK+16
          LD    6,TK+24
          RETURN (14,12)
          CNOP  0,8
CON       DC    X'46000000'
WUN       DC    F'1'
TE        DS    F
TG        DC    15F'0'
TK        DC    4D'0'
TH        DC    F'0'
          END
```

Appendix A.7.2

```
      SUBROUTINE GMPRD(A,B,R,N,M,L)
      DIMENSION A(1),B(1),R(1)
      IR=0
      IK=-M
      DO 10 K=1,L
      IK=IK+M
      DO 10 J=1,N
      IR=IR+1
      JI=J-N
      IB=IK
      R(IR)=0.
      DO 10 I=1,M
      JI=JI+N
      IB=IB+1
10    R(IR)=R(IR)+A(JI)*B(IB)
      RETURN
      END
```

Appendix A.8 Cathode Emission

```
      SUBROUTINE KATE
      COMMON/TIM/TIME,STEPN,IM,C,P,TH,PD,THD,ER,ETH,ERS,ETHS,
     1VE,QE,QP,QPP,ACE,VE,VB,VDC,VIN,NE,ZN,BETA,          HT,TMAX,G,GG,
     2EMIN,CSAT,UTHERM,CNST,ALP,DB,DC,DA,DD,DDG,DAG,DBG    ,CE,THK,CK,CA,
     3THA,WA,JP,ND,NK,MA,MX,  PI,TPI,
     4MP,MC,MD,ICH,SZ,MM,MDM,HS,NM,NMM,HTH,PSS,MMP,MMPM,HSP,NMP,NMPM,
     5HTHP,     GAP,DDT,QA,QB,MF,F,PSI
      EQUIVALENCE(FD,F),      (CONFIG,TIME)
      DIMENSION C(600),P(600),TH(600),PD(600),THD(600),ER(600),ETH(600),
     1ERS(600),ETHS(600)
     1,FD(5832),VE(20),QE(20),QP(20),VE(80),VB(80),CE(50),THK(50),
     2CK(50),CA(10),THA(10),ICH(15),QA(30),QB(30),CONFIG(13551),
     3PSI(50,50),EK(50),F(18,18,18)
      INTEGER STEPN
      MMM=MM-1
      THCR=PI/FLOAT(NK)
      TX=((WA/PI)**2)*2.
      DO 4 I=1,NK
4     EK(I)=0.
3     DO 60 I=1,NK
      TE=TPI*FLOAT(I-1)/FLOAT(NK)
      DO 60 J=1,IM
      IF(C(J))60,60,8
8     AL=P(J)/HS
      CALL FIXER(AL,FM,M)
  9   IF(M-MMM)10,11,60
11     M=M-1
      FM=FM+1.
  10  DTH=TH(J)-TE
 130  IF(DTH-PI)132,131,131
 131  DTH=DTH-TPI
      GO TO  130
 132  IF(DTH+PI)133,16,16
 133  DTH=DTH+TPI
      GO TO 132
16    DDTH=ABS (DTH)
      AL=DDTH/HTH
      CALL FIXER (AL,FTH,N)
90    IF(DDTH-THCR)161,161,171
161   IF(M-1)60,165,169
165   TXX=-C(J)*TX*P(J)
      TXY=TXX/2.
      L=1
      IF(DTH.LT.0.) L=-L
      II=I-L
      IF(II.EQ.0) II=NK
       IF(II.GT.NK) II=1
      IJ=I+L
      IF(IJ.EQ.0) IJ=NK
      IF(IJ.GT.NK) IJ=1
```

```
      ALF=.5*DDTH/THCR
      EJ=C(J)*WA-TXX
      EK(I)=EK(I)+(1.-ALF)*EJ+ALF*TXY
      EK(II)=EK(II)+(1.-ALF)*TXY
      EK(IJ)=EK(IJ)+ALF*EJ+TXY
      GO TO 60
169   IF(M-3)180,181,17
180   FM=FM-2.
      GO TO 182
181   FM=FM-1.
182   M=4
      GO TO 17
171   IF(N-NMM)172,60,60
172   IF(M-4)60,17,17
17    B3=2.*F(2   ,M,N)
923   B5=.5*F(3   ,M,N)
  33  A=B3-B5
40    G1=F(2   ,M+1,N)-F(2   ,M,N)
      G3=F(2   ,M,N+1)-F(2   ,M,N)
50    EK(I)=EK(I)-C(J)*(A+G1*FM+G3*FTH)/HS
  60  CONTINUE
      GO TO (52,61),MD
52    CALL PDUMP(EK,EK(NK),5)
61    DO 600 I=1,NK
      TE    =6.2831853*FLOAT (I-1)/FLOAT (NK)
  70  DO 600 NA=1,NE
 213  DTH=(FLOAT (NA-1)+0.5)*DDT-TE
2130  IF(DTH-PI) 2132,2131,2131
2131  DTH=DTH-TPI
      GO TO 2130
2132  IF(DTH+PI)2133,2139,2139
2133  DTH=DTH+TPI
      GO TO 2132
2139  AL=ABS (DTH/HTHP)
      CALL FIXER(AL,FTH,N)
91    IF(N-NMPM)2000,600,600
2000  B3=2.*PSI(2,N)
2923  B5=.5*PSI(3   ,N)
2033  A=B3-B5
2040  G1=PSI(2,N+1)-PSI(2,N)
500   EK(I)=EK(I)+VE(NA)*(A+G1*FTH)/HSP
 600  CONTINUE
      DO 900 I=1,NK
      IF(EK(I))650,890,890
650   IF(EK(I)-EMIN)652,891,891
652   CE(I)=0.
      GO TO 900
890   CE(I)=CNST
      GO TO 900
891   CE(I)=CNST*(1.-EK(I)/EMIN)
```

```
 900 CONTINUE
     MA=1
     GO TO (960,965),MD
 960 CALL POUMP(EK,EK(NK),5,CE,CE(NK),5)
 965 RETURN
     END
```

Appendix A.9 Trajectory Calculation

```
      SUBROUTINE NW01
C     JUNE 6
      EQUIVALENCE(LNWT,ME)
      COMMON/PROB/JP,SZ,THM,MM,NM,PS,NE,GAP,THMP,MMP,NMP,ND,NKD,
     1VDC,NG,VDR,ZA,CB,CC,GAMA,GAMB,GAMC,GA,GB,GC,C1,C2,GAM1,GAM2,G1,G2,
     2CIN1,CIN2,COUT1,COUT2,FREQ,THTC,
     3HT,G,GG,TMAX,NK,KM,LNWT,EMIN,CSAT,CNST,UTHERM,PIN,PDIN,THDIN,TAU
     4,KDIS,TD
      COMMON/CHARGE/IM,C,P,TH,UY,UX,ER,ETH,ERS,ETHS
      DIMENSION C(600),P(600),TH(600),UX(600),UY (600),ER(600),ETH(600),
     1ERS(600),ETHS(600)
      COMMON/CONSTS/ALP,DA,DB,DC,DD,DAG,DBG,DCG,DDG,WA,MMM,HS,NMM,HTH,PS
     1S,MMPM,HSP,NMPM,HTHP,PI,TPI,MPI,MA,MB,MC,MD,ICH,HHT,  GU,THCR ,GAM
     2P,GAMM,GV,GQ,GAMN,OMEGA,THS,PMT,GBT,GTHS,PMAX,FNS,AB,AC,AA,TP,TPT,
     3DUM
      DIMENSION ICH(15)
      COMMON/MARDAT/CAN,WAN,SWK,SCK,SAN,WAT,CE,CA,THA,CK,THK
      DIMENSION CE(50),CA(20),THA(20),CK(50),THK(50),CAN(80),WAN(80)
      ENTRY NEWT
      THS=TPI/FLOAT(NE)
      GTHS=GAP*THS
      PMAX=1.  -SZ
      PMT=PMAX-.00001
      DB=2.*GG*HT/FLOAT(LNWT)
      DA=DB**2/2.
      DD=DB**3/6.
      DC=DB**4/24.
      DAG=DA*G
      DBG=DB*G
      DCG=DC*G
      DDG=DD*G
      DEG=DBG*DC/5.
      CA(1)=0.
      CK(1)=0.
      L=1
      J=1
      SWK=0.
      SCK=0.
      SAN=0.
      WAT=0.
      DO 11 I=1,NE
      CAN(I)=0.
   11 WAN(I)=0.
      DO 20 LCN=1,LNWT
    3 DO 10 I=1,IM
      IF(C(I))10,10,7
    7 S=SZ+P(I)
      IF(P(I).EQ.PMT) GO TO 10
      EX=ETH(I)/S
      EY=ER(I)
```

```
      BET =G*EY/S
      DEL=-G*EX/S
      AA=UY(I)
      AM=UX(I)
      AB=EY+AM
      AN=EX-AA
      AC=AN+DEL*AM
      AP=BET*AM-AB
      AD=AP+DEL*AN
      AQ=BET*AN-AC
      AE=DEL*AP+AQ
      AR=BET*AP-AD
      UYT=AA+AB*DB+AC*DA+AD*DD+AE*DC
      UXT=AM+AN*DB+AP*DA+AQ*DD+AR*DC
      YT=S+AA*DBG+AB*DAG+AC*DDG+AD*DCG+AE*DEG
      XT=AM*DBG+AN*DAG+AP*DDG+AQ*DCG+AR*DEG
      S=SQRT(XT**2+YT**2)
      DETH=ATAN(XT/YT)
9     CD=YT/S
      SD=XT/S
      P(I)=S-SZ
      TH(I)=TH(I)+DETH
      IF(TH(I).LT.0.)TH(I)=TH(I)+TPI
 95   UX(I)=UXT*CD-UYT*SD
      UY(I)= UXT*SD+UYT*CD
   10 CONTINUE
      DO 20 I=1,IM
      IF(C(I))20,20,31
 31   IF(P(I))40,20,120
   40 CK(J)=C(I)
      SCK=SCK+C(I)
      SWK=SWK+C(I)*(UX(I)**2+UY(I)**2)
      THK(J)=TH(I)  *57.29578
      C(I)=-1.
      ER(I)=0.
      ETH(I)=0.
      IF(J-50)19,20,20
   19 J=J+1
      GO TO 20
 120  IF(P(I)-PMT )20,132,130
 130  SIG=TH(I)/THS
      ISE=SIG +.5
      FISE=ISE
      PSIP=(SIG-FISE   )/GAP+.5
      IF(PSIP.LE.0..OR.PSIP.GT.1.)GO TO 131
      GO TO 20
 131  CA(L)=C(I)
      IF(PSIP.GT.1.)ISE=ISE+1
      IF(ISE.EQ.0)ISE=NE
      CAN(ISE)=CAN(ISE)+C(I)
```

```
      W=C(I)*(UX(I)**2+UY(I)**2)
      WAN(ISE)=WAN(ISE)+W
      SAN=SAN+C(I)
      WAT=WAT+W
      THA(L)=TH(I) *57.29578
      P(I)=PMT
      IF(L.EQ.10)GO TO 20
  140 L=L+1
      GO TO 20
  132 C(I)=-1.
   20 CONTINUE
      LM=L
      JM=J
      DO 311I=LM,10
  311 CA(I)=0.
      DO 30 J=JM,50
   30 CK(J)=0.
      GO TO (200,220),MD
  200 CALL PDUMP(UX,UX(IM),5,UY ,UY (IM),5)
  220 RETURN
      END
```

Appendix A.10 Merge, Collect and Output

```
      SUBROUTINE MAR2
C     JUNE 19
      COMMON/PROB/JP,SZ,THM,MM,NM,PS,NE,GAP,THMP,MMP,NMP,ND,NKD,
     1VDC,NQ,VDR,ZA,CB,CC,GAMA,GAMB,GAMC,GA,GB,GC,C1,C2,GAM1,GAM2,G1,G2,
     2CIN1,CIN2,COUT1,COUT2,FREQ,THTC,
     3HT,G,GG,TMAX,NK,KM,LNWT,EMIN,CSAT,CNST,UTHERM,PIN,PDIN,THDIN,TAU
     4,KDTS,TD
      COMMON/STATUS/TIME,STEPN,M4,QPP,ACF,XX,LG,CCAT,JT,QA,QB
      COMMON/CHARGE/IM,C,P,TH,UY,UX,ER,ETH,ERS,ETHS
      COMMON/CONSTS/ALP,DA,DB,DC,DD,DAG,DBG,DCG,DDG,WA,MMM,HS,NMM,HTH,PS
     1S,MMPM,HSP,NMPM,HTHP,PI,TPI,MPI,MA,MB,MC,MD,ICH,HHT,  GU,THCR ,GAM
     2P,GAMM,GV,GQ,GAMN,OMEGA,THS,PMT,GBT,GTHS,PMAX,FNS,AB,AG,AA,TP,TPT,
     3DDT
      DIMENSION M(6400)
      EQUIVALENCE (TAU,TLIFE)
      COMMON/MARDAT/CAN,WAN,SWK,SCK,SAN,WAT,CE,CA,THA,CK,THK
      COMMON/NETWRK/VE,VF,VI,QE,QP,M
      DIMENSION VE(80),VF(80),VI(80),QE(80),QP(80)
      DIMENSION QA(100),QB(100)
      DIMENSION C(600),P(600),TH(600),UX(600),UY (600),ER(600),ETH(600),
     1ERS(600),ETHS(600)
      DIMENSION ICH(15)
      DIMENSION CE(50),CA(20),THA(20),CK(50),THK(50),CAN(40),WAN(40)
      INTEGER AND,OR,CFF,CFO,CNST
      INTEGER STEPN
      EQUIVALENCE (ID,DI)
      DIMENSION KC(10),JA(10)
     5,DQE(90)     ,WCP(20),PCO(20),UXC(20),UYC(20),CCP(20)
      EQUIVALENCE (TIME,CNF)
     1,(ICE,CE(1)),(KC(1),CK(1)),(JA(1),CA(1))
      DIMENSION MN(12)
      DATA MN/'JAN.FEB.MAR.APR. MAYJUNEJULYAUG.SEP.OCT.NOV.DEC.'/
      DATA CFF/Z FFFFFE00/,CFO/Z000001FF/,JEN/1/
      ENTRY MARGE
      GO TO (1,2),JEN
1     JEN=2
      AC=0.
      MXJ=.5+TLIFE/.1
      LLL=MXJ-512
      GBT=G/2.
      RGBT=SQRT(GBT)
      CALL DATE(JMN,JDA,JYR)
        PMT=(1.-SZ)-.00001
2     JST=.5+TIME/.1
      ICE  =OR(AND(CNST,CFF),AND(CFO,JST) )
      IF(MA.EQ.3) GO TO 799
      IF(STEPN.NE.0)GO TO 3
      CCAT=0.
      XX  =0.
      DO 4 J=1,100
```

```
      QA(J)=0.
 4    QB(J)=0.
 3    IA=1
      CCO=0.
      DCO=0.
      WCO=0.
      LCO=0
C     CLEAN-OUT
      K=JST-MXJ
      DO 60 I=1,IM
      IT=1
      IF(C(I).EQ.-1.)GO TO 59
      LST=AND(C(I),CFO)
      IF(P(I).EQ.PMT)GO TO 60
      LSTK=LST-K
 62   IF(LSTK.GT.0)GO TO 60
      IF(LSTK.EQ.0)GO TO 70
      IF(LSTK.GT.LLL)GO TO 61
      LSTK=LSTK+512
      GO TO 62
 70   ID  =OR(AND(CFF,C(I)/2.          ),AND(C(I),CFO))
      C(I)=DI
      IT=2
 61   CCO=CCO+C(I)
      IF(LCO.GE.20)GO TO 60
      LCO=LCO+1
      CCP(LCO)=C(I)
      PCO(LCO)=P(I)
      WCP(LCO)=GBT*C(I)*(UX(I)**2+UY(I)**2)
      WCO=WCO+WCP(LCO)
      UXC(LCO)=UX(I)*RGBT
      UYC(LCO)=UY(I)*RGBT
      IF(IT.EQ.2)GO TO 60
      C(I)=-1.
 59   P(I)=10.
 60   CONTINUE
      DCO=CCO/HT
      SCE=0.
      DO 100 K=1,NK
 80   DO 90 I=IA,600
      IF(C(I))81,81,90
 81   C(I)=CE(1)
      SCE=SCE+C(I)
      P(I)=PIN
      UY(I)=PDIN
      TH(I)=TPI*FLOAT(K-1)/FLOAT(NK)
      UX (I)=THDIN
      GO TO 92
 90   CONTINUE
 92   IA=I
```

```
      IF(IA-600)100,100,110
  100  CONTINUE
      DO 101 I=IA,600
      IF(C(I)) 101,101,102
  102   IA=IA+1
  101 CONTINUE
      GO TO 120
  110 IM=600
      GO TO 131
   120 DO 125 L=1,IM
      J=IM+1-L
      IF(J)123,130,123
  123 IF(C(J))125,125,126
   125 CONTINUE
   126 IM=J
  130  IMP=1
  131  IF(IM.GT.1) IMP=IM
      DO 132 J=IMP,600
      IF(C(J))134,134,132
   132 CONTINUE
   134 IM=J-1
      DO 400 N=1,9
  400   ICH(N)=FLOAT(ICH(N))/100.
      CALL TIMEGN(M4,IC)
      ACL=AC
      AC=FLOAT(IC)/6000.
      IA=IA-1
      ACL=AC-ACL
      DO 440 N=1,NE
  440  DQE(N)=(QE(N)-QP(N))/HT
      GO TO (401,402),MD
  401  PRINT 500,JP,STEPN,TIME,(N,ICH(N),N=1,9)
  500  FORMAT(5H1 SN I20,40X,9HSTEP NO. I5,7HTIME = 1PE15.3//26H TIME SPE
     1NT IN CHAIN LINKS/(I10,I10,14H        SECONDS))
      PRINT 501,AC,ACL,IA
  501  FORMAT(1H0,2F30.3,I10)
  402  PRINT 509,MN(JMN),JDA,JYR,JP,STEPN,TIME
  509  FORMAT(1H1,5X,A4,I3,4H, 19,I2, 5X,8HSER. NO.  ,I8, 5X,9HSTEP NO.
     1I3,5X,5HTIME  ,F8.3///
     1 9H0   ANODE  ,2X,7HVOLTAGE,5X,7HINDUCED,5X,7HINDUCED,4X,9HCOLLECT
     2ED,2X,11HBOMBARDMENT/5X,3HNO. 15X,6HCHARGE,6X,7HCURRENT ,5X,6HCHAR
     3GE,6X,6HENERGY/ )
      DO 300 N=1,NE
  300  WAN(N)=WAN(N)*GBT
      PRINT 510,((N,VF(N),QE(N),DQE(N),CAN(N),WAN(N)),N=1,NE)
  510  FORMAT(I7,F11.5,3F12.5,F13.5)
      VK=-VDC
  511  FORMAT( 8H0  SOLE      ,F10.5,24X,F12.5,F13.5)
  512  FORMAT(/8H   ANODE,10X,3F12.5,F13.5)
  513  FORMAT(/12H   COLLECTOR,18X,2F12.5,F13.5)
```

```
514  FORMAT(//19H CONVERTED ENERGY =,F13.5////)
515  FORMAT('0  INJECTION        ',11X,F12.5,'    ',F9.5,F13.5/)
     SKK=(SCE    )/HT
     SWK=SWK*GBT
     WEM=SCE*(PDIN**2+THDIN**2)*GBT
     WAT=WAT*GBT
     DQAT=SAN/HT
     QAT=0.
     DO 150 N=1,NE
150  QAT=QAT+QE (N)
     PRINT 512,QAT,DQAT,SAN,WAT
     PRINT 511,VK,SCK,SWK
     PRINT 513,DCO,CCO,WCO
     PRINT 515             ,SKK,SCE,WEM
     IF(LCO.LE.0)GO TO 152
     PRINT 516
516  FORMAT(30X,'COLLECTED STREAM'//6X,'CHARGE',5X,'RAD. LOC.',3X,'KIN.
    1 EN.',4X,'RAD. VEL.',2X,'AZIM. VEL.'/)
     PRINT 517,(CCP(I),PCO(I),WCP(I),UYC(I),UXC(I),I=1,LCO)
     IF(TIME.GE.TMAX-1.)
    1PUNCH 518,(CCP(I),PCO(I),WCP(I),UYC(I),UXC(I),TIME,JP,I=1,LCO)
517  FORMAT( 5 F12.5)
518  FORMAT( 5 F12.5,F12.5,I8)
152  NG=1./HT+.5
     K=MOD(STEPN,NG)+1
     XX=XX+QA(K)*(QE(1)-QB(K))
     CCAT=CCAT+QE(1)**2-QA(K)**2
     ACF=XX/CCAT
     QB(K)=QA(K)
     QA(K)=QE(1)
     PRINT 590,ACF
590  FORMAT(29H01-CYCLE RUNNING AUTO CORREL.F10.6)
     PRINT 501,AC,ACL,IA
     IF(MD.EQ.2)GO TO 220
     CKK=0.
     IF(CK(1))410,215,410
410  PRINT       530
530  FORMAT(1H1,25X,12HCATHODE DATA/)
     DO 211 I=1,50
     IF(CK(I)) 210,215,210
210  CKK=CKK+CK(I)
     ISS=AND(CK(I),CFO)
     KC(I)=AND(CK(I),CFF)
211  PRINT 520,CK(I),THK(I),ISS
215  PRINT 820,CKK,IM
     CAT=0.
     IF(CA(1))216,220,216
216  PRINT 540
540  FORMAT(1H1,25X,10HANODE DATA/)
     DO 226 I=1,10
```

```
      IF(CA(I))225,220,225
  225 ISS=AND(CA(I),CFD)
      JA(I)=AND(CA(I),CFF)
      CAT=CAT+CA(I)
  226 PRINT 520,CA(I),THA(I),ISS
  220 TIME=TIME+HT
  520 FORMAT(  E20.7,F20.4,I10)
      STEPN=STEPN+1
  200 IF(TIME-TMAX)222,799,799
  820 FORMAT(E20.6,I15)
  121 FORMAT(20A4)
  799 PUNCH 820,TIME,JP
      PUNCH 820,TIME,IM
      PUNCH121,(C(I),P(I),TH(I),UY(I),UX (I),I=1,IM)
      PUNCH 121,(QE(J)  ,J=1,NF)
      PUNCH 121,(QP(J)  ,J=1,NE)
      PUNCH 121,(VE(J)  ,J=1,NE)
      PUNCH 121,(VF(J)  ,J=1,NE)
      PUNCH 121,(VI(J)  ,J=1,NF)
      PUNCH 820,XX,NG,CCAT,STEPN
      PUNCH 121,(QA(K),K=1,NG)
      PUNCH 121,(QB(K),K=1,NG)
   77 CONTINUE
   78 RETURN
  222 RETURN
      END
```

Appendix A.10.1

```
          TITLE 'REAL/INTEGER FUNCTION AND(I,J)'
          ENTRY AND
          BALR  15,0
          USING *,15
AND       SAVE  (14,5)
          L     14,0(1)
          L     0,0(14)
          L     14,4(1)
          N     0,0(14)
          ST    0,T
        LE      0,T
       RETURN   (14)
T         DS    1F
          END
```

Appendix A.10.2

```
          TITLE 'REAL/INTEGER FUNCTION OR (I,J)'
          ENTRY OR
          BALR  15,0
          USING *,15
OR        SAVE  (14,5)
          L     14,0(1)
          L     0,0(14)
          L     14,4(1)
          O     0,0(14)
          ST    0,T
        LE      0,T
       RETURN   (14)
T         DS    1F
          END
```

Appendix A.11 Fourier Analysis

```
      SUBROUTINE AN06
C     JUNE 27
      COMMON/PROB/JP,SZ,THM,MM,NM,PS,NE,GAP,THMP,MMP,NMP,ND,NKD,
     1VDC,NG,VDR,CA,CB,CC,GAMA,GAMB,GAMC,GA,GB,GC,C1,C2,GAM1,GAM2,G1,G2,
     2CIN1,CIN2,COUT1,COUT2,FREQ,THTC,
     3HT,G,GG,TMAX,NK,KM,LNWT,EMIN,CSAT,CNST,UTHERM,PIN,PDIN,THDIN,TAU
     4,KDIS,TD
      COMMON/CONSTS/ALP,DA,DB,DC,DD,DAG,DBG,DCG,DDG,WA,MMM,HS,NMM,HTH,PS
     1S,MMPM,HSP,NMPM,HTHP,PI,TPI,MPI,MA,MB,MC,MD,ICH,HHT,  GU,THCR ,GAM
     2P,GAMM,GV,GQ,GAMN,OMEGA,THS,PMT,GBT,GTHS,PMAX,FNS,UB,UC,UA,TP,TPT
      COMMON/STATUS/TIME,STEPN,M4,QPP,ACF,XX,LG,CCAT,JT
      COMMON/CHARGE/IM,C,P,TH,UY,UX,ER,ETH,ERS,ETHS
      DIMENSION C(600),P(600),TH(600),UX(600),UY (600),ER(600),ETH(600),
     1ERS(600),ETHS(600),ICH(15)
      COMMON/NETWRK/VE,VF,VI,QE,QP,M
      DIMENSION VE(80),VF(80),VI(80),QE(80),QP(80)
      DIMENSION VB(80,8),QB(80,8),VET(80,50),QET(80,50)
      INTEGER STEPN
      DATA J3/0/
      ENTRY ANAL
      FNS=1./(FREQ*HT)
      AB=2./(3.*FNS)
      AC=2.*AB
      AA=4.*AB
      TP=TPI/FNS
      TPT=TPI*FREQ*TIME
      J=1.+FNS *AMOD(TIME+HHT,1./FREQ)
      A=AA
      IF(AND(J,1).NE.0.)A=AC
      IF(JJJ.EQ.123456)GO TO 4
      JJJ=123456
      THTC=THTC*PI/180.
      DO 100 N=1,NE
      DO 50 K=1,8
      VB(N,K)=0.
50    QB(N,K)=0.
      DO 100 K=1,50
      VET(N,K)=0.
100   QET(N,K)=0.
4     DO 6 N=1,NE
      B=VF(N)-VET(N,J)
      D=QE(N)-QET(N,J)
      DO 5 K=1,2
      ARG=FLOAT((K-1))*TPT
      CO=COS(ARG)
      SI=SIN(ARG)
      VB(N,K)=VB(N,K)+A*(B)*CO
      VB(N,K+4)=VB(N,K+4)+A*(B)*SI
      QB(N,K)=QB(N,K)+A*D*CO
5     QB(N,K+4)=QB(N,K+4)+A*D*SI
      QET(N,J)=QE(N)
6     VET(N,J)=VF(N)
      IF(MOD(J,KM ).NE.1)RETURN
```

```
      QR=0.
      QQ=0.
      DO 200 N=1,NE
      IF(MOD(N,55).EQ.1)PRINT 10,JP,STEPN,TIME
      K=2
      J=K-1
      VM=SQRT(VB(N,K)**2+VB(N,K+4)**2)
      VANG=ATAN2(VB(N,K+4),VB(N,K))*57.2957795
      QM=SQRT(QB(N,K)**2+QB(N,K+4)**2)
      QANG=ATAN2(QB(N,K+4),QB(N,K))
      THT=QANG+FLOAT(N-1)*THTC
      QANG=QANG                          *57.2957795
      IF(N.GT.NG)GO TO 200
      QR=QR+QM*COS(THT)
      QQ=QQ+QM*SIN(THT)
  200 PRINT 12,N,VM,VANG,QM,QANG
      QM=SQRT(QR**2+QQ**2)
      QANG=ATAN2(QQ,QR)                  *57.2957795
      PRINT 22,QM,QANG
      J3=J3+1
      IF(J3.EQ.5)GO TO 20
      RETURN
   20 CO=COS(TPT)
      SI=SIN(TPT)
      J3=6
      PRINT 23,(L,VF(L),VI(L),L=1,NG)
      DO 30 N=1,NG
      VF(N)= VB(N,2)*CO+VB(N,6)*SI
   30 VI(N)=(VB(N,2)*SI-VB(N,6)*CO)/TPI
      PRINT 23,(L,VF(L),VI(L),L=1,NG)
      RETURN
   10 FORMAT(1H1,7X,I20,10X,'STEP NO.',I4,10X,'TIME=',F9.3///11X,'ELEC.'
     1,5X,'VOLTAGE',14X,'CHARGE'/12X,'NO.',2X,'MAGN.    ANGLE',5X,'MAGNIT
     2UDE',4X,'ANGLE'//)
   12 FORMAT(I14,F8.3,F9.2,1PE13.4,0PF9.2)
   22 FORMAT(31X,1PE13.4,0PF9.2)
   23 FORMAT('1'/(I15,2F10.4))
      END
```

```
      FUNCTION ATAN3(A,B)
      IF(A.EQ.0..AND.B.EQ.0.)GO TO 1
      ATAN3=ATAN2(A,B)
2     RETURN
1     ATAN3=0.
      RETURN
      END
```

REPORT DISTRIBUTION LIST FOR CONTRACT NO. NAS3-9710

National Aeronautics and Space Administration
Headquarters
Washington, D. C. 20546
Attention: SA/L. Jaffe - 1 cy.
SAC/A. M. G. Andrus - 10 cys.

National Aeronautics and Space Administration
Lewis Research Center
21000 Brookpark Road
Cleveland, Ohio 44135
Attention: C. C. Conger, MS 54-1 - 1 cy.
R. E. Alexovich, MS 54-3 - 1 cy.
Dr. H. G. Kosmahl, MS 54-3 - 1 cy.
Technology Utilization Office, MS 3-19 - 1 cy.
Agena & Support Procurement Sec., MS 500-110 - 1 cy.
Library, MS 60-3 - 2 cys.
Report Control Office, MS 5-5 - 1 cy.
N. T. Musial, MS 501-3 - 1 cy.
G. J. Chomos, MS 54-3 - 5 cys.

Communication Systems, Inc.
5817 Columbia Pike
Falls Church, Virginia 22046
Attention: J. Bisaga - 1 cy.

Rand Corporation
1700 Main Street
Santa Monica, California 90404
Attention: Dr. J. Holt - 1 cy.

NASA Electronics Research Center
575 Technology Square
Cambridge, Massachusetts 02139
Attention: E/Dr. L. Van Atta - 1 cy.
EM/C. Veronda - 1 cy.
Library - 1 cy.

National Aeronautics and Space Administration
George C. Marshall Space Flight Center
Huntsville, Alabama 35812
Attention: RASTR-A/E. C. Hamilton - 1 cy.
Library - 1 cy.

National Aeronautics and Space Administration
Goddard Space Flight Center
Greenbelt, Maryland 20771
Attention: 733/R. Pickard - 1 cy.
Library - 1 cy.

National Aeronautics and Space Administration
Ames Research Center
Moffett Field, California 94035
Attention: OART-MAO/E. Van Vleck, MS 202-6 - 1 cy.
Library - 1 cy.

National Aeronautics and Space Administration
Langley Research Center
Langley Station
Hampton, Virginia 23365
Attention: B. Kendall, MS 173 - 1 cy.
Library, MS 185 - 1 cy.

National Aeronautics and Space Administration
Manned Spacecraft Center
Houston, Texas 77001
Attention: Library - 1 cy.

Jet Propulsion Laboratory
4800 Oak Grove Drive
Pasadena, California 91103
Attention: L. Derr - 1 cy.
Library - 1 cy.

National Aeronautics and Space Administration
Scientific and Technical Information Facility
P. O. Box 5700
Bethesda, Maryland
Attention: NASA Representative - 3 cys.

Radio Corporation of America
Astro-Electronics Division
Princeton, New Jersey 08540
Attention: R. B. Marstin - 1 cy.

TRW Systems
One Space Park
Redondo Beach, California 90278
Attention: W. A. Finley/Space Vehicle Division - 1 cy.

General Dynamics Corporation
Convair Division
P. O. Box 1128
San Diego, California 92112
Attention: F. J. Dore/Advanced Programs Laboratory - 1 cy.

Hughes Aircraft Company
Space Systems Division
1194 West Jefferson Boulevard
Culver City, California 90230
Attention: H. A. Rosen/Satellite Systems Laboratory - 1 cy.

General Electric Company
Missile and Space Division
Valley Forge Space Technology Center
P. O. Box 8555
Philadelphia, Pennsylvania 19101
Attention: H. Collins - 1 cy.
P. Nadler - 1 cy.

Federal Communications Commission
521 Twelfth Street
Washington, D. C. 20554
Attention: H. Fine - 1 cy.

U. S. Information Agency
25 M. Street S.W.
Washington, D. C. 20547
Attention: IBS/EF/G. Jacobs - 1 cy.

General Electric Company
Tube Department
Microwave Tube Business Section
Schenectady, New York
Attention: R. Dehn - 1 cy.

Litton Industries
Electron Tube Division
960 Industrial Road
San Carlos, California 94070
Attention: Dr. G. Pokorney - 1 cy.
J. Orr - 1 cy.

S-F-D Laboratories, Inc.
800 Rahway Avenue
Union, New Jersey 07083
Attention: Dr. G. Farney - 1 cy.

Hughes Aircraft Company
Electron Dynamics Division
P. O. Box 2999
Torrance, California 90509
Attention: Dr. J. Mendel - 1 cy.

Watkins Johnson Co.
333 Hillview Avenue
Palo Alto, California 94304
Attention: Dr. D. Watkins - 1 cy.

Varian Associates
611 Hansen Way
Palo Alto, California 94303
Attention: F. Melzer - 1 cy.

RCA
Industrial Tube Division
Lancaster, Pennsylvania
Attention: W. P. Bennett - 1 cy.